UiT The Arctic University of Norway

FACULTY OF HEALTH SCIENCES, DEPARTMENT OF MEDICAL BIOLOGY,
MOLECULAR PHARMACOLOGY AND TOXICOLOGY RESEARCH GROUP

The search of new negative allosteric $GABA_B$ receptor modulators using in silico and in vitro approaches

Ali Muataz Hadi

Master thesis in pharmacy (FAR-3911) May 2020

Table of Contents

Foreword

This master thesis serves as a documentation and is the final work of my master's study at University in Tromsø – The Arctic University of Norway. This project was achieved along with the Medical Pharmacology and Toxicology Research Group, Department of Medical Biology, Faculty of Health Science, between August 2019 and May 2020.

I would like to sincerely express my gratitude to my supervisors, Associate Professor Mari Gabrielsen and Chief Engineer Imin Wushur, as I attained a vast knowledge and learning experience. I could not accomplish this work without their support and guidance.

It was a great pleasure working with my project partner Ibrahim Touré (Quttuz). Thank you for the companionship and laughter throughout this project, making every step enjoyable.

I also want to thank my friends Luqman Ahsan (Ibn Sina) and Kasi Shorshan (Ibn Rushd). I am truly grateful for the memories and for making ordinary moments, extraordinary.

I want to honor my parents for continuously believing in my abilities and supporting my accomplishments. Finally, I wish to thank my girlfriend Jamelle, for being so patient, understanding and encouraging despite the long distance.

Abstract

γ-aminobutyric acid (GABA) is the primary inhibitory neurotransmitter in the CNS. GABA exerts its function on both ionotropic ligand-gated $GABA_A$ receptors and metabotropic $GABA_B$ G-protein coupled receptors (GPCRs). Disruption in the GABAergic system has been associated with numerous neurological and psychiatric disorders in humans. These include developmental dysfunctions, epilepsy, sleep disorders, drug and alcohol dependence, schizophrenia, motor coordination disorders, anxiety, autism, inability to regulate emotions, Huntington's disease, and Parkinson's disease. Hence, developing drugs to act on such a remarkable system can attract much attention and be beneficial.

In recent years, there has been colossal attention toward development of allosteric modulators of GPCRs. These compounds provide high selectivity, novel modes of action and may lead to unique therapeutic agents for the treatment of many neurological and psychiatric human disorders. Baclofen, a $GABA_B$ receptor agonist, is still the only $GABA_B$ receptor approved drug, and is used for the treatment of muscle spasticity associated with spinal cord injury and multiple sclerosis; however, numerous side effects hamper its clinical use. Allosteric modulators, on the other hand, are expected to have a much better side-effect profile than traditional orthosteric drugs.

In the current study, in silico and in vitro methods were adopted to screen for potential negative allosteric modulators within the MolPort database. A sequential combination of ligand- and structure-based virtual screening was first performed to reduce the significant number of chemical compounds followed by the in vitro experimental testing. The virtual screening procedure facilitated the selection of 16 hit compounds that were purchased and tested experimentally using an in vitro functional assay. Only one compound, A-8, was tested in a dose-response cAMP assay, and results indicate that it is a negative allosteric modulator. In addition, analysis of the initial test results suggests that A-9 might be a negative allosteric modulator and that A-20 might be a positive allosteric modulator. Further accurate experimental tests are required for these compounds.

Abbreviations

Å	Ångström
ADME	Absorption, Distribution, Metabolism, Excretion
AMP	Adenosine monophosphate
ATP	Adenosine triphosphate
BBB	Blood brain barrier
BLAST	Basic Local Alignment Search Tool
CADD	Computer-aided drug design/discovery
CasR	Calcium-sensing receptor
cDNA	complementary DNA
CHO-K1 cells	Chinese Hamster ovary cells
CNS	Central nervous system
CRD	Cysteine rich domain
CYP enzymes	Cytochrome P450 enzymes
DMSO	Dimethyl sulfoxide
DNA	Deoxyribonucleic acid
EA	Enzyme acceptor
E_{angle}	Angle binding energy
E_{bonded}	Bonded energy
EC	Effective concentration
ECD	Extracellular domain
ECL	Extracellular loop
ED	enzyme donor
$E_{dihedral}$	Torsional energy
E_{elec}	Electrostatic energy
EFC	Enzyme fragment complementation
EM	Electron microscopy
$E_{non\text{-}bonded}$	Non-bonded energy
ER	Endoplasmatic reticulum
E_{vdw}	Van der Waals energy
FDA	Food and Drug Administration
GABA	Gamma aminobutyric acid
GAT	GABA transporters
GAD	Glutamic acid decarboxylase
GDP	Guanosine diphosphate
GERD	Gastroesophageal Reflux Disease
GIRK	G protein-coupled inwardly-rectifying potassium channels
GPCR	G-protein coupled receptors
GRAFS	Glutamate, Rhodopsin, Adhesion, Frizzled/Taste2, and Secretin
GRK	G-protein coupled kinases
GTP	Guanosine triphosphate

GUI	Graphical user interface
HBA	Hydrogen bond acceptor
HBD	hydrogen bond donor
HBSS	Hank's Balanced Salt Solution
HEK cells	Human Embryonic Kidney cells
HEPES	4-(2-hydroxyethyl)-1-piperazineethanesulfonic acid
HTS	High-throughput screening
ICL	Intracellular loop
ICM	Internal Coordinate Mechanics software
IFD	Induced fit docking
IPSC	Inhibitory postsynaptic current
KCTD	Potassium channel tetramerization domain
K_d	Dissociation constant
LAF	Laminar flow
LBDD	Ligand-based drug design/discovery
LBVS	Ligand-based virtual screening
LCP	Lipid Cubic Phase
MC	Monte Carlo simulation
MD	Molecular dynamics simulation
mGlu receptor	Metabotropic glutamate receptor
MM	Molecular mechanics
MSA	Multiple sequence alignment
MW	Molecular weight
NAM	Negative allosteric modulator
NAL	Neutral allosteric ligand
NMDAR	N-methyl-D-aspartate receptor
OPLS	Optimized Potentials for Liquid Simulations
PAINS	Pan-assay interference compounds
PAM	Positive allosteric modulator
PBS	Phosphate buffered saline
PDB	Protein Data Bank
PKA	Protein kinase A
PNS	Peripheral nervous system
PRAF	Prenylated Rab acceptor family
PSA	Polar surface area
QM	Quantum mechanics
QSAR	Quantitative structure-activity relationship
RB	Rotatable bonds
RLU	Relative Light Unit
RMSD	Root Mean Square Deviation
RSRR	Endoplasmatic reticulum retention motif
SAM	Silent allosteric modulator
SAVES	Structural analysis and verification server

SBDD	Structure-based drug design/discovery
SBVS	Structure-based virtual screening
SD	Sushi domain
SLC6	The solute carrier 6
SP docking	Standard precision docking
TAS	Taste receptors
TM	Transmembrane
TREK2	Twik-related K_+ channels
UniProtKB	Universal Protein Resource Knowledgebase
VFT	Venus fly trap
VGAT	Vesicular GABA transporter
VGCC	Voltage-gated calcium channels
VS	Virtual screening
XP docking	Extra precision docking

1 Introduction

1.1 The central nervous system

The nervous system is the control system of the human body. It is highly sophisticated, enabling the body to receive, interrupt, and respond to changes in the surrounding environment. It controls both voluntary processes and involuntary processes, including circulation, respiration, and digestion (1).

Structurally, the nervous system is divided into two principal regions: the central nervous system (CNS) and the peripheral nervous system (PNS). The CNS consists of two main components: the brain and the spinal cord. The brain is attached to the spinal cord, which provides information from different parts of the body to and from the brain. The brain is the control system involved in many body functions, including sensation, thinking, movement, and memory. The PNS comprises all the nervous structures outside the CNS and connects CNS to muscles and organs (1).

Nervous tissue is one of the major classes of tissues. It consists of multiple nerve cells, also referred to as neurons, and glial cells. Control and communication occur by receiving or sending signals (messages) via a network of neurons. The neuron consists mainly of the cell body (soma) and other extensions referred to as processes (Fig. 1). Axon and dendrites are such extensions, which receive or pass information from or to other neurons at specific areas called synapses. Neurons are not directly attached to target cells, whether other neurons or muscle tissue, and there is a gap between the cells known as the synaptic cleft. The messages are carried between synapses by the release of chemical messengers, known as neurotransmitters (1). The other type of cells found in the nervous tissues is the aforementioned glial cells. Generally, they are recognized as supporting cells that maintain the concentration of chemicals in the extracellular space, eliminate excess signaling molecules, respond to tissue damage, and contribute to the blood-brain barrier (BBB) (2).

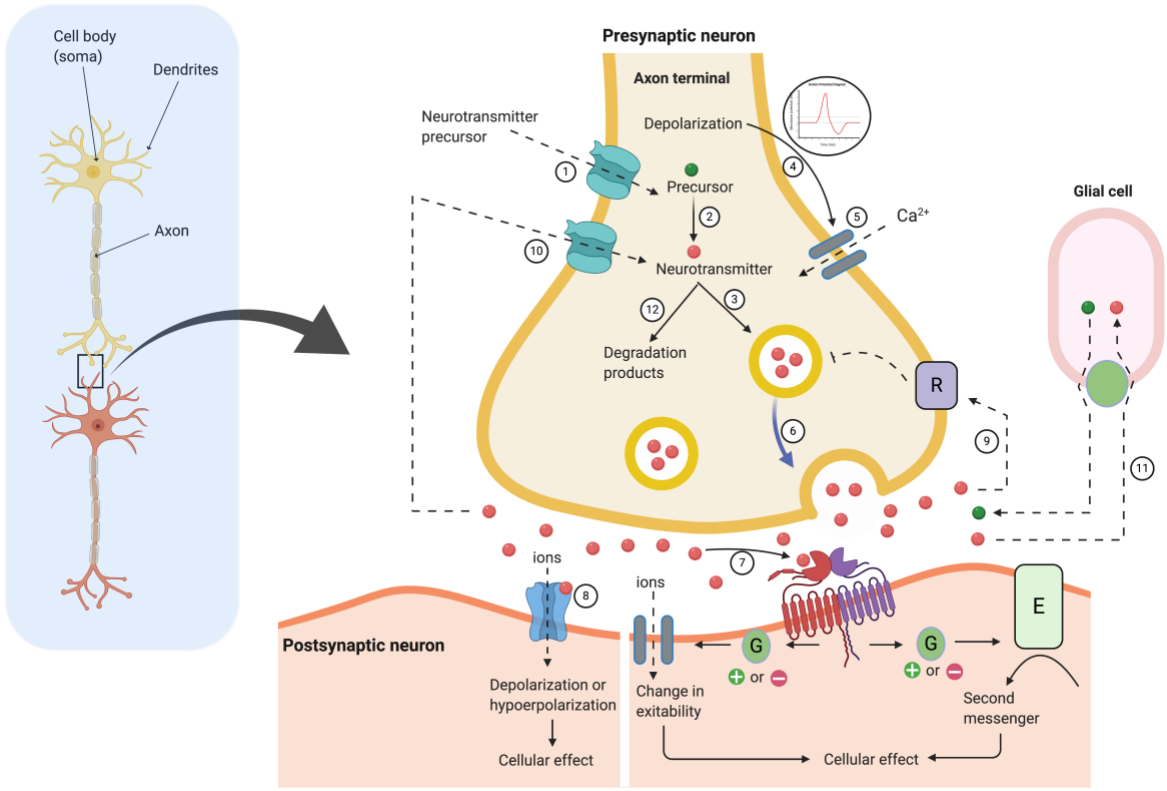

Figure 1 Schematic representation of neurons and the main processes involved in neurotransmission. *1. Uptake of neurotransmitter precursors; 2. Synthesis of neurotransmitter; 3. Uptake of neurotransmitter into storage vesicles; 4. Depolarization by generated action potential; 5. Influx of Ca^{2+} in response to depolarization; 6. Release of neurotransmitter into synaptic cleft by exocytosis; 7. Binding of neurotransmitter and activation of postsynaptic metabotropic receptors (e.g., G-protein coupled $GABA_B$ receptor); 8. Binding of neurotransmitter and activation of ligand-gated ion channel (e.g., postsynaptic ionotropic $GABA_A$ receptors); 9. Interaction with presynaptic receptors. Neurotransmission termination occurs either by, 10. Reuptake of the neurotransmitter into the presynaptic neuron (11; reuptake into glia cells) or by, 12. Inactivation of the neurotransmitter inside the synapses. The metabotropic postsynaptic receptor presented is the heterodimer $GABA_B$ receptor. The design of the figure is adopted from (3).*

Neurons are surrounded by and filled with charged particles (ions). At resting state, there is a balance between positively charged ions inside and outside of the neuron. The concentration of sodium ions (Na^+) on the outside of the neuron is higher than inside, whereas there is more potassium ion (K^+) on the inside of the neuron compared to outside. The distribution of these ion concentrations yields a net negative charge of -60 to -70 mV inside the neuron relative to the outside, and this is called the resting membrane potential (4). In order to release neurotransmitters, the neuron must be activated, and a shift in this ion balance has to occur. In the initiation stage of activation, a few positively charged sodium ions enter the neuron across the cell membrane via Na^+-channels. This process results in a more positively charged ions inside the neuron compared to the outside. As a result, the resting membrane potential becomes less negative, a process referred to as depolarization. Membrane depolarization from -70 mV to -55 mV (known as the threshold), opens the voltage-gated Na^+ channels, and an action potential is initiated. Depolarization that does not change the membrane potential to -55 mV or higher, will not reach the threshold and thus will not result in an action potential. As the membrane potential reaches +30 mV, specific voltage-gated potassium channels open in the membrane. The membrane potential moves back to its resting state because K^+ ions leaves the cell, a process referred to as repolarization. Those voltage-gated potassium channels are somewhat delayed in closing, causing the membrane potential to go below -70

mV, a process known as hyperpolarization (1). Diagram of the action potential is shown in Fig. 2.

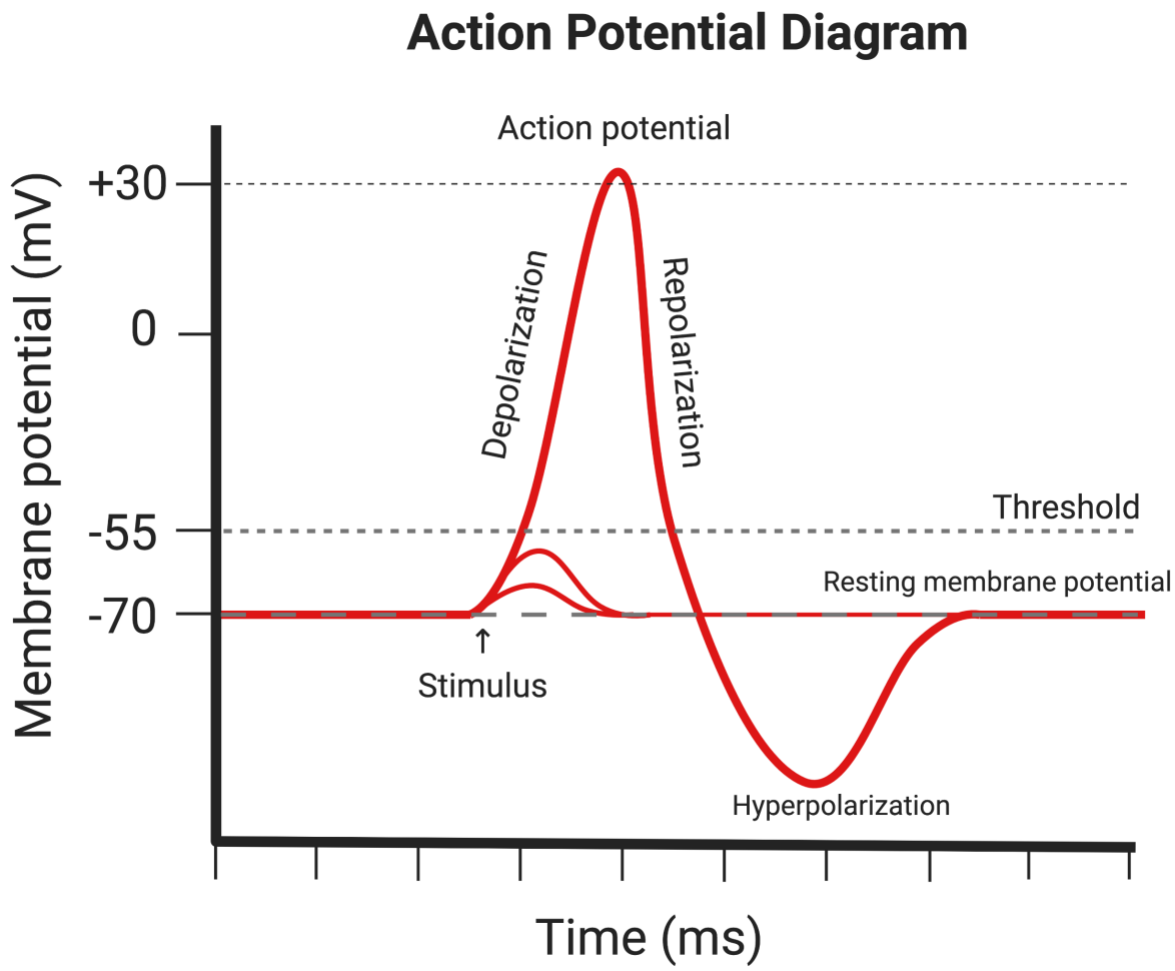

Figure 2 Graph of action potential. *The graph shows the millivoltage (mV) plotted against time in milliseconds (ms).*

Neurotransmitters are either monoamines (e.g., acetylcholine, noradrenaline, dopamine, and serotonin, also known as 5-hydroxytryptamine (5-HT)) or amino acids (e.g. γ-aminobutyric acid (GABA), glutamate, and glycine). They are usually stored in vesicles of the presynaptic neuron and are released to the synaptic cleft once the action potential reaches the axon terminal. Following their release, they diffuse to the postsynaptic target, where they bind to specific cell-surface receptors. The types of neurotransmitters released and the type of receptors present, determine the type of communication that can occur. This process of binding initiates a cascade of secondary effects that result in a biological response (2).

Drugs that affect the CNS work on neurons, by mimicking or interfering with the neurotransmission. For example, drugs can interfere with the neurotransmitter synthesis, blocking neurotransmitter transporters, or enhancing/decreasing receptor activation. Hence, increasing brain activity in specific regions or decreasing activity in others (1).

The principles of drug-receptor and neurotransmitter-receptor interactions are explained by the Law of Mass Action. A drug molecule, D, is supposed to combine with a receptor, R, to make a drug-receptor complex, DR (3). The equation can be written as follows:

$$D + R \underset{K_{-1}}{\overset{k_{+1}}{\rightleftharpoons}} DR \qquad \text{Eq. (1)}$$

where k_{+1} is the association rate constant, and k_{-1} is the dissociation rate constant. Drugs are described by their dissociation equilibrium constant K_d, which is the ratio of dissociation to association rate constants or the ratio of association to dissociation rate, known as association constant or affinity. The higher the affinity of the drug for the receptors, the lower will be the value of K_d. This principle also explains the termination of drug action or termination of neurotransmission. When the concentration of the unbound drug, D, (or neurotransmitter) decreases, the equilibrium is driven toward the unbound drug, which results in less drug-receptor complex, hence termination of the action (Fig. 1) (3,5).

1.1.1 Drug distribution to the CNS

Blood supply to the brain is critical for our survival because it transports vital nutrients (e.g., glucose) and oxygen to the brain and removes toxins and waste products from the brain. However, blood may also carry foreign substances that can put us at risk. Therefore, we have a security system in our blood vessels of the CNS called the blood-brain barrier (BBB). It is a physiological barrier that protects our neural tissue from toxins and pathogens, allows for a precise neural function, and helps to maintain a stable and safe microenvironment (6). The capillaries in the brain, like other blood vessels in the body, are composed of endothelial cells that line the wall of the blood vessels. However, in the CNS, the endothelial cells are held together with tight junctions that serve as physical barriers restricting passages of substances through space between cells.

In addition to the endothelial cells, mural cells (pericytes) and glial cells (astrocytes) are other types of cells that form the BBB. The mural cells cover the endothelial cells and contain contractile proteins, and therefore can contract to control the capillary's diameter. The astrocytes connect the neuronal network activity to blood vessels (6). These biological systems prevent potentially dangerous substances from penetrating the brain. On the other hand, it creates challenges in designing drugs reaching the CNS. Almost more than 98% of all small-molecule drugs do not reach the CNS (7). A sample of the BBB is presented in Fig. 3.

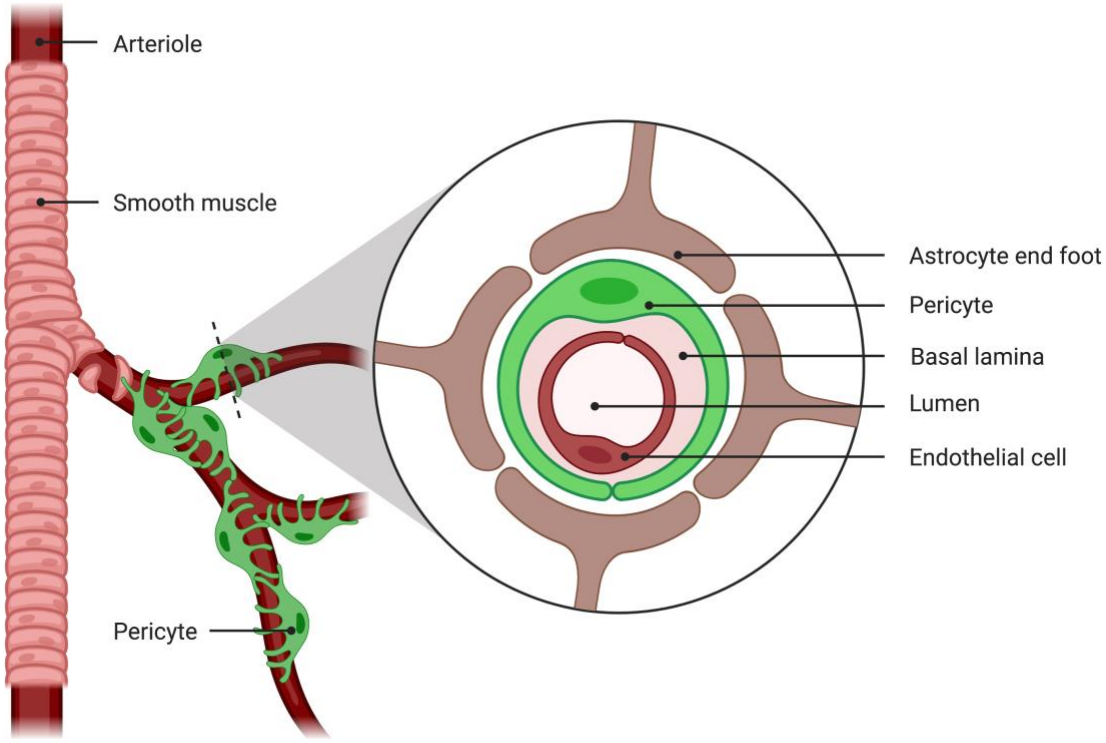

Figure 3 Elements of the blood-brain barrier. *The blood-brain barrier consists of specialized capillary endothelial cells that are embraced by the basal lamina, pericytes, and astrocytic end-feet.*

Most drugs in clinical use that act in the CNS are small, lipid-soluble molecules that cross the BBB by transmembrane passive diffusion (8). It is a nonsaturable diffusion that highly depends on the physicochemical properties of drugs. Drugs with low molecular weight and high lipid solubility are most likely to cross the membrane by this mechanism.

Many drugs are weak acids or bases and can exist in both uncharged and charged forms, where the ratio of these is dependent on the pH (3). For example, the ionization reaction of a weak base can be written as follows:

$$BH^+ + H_2O \underset{}{\overset{K_a}{\rightleftharpoons}} B + H_3O^+ \qquad \text{Eq. (2)}$$

Where HB_+, is the ionized form of the base, and B is the unionized form. B can accept a proton when pH is below its specific pK_a value (dissociation constant) to become cationic, BH_+. The dissociation constant, pK_a, is given by Henderson-Hasselbalch equation:

$$pK_a = pH + \log_{10}\frac{[A^-]}{[HA]} \qquad \text{Eq. (3)}$$

Similarly, for weak acid, the ionization can be written as:

$$HA + H_2O \underset{}{\overset{K_a}{\rightleftharpoons}} A^- + H_3O^+ \qquad \text{Eq. (4)}$$

where HA becomes anionic, A^-, when pH is above the specific pK_a value of the molecule. The dissociation constant for weak acids given by the Henderson-Hasselbalch equation is:

$$pK_a = pH + \log_{10} \frac{[BH^+]}{[B]} \qquad \text{Eq. (5)}$$

The ionized forms have very low lipid solubility and are unable to cross the lipid membrane by passive diffusion. The Henderson-Hasselbalch equation describes that the ratio of ionized proportion to unionized depends on the pK_a of the drugs and the environment pH. The ionization state of a drug does affect not only drug permeability but also the distribution between body compartments. For example, all acidic drugs are unionized in the stomach (approx. pH=3), and the portion of the ionized drug increases when it reaches the intestine (approx. pH=7.4) (3). The unionized portion of the acidic drug is well absorbed from the stomach; however, the surface area in the stomach is less than in the intestine which makes most of the drug to be absorbed from the intestine even though pH is higher than in the stomach. Drugs pharmacokinetic properties, such as rate of absorption from the gut, penetration into different tissues, and the extent of renal elimination, are of equal value as pharmacodynamic properties (3).

The movement of ions and molecules between blood and brain are controlled with specific transporters. There are two main types of transporters expressed in the CNS: efflux transporters and nutrient transporters (6). Efflux transporters, including P-glycoprotein, use hydrolysis ATP to transport substances against their concentration gradient. They are specialized to recognize molecules that should not be in the brain and pump them out to the vascular system (9). Nutrient transporters facilitate the transport of specific nutrients down its concentration gradients from the blood to the brain. Many of these transporters belong to the solute carrier-class, including SLC2A1 (glucose), also called Glut1, that transport glucose and other essential amino acids (6). Some drugs cross the BBB by the use of saturable transport systems. L-DOPA and caffeine are examples, as are vitamins such as B_{12} and B_6 (8).

1.2 The GABAergic system

GABA is the primary inhibitory neurotransmitter in the mature CNS that mediates more than 50% of the inhibitory signals in the CNS (10). In some regions of the brain, GABA is presented at high concentration (millimolar); these concentrations are actually 1000 times higher compared with the concentrations of classical monoamine neurotransmitters in the same region (11).

Disruption in the GABAergic system has been associated with numerous neurological and psychiatric disorders in humans. These include developmental dysfunctions, epilepsy, sleep disorders, drug and alcohol dependence, schizophrenia, motor coordination disorders, anxiety, autism, inability to regulate emotions, Huntington's disease, and Parkinson's disease

(10). Hence, developing drugs to act on such an impressive system can attract much attention and be to good profit (10,11).

GABA is also found beyond the nervous system at relatively high concentrations. However, the knowledge about GABA beyond the nervous system is yet to be fully studied. It is synthesized in the insulin-producing β-cells in pancreas, along with insulin, and serves to increase insulin secretion (12). Moreover, GABA is also discovered in α-cells and aids in suppressing glucagon secretion in animal research (13). These findings may lead to the development of novel antidiabetic drugs. Interestingly, immune cells exhibit GABA receptors and can produce GABA. Such feature could be beneficial in treating autoimmune diseases (14). GABA has likewise been discovered in other peripheral tissues such as liver, spinal cord, intestine, eyes, bladder, and stomach in fewer concentrations (15,16).

1.2.1 GABA synthesis and degradation

GABA is synthesized in presynaptic neurons from its precursor glutamate by the support of glutamic acid decarboxylase (GAD) together with its cofactor, pyridoxal phosphate (active form of vitamin B_6). The synthesized GABA is stored in vesicles with the help of a specific vesicular GABA transporter (VGAT). GABA is then released to the synaptic cleft to mediate its action via ionotropic $GABA_A$ receptor and the metabotropic $GABA_B$ receptor (10,11). To terminate GABAergic neurotransmission, GABA is removed from the synaptic cleft via GABA transporters (GATs) located at the cell surface of presynaptic neurons or surrounding glial cells. The GATs belong to a large family of neurotransmitter: sodium symporters also referred to as the solute carrier 6 (SLC6) in humans (17), and require extracellular Na^+ and Cl^- ions in order to operate. The GABA that has been taken back to the presynaptic neurons is taken up to the presynaptic storage vesicles and recycled, while the GABA that has been taken by glial cells is metabolized to glutamine by the GABA transaminase (GABA-T) (11). Glutamine is taken up by the GABAergic neurons where it is converted to glutamate and then to GABA (18). An illustration of a GABAergic synapse is shown in Fig. 4.

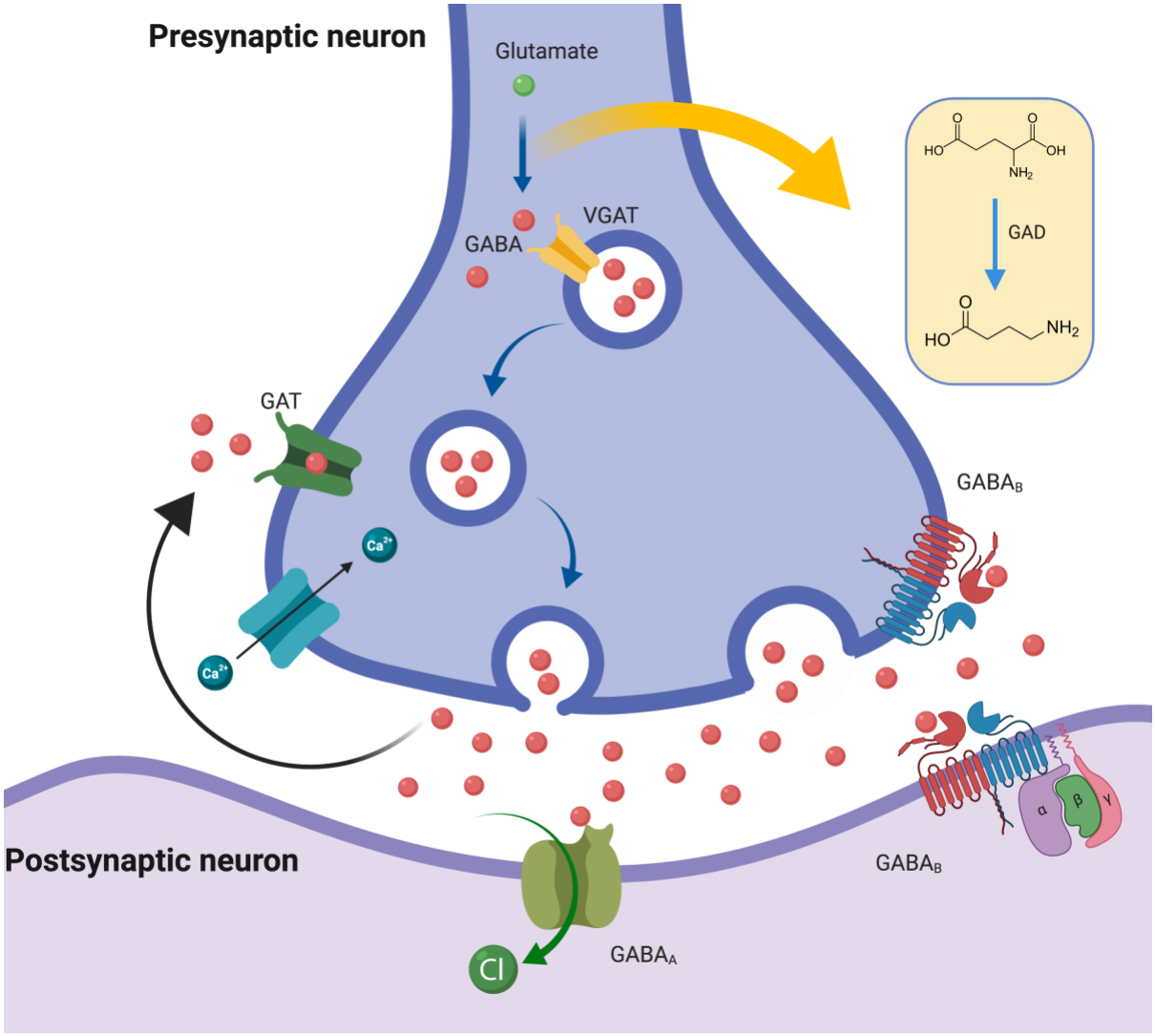

Figure 4 Aspects of the GABAergic synapse*: synthesis of GABA from glutamate, inserting into synaptic vesicles by VGAT; vesicular GABA transporter, the release of GABA, binding of GABA to the receptors, and reuptake of GABA by GAT; GABA transporter. GAD; glutamic acid decarboxylase.*

1.2.1.1 GABA$_A$ receptors

GABA$_A$ receptors are pentameric complexes consisting of multiple subunit types, but the major isoform is comprised of five subunits (α-β-α-β-γ) (Fig. 5). These subunits are organized in a circular shape around the channel pore, with a GABA binding site between the α and β subunits, giving a total of two potential GABA binding sites on each GABA$_A$ receptor. Ethanol also binds between the α and β subunits, but at a different location from GABA and allosterically modulate the action of GABA. There are even multiple versions of each subunit type, for example, there is six different α subunits, and each subtype is associated with a different function. On the other hand, there is only one bindings site for a drug group, known as benzodiazepines, between the γ and α subunit (10,11).

Ionotropic GABA$_C$ receptors are only comprised of rho subunits, unlike GABA$_A$, which consists of different types of subunits. They are so similar to GABA$_A$ that they are considered a sub-class of GABA$_A$ receptors, and the name was changed several years ago to the GABA$_A$-rho receptor. GABA$_A$ receptors are located postsynaptically, and its activation

results in the opening of the ion channel, which allows the Cl- ions entrance to the cell. The entry of Cl- ions hyperpolarize the cell membrane potential, which makes the action potential less likely to occur (Fig. 2). This again makes the cell less responsive to excitatory neurotransmitters (10,11).

Benzodiazepines and barbiturates are drug classes that positively modulate the $GABA_A$ receptors. They act as a positive allosteric modulator by increasing the influx of Cl- ions across the cell membrane. Like other positive allosteric modulators, they act when GABA is already bound to the receptor. The increased influx of chloride ions makes the action potential less likely to occur. They have beneficial effects such as sedatives (also known as tranquilizers), anticonvulsant, anxiolytic, and hypnotics (19).

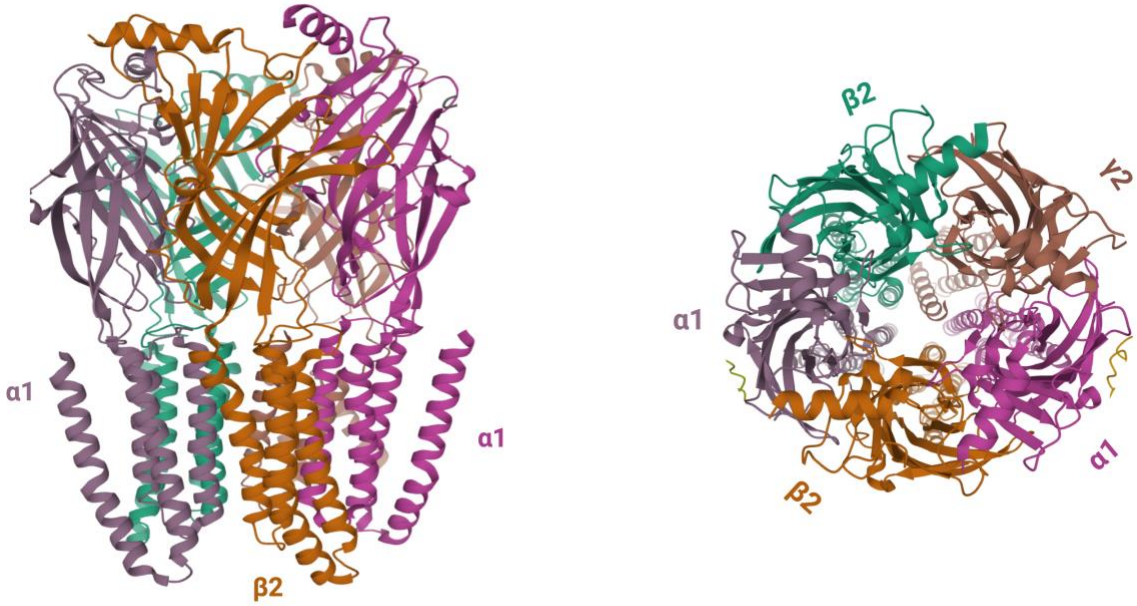

***Figure 5 Structure of the $GABA_A$ receptor (PDB: 6D6T)**. Left structure is the membrane view of the $GABA_A$ receptor, whereas the right structure is the view of the structure from the extracellular face. The figure shows the different subunits of the $GABA_A$ receptor labeled with different colors. The structure is generated using the PDB database.*

1.2.1.2 $GABA_B$ receptors

Bowery first identified the $GABA_B$ receptor in 1980 (20), and 17 years later was $GABA_B$ first cloned by Kaupmann (21). $GABA_B$ receptor is involved in critical neurological and psychiatric disorders, such as epilepsy, schizophrenia, anxiety, depression, autism spectrum disorder, stroke, drug addiction, and neurodegenerative disorders, including Parkinson's disease, Huntington's disease, and Alzheimer's disease (22). $GABA_B$ receptors have also been involved with muscle spasticity disorders, pain, and gastroesophageal reflux disease (GERD) (22,23).

$GABA_B$ receptors are G-protein coupled receptors (GPCRs) that mediate slow inhibitory neurotransmission in the CNS and is found on both presynaptic and postsynaptic neurons. Presynaptic $GABA_B$ receptors located at GABAergic synapses are autoinhibitory receptors

that upon activation inhibits the release of GABA upon activation. Presynaptic $GABA_B$ receptors at other systems than GABAergic function as hetero-receptors, which upon activation inhibits the release of other neurotransmitters, such as dopamine, acetylcholine, and 5-hydroxytryptamine (22). $GABA_B$ receptors are expressed in different regions of the brain. The brain regions possessing the most significant density of $GABA_B$ receptors are the hippocampus, thalamic nuclei, cerebellum, and cortex (10).

The heterodimeric G-proteins are located intracellularly and interact with the intracellular region of the GPCRs upon activation. The G protein contains three subunits: G_α, G_β, and G_γ. There are 21 G_α subunits, 6 G_β subunits, and 12 G_γ subunits in the human body (24). Based on the query sequence similarity between G_α subunits, G-proteins are classified into four principal classes: $G_{\alpha s}$, $G_{\alpha i}$, $G_{\alpha q}$, and $G_{\alpha 12}$ (25). The structures of the G_α subunit is composed of a GTPase domain (Ras-like domain), and a helical domain. The GTPase domain is preserved in all G-proteins, while the helical domain is different in each type of G_α protein. The first X-ray crystal structure of the G-protein- β_2 adrenergic receptor complex exposed a nucleotide-binding pocket located between these two domains (26). The G-protein β- and γ-subunits usually are fastened by coiled-coil motif interaction to form a functional assembly (25).

The G_α subunit harbors guanosine diphosphate (GDP) at the inactive resting state. Upon GPCR receptor activation, the 7TM region undergoes a conformational rearrangement. This process allows the 7TM domain to interact with the G_α subunit, by the insertion of the C-termini (known as α5-helix) of G_α subunit inside the pocket enclosed by the 7TM domain (27). This affects the establishment of the nucleotide-binding pocket leading to the dissociation of GDP from the G_α subunit. The G_α subunit undergoes an intermediate state that the binding pocket is nucleotide-free (28). Afterwards, guanosine triphosphate (GTP) replaces GDP and causes structural changes in the G_α-GTP, $G_{\beta\gamma}$, and the receptor. The GTP attachment drives a disengagement between G_α-GTP and $G_{\beta\gamma}$ subunits. The G_α-GTP and $G_{\beta\gamma}$ complexes then stimulate or inhibit specific effector proteins leading to cellular effects (25). The G-protein goes back to its resting inactive state with the help of the Ras-like domain of the G_α subunit. This domain hydrolyses a phosphate group from GTP and converts it to GDP, which provides a bindings site for the $G_{\beta\gamma}$ subunit (27).

The activation of the $GABA_B$ receptor (Fig. 6) causes the activation of the heterotrimeric G-protein (G_i/G_0), and consequently, the dissociation of $G_{\alpha i}$ from $G_{\beta\gamma}$. The $G_{\beta\gamma}$ complex inhibits neurotransmitter release from presynaptic terminals by the inhibition of voltage-gated calcium channels (VGCC). This results in a decrease in Ca^{2+} inside the synapse that drives the cell hyperpolarization, making the action potential less likely to occur. Moreover, the $G_{\beta\gamma}$ complex and the $G_{\alpha i}$ restricts vesicle fusion and hence neurotransmitter release (29).

$GABA_B$ can also mediate slow inhibitory postsynaptic current (IPSC) by the activation of the G protein-coupled inwardly-rectifying potassium channels (GIRKs) through the $G_{\beta\gamma}$ complex. This results in the efflux of K^+ and hence cell hyperpolarization, making the action potential less likely to occur (29). The activation of postsynaptic $GABA_B$ receptors can also reduce the level of cyclic adenosine monophosphate (cAMP), second messenger, by inhibiting adenylyl cyclase (30).

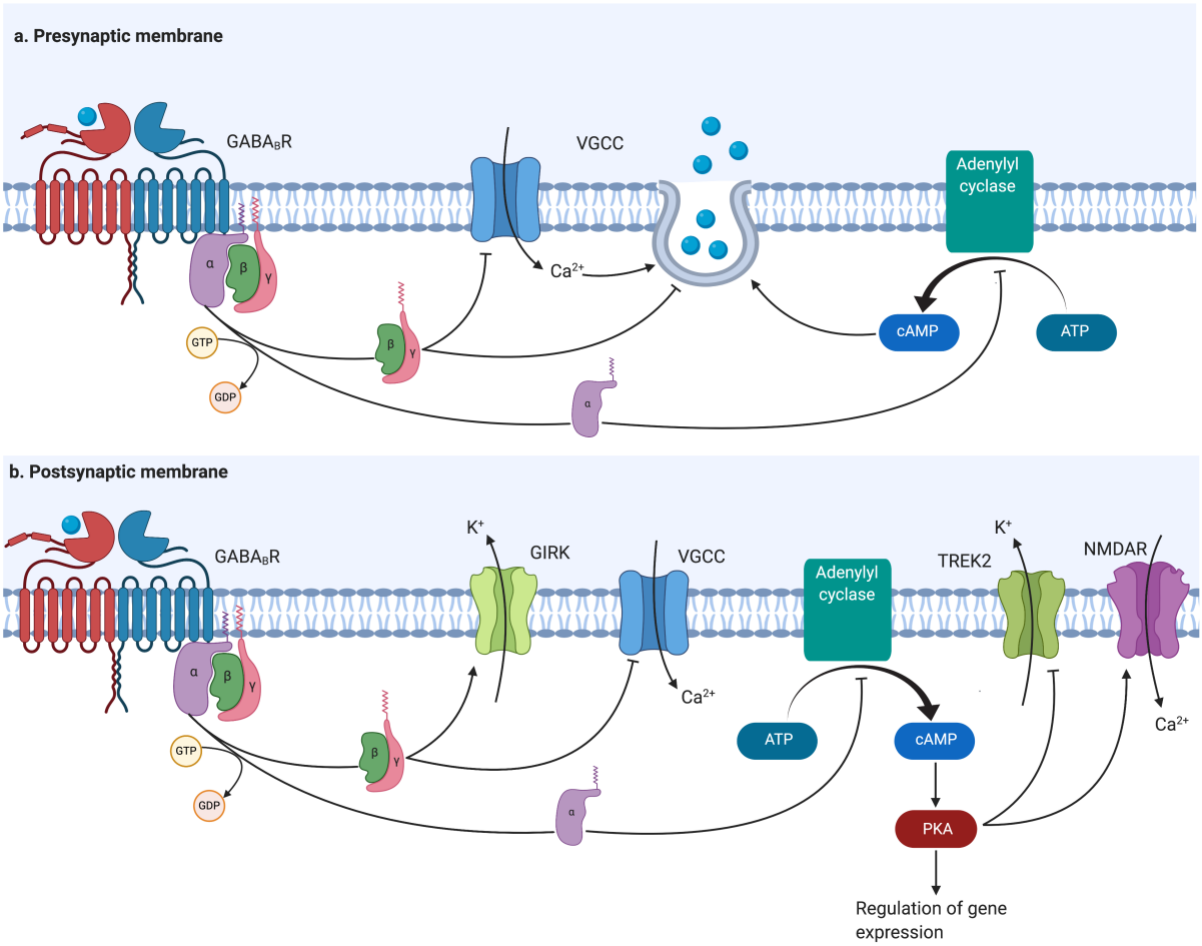

Figure 6 Schematic representation of GABA$_B$ receptor downstream effectors and their physiological roles. *a. In presynaptic compartments, GABA$_B$ receptor activates G$_{i/o}$ proteins that inhibit adenylyl cyclase from increasing the level of cyclic adenosine monophosphate (cAMP) in the cell. Downregulation of cAMP prevents vesicle fusion and neurotransmitter release. Released G$_{\beta\gamma}$ complex inhibits voltage-gated Ca^{2+} channels (VGCCs) and consequently inhibits neurotransmitter release. In addition, G$_{\beta\gamma}$ directly inhibits vesicle fusion, thereby limiting neurotransmitter release. b. In postsynaptic compartments, released G$_{\beta\gamma}$ opens G-protein activated inwardly rectifying potassium channels (GIRKs) and inhibits VGCCs, which inhibits neuronal excitability. Released G$_{\alpha i/o}$ proteins decrease the level of cAMP that reduces protein kinase A (PKA) activity, thereby reducing inhibition of TREK2 channels. Reduction of PKA activity inhibits the Ca $^{2+}$ permeability of NMDA-type glutamate receptors (NMDARs). GABA$_B$-mediated downregulation of PKA activity also influences gene expression. The figure is modified from (29).*

1.3 G-protein coupled receptors

The majority of drugs act on protein targets, which generally are divided into receptors, ion channels, enzymes, and transporters. G-protein coupled receptors (metabotropic receptors), ligand-gated ion channels (ionotropic receptors), kinase-linked receptors, and nuclear receptors are different types of receptors (3), and that is the absolute majority of drug targets (31). The human genome contains genes that encode for approximately 800 GPCRs (32), and as for 2017, approximately 700 (~35%) of FDA-approved drugs target one or more GPCRs. Currently, approx. 128 (~16%) of all GPCRs in human are targeted by a marketed drugs (33). During the same year, 320 potential drugs were in the clinical trials targeting GPCRs (34). This indicates that only a small fraction of GPCRs are currently targets for drugs in the market.

Various classification schemes have been used to categorize the GPCRs superfamily. The first classification system divided the GPCRs into six classes, from A to F (35). This A–F system is intended to cover all GPCRs, not only in human. Therefore, an alternative classification system categorized GPCRs, based on sequence similarity, into five main families: Glutamate family (class C), Rhodopsin family (class A), Adhesion family, Frizzled/Taste family (class F), and Secretin family (class B), referred to as GRAFS classification system (32,36). The extracellular messengers are various ligands, including neurotransmitters, hormones, proteins, peptides, ions, organic compounds, photons, and odors. Signals via GPCRs are crucial for many physiological processes, such as control of blood pressure, muscle contraction, allergic response, metabolism, secretion, nerve system regulation, immune response, vision, smell, and taste (37). Consequently, the malfunction of GPCRs results in many diseases, such as diabetes, obesity, cardiovascular disease, neurodegenerative disorders, inflammation, and even cancer (38), making these receptors drug targets for multiple diseases. Table 1 shows some of the GPCRs and their therapeutic targets.

Among the five GPCR families, the Rhodopsin family is the largest, and the most studied, consisting of about 670 protein receptors, including 388 olfactory receptors (37). Despite the fact that Rhodopsin family is the largest with the most discovered drugs, GPCRs belonging to other families, such as the Glutamate family (Class C), can also be targeted by drugs. Class C/Glutamate family of GPCRs is broadly expressed in the human body. They play an essential role in many physiological processes, such as taste sensation, calcium homeostasis, and the most vital modulation of neuronal excitability and inhibition throughout the CNS, mediated by GABA and glutamate. Moreover, they are drug-targets for a variety of psychiatric, neurological, and metabolic disorders such as Alzheimer's, schizophrenia, depression, anxiety, Parkinson's, among others (39,40).

The 800 human GPCRs are ubiquitously expressed throughout the body. Moreover, new GPCR research fields revealed that GPCR activation is translated to various signals. These signals are mediated not only via G-proteins but also through scaffolding proteins, such as β-arrestins and kinases, and that some allosteric and orthosteric ligands selectively activate or modulate distinct signaling pathways (41). GPCR kinases (GRKs) usually identify and phosphorylate activated GPCRs. GPCRs that are phosphorylated by GRKs can bind to β-arrestin, which prevents the stimulation of G-proteins. It is assumed that β-arrestins can also interact with some of the GPCRs directly by binding to the 7TM domain of the GPCR (42). The examination of the β-arrestin-signaling pathway led to the identification of so-called biased activation. Biased agonists mediate this kind of activation that selectively stimulates either the G-protein pathway or the β-arrestin pathway (42). Carvedilol, a drug used to treat heart failure, is a β-arrestin-biased agonist for β_2-adrenoreceptors. It stimulates the cell survival mediated by β-arrestin and represses the unwanted toxic effect mediated by G-protein (43). This indicates that a clear illustration of the activation mechanism of GPCRs would promote the discovery of more selective and effective drugs. However, it is still unknow whether $GABA_B$ receptor activation stimulate β-arrestin pathway or not.

The common characteristic feature of all the GPCRs is the seven transmembrane (7TM) domain (44). Accordingly, the term "7TM receptor" is regularly used correspondently with "GPCR". GPCRs share a common method of signaling by passing signals from a variety of extracellular messengers to modulate intracellular pathways through the activation of G-proteins and other signaling molecules. The GPCRs undergo different conformational changes, ranging between several active and several inactive conformations (44). Agonist

binding to the orthosteric binding site induces the active conformational states of the receptor. In contrast, antagonists or inverse agonists stabilize the inactive conformational states. During activation, the 7TM domain of the receptor shifts its conformation in order to interact with G-proteins or other intracellular effectors (22). Receptors can show some level of activation, even when no ligand is bound, called constitutive activation. Some ligands can reduce the level of constitutive activation, known as inverse agonists. Therefore, an inverse agonist can be considered as drugs with negative efficacy, while agonists been drugs with positive efficacy and antagonists with zero efficacy (3).

Table 1 shows some of GPCRs with their endogenous ligands, GPCR class, drugs in the marked for the corresponding GPCR and their indication. *(45,46).*

Endogenous agonist(s)	**Receptor**	**GPCR class**	**Drug (mode of action)**	**Indication**
Serotonin (5-HT)	5-Hydroxytryptamine receptors	Class A (Rhodopsin)	Eletriptan (agonist)	Anti-migraine
Melatonin	Melatonin receptors	Class A (Rhodopsin)	Melatonin (agonist)	Hypnotics and sedatives
Acetylcholine	Muscarinic receptors	Class A (Rhodopsin)	Atropine (antagonist)	Bradycardia
Dynorphins, enkephalins, endorphins, endomorphins, and nociceptin	Opioid receptors	Class A (Rhodopsin)	Fentanyl and morphine (agonists)	Analgesics
Adrenaline and Noradrenaline	β_2 adrenergic receptors	Class A (Rhodopsin)	Propranolol (antagonist)	Antihypertensive
Parathyroid hormone	Parathyroid hormone receptors	Class B	Teriparatide (agonist)	Osteoporosis
Glucagon and glucagon-like peptide-1	Glucagon receptor family	Class B	Dulaglutide (agonist)	Antidiabetic
GABA	$GABA_B$ receptors	Class C (glutamate)	Baclofen (agonist)	Anti-spastic
Glutamate	Metabotropic glutamate receptors	Class C (glutamate)	Acamprosate (antagonist)	Antineoplastic; halt development of tumor
Calcium	Calcium-sensing receptors	Class C (glutamate)	Cinacalcet (PAM)	Hyperparathyroidism
Patched	Smoothened receptors	Class F (Frizzled)	Itraconazole (antagonist)	Antineoplastic

1.3.1 Structure determination of GPCRs

Until recently, structure-based drug development has been impeded by the absence of three-dimensional (3D) structure information about GPCRs and how compounds interact with these receptors. X-ray crystallography is one of the most used experimental techniques in determining the atomic and molecular structure of GPCRs. However, the traditional x-ray crystallography requires a large amount of purified GPCR samples in order to form an appropriate crystal.

The predominant obstacle in determining GPCR structures and other membrane proteins that are unstable and lose their highly organized structure once extracted from the cell membrane (47). GPCRs are also conformationally unstable due to the amphipathic nature of their

surface. They have a hydrophobic surface area in contact with membrane phospholipids and polar surface area in contact with an aqueous phase on both sides of the membrane (48). Furthermore, the majority of GPCRs are present on the cell surface in native tissues at very low concentrations making over-expression a prerequisite.

During the last two decades, the structural determination of GPCRs has experienced significant progress through the technology improvement of expression, purification, and stabilization. Detergents are usually used to extract GPCRs from the cell membrane and to maintain their structural and functional properties in solutions (49). Detergents have also been used in combination with lipids and cholesterols since they play an important role in maintaining the normal function of GPCRs (50). Many expression strategies have been developed to increase the low abundance of GPCRs at the cell surface. For instance, glycosylation, fatty acylation, and phosphorylation are some of the methods used to modify the protein fold and thus express them (51). Ligands are often added to GPCRs to maintain the receptor in one specific conformation state because GPCRs can have multiple conformation rearrangements (52). Another widely used strategy to improve protein expression and stability is the mutagenesis of GPCRs (53). Unfortunately, despite all these improvements in GPCR expression, purification, and stabilization, the traditional x-ray crystallography method continues to be challenging. However, more helpful approaches have been developed and nowadays are essential tools for GPCR crystallization. For example, the Lipid cubic phase (LCP) provides a highly organized crystal by mimicking the membrane environment for GPCRs (54).

Apart from x-ray crystallography, Cryo-EM is another attractive approach used to determine the structure of macromolecules that are unachievable by other approaches. Electron cryo-microscopy (cryo-EM) has revolutionized the structure determination of GPCRs and have a significant impact on structure-based drug discovery (55,56) (Garcia2020)(Garcia2019). Compared to X-ray crystallography, cryo-EM does not require crystals and allows the proteins to be observed in various conformations in solution (57). Cryo-EM is an imaging technique that makes it possible to view large protein molecules with atomic precision. Cryo-EM gets around most of the problems associated with X-ray crystallography without affecting the resolution. It uses an electron beam, rather than light, to obtain samples with an increased atomic resolution. Electrons microscopy (EM) work in a vacuum and hit molecules with electrons, which can destroy the sample. In 1982, cryo-cooling techniques were introduced, where a thin layer of verified water protects molecules from the two problems mentioned above (58). Nevertheless, other obstacles remained, such as image processing power, including low contrast and a large amount of noise. The development of algorithms that enabled computers to average a collection of noisy micrographs into one sharp image. In the last decades, computers get way better in using techniques in addition to the advances of electron detector technologies, which led to the high-resolution of cryo-EM structures (58).

1.3.2 X-ray and cryo-EM structures of class C GPCRs

Class C GPCRs cover the metabotropic glutamate receptors (mGlu1 to mGlu8), γ-aminobutyric acid receptor B ($GABA_B$), taste 1 receptors (TAS1), the calcium-sensing receptor (CaSR), pheromone (V2) receptors (absent in human), and few orphan receptors (59). Class C of GPCRs, unlike class A GPCRs, have a large N-terminal extracellular domain (ECD). The ECD is connected to the 7TM domain by cysteine-rich domain CRD (except for $GABA_B$ receptors) (21). Class C GPCRs are obligate dimers, either homodimers (e.g.,

mGlus, CaSR) or heterodimers (e.g., GABAB, TAS1). The VFTs within the ECDs of the homodimeric receptors, mGlu and CaSR, are crosslinked via a covalent disulfide bond. In contrast, heterodimeric receptors, GABAB, and TAS1 are not covalently linked. A large ECD, containing the Venus flytrap domain (VFT), distinguishes class C GPCRs and contains the orthosteric binding site. This orthosteric binding site is located within the bi-lobed N-terminal domain forming a cleft. These two lobes are flexible and fold around the orthosteric agonists, merely similar to a Venus flytrap plant. The class C GPCRs agonists, stabilize the "closed" VFT conformations, while antagonists maintain the "open" VFT conformations. Within the 7TM domain, another binding site is located referred to as the allosteric binding site (60). Interestingly, the crystal structures of the mGlu1(61) and mGlu5 (61–63) 7TM domains show that the allosteric ligand-binding pockets overlap with those of orthosteric ligands in family A GPCRs (64).

Currently, the only available structures of the 7TM domain are the X-ray and cryo-EM structures of mGlu1 and mGlu5, including the inactive and active full-length structures of mGlu5 (61–63,65,66). In addition, two pre-print papers describing the full-length GABAB receptor cryo-EM structure were released in April 2020 (structures not released yet) (67,68). There are, however, also x-ray crystal structures available of the extracellular domains of GABAB and mGlu receptors which show that the VFT is in a closed conformation when bound to an agonist but in an open conformation in presence of antagonists or without ligands (60,69–72). As the only structures of the 7TM domain are those of mGlu1 and mGlu5, these receptors are important tools for studying other class C members as well. The first X-ray crystal structure of the 7TM domains of both mGlu1 (61) and mGlu5 were released in 2014 (62,63,65). The X-ray crystal structures show that this region is arranged similarly to that of other GPCRs but with a more compressed shape. The conformational rearrangement of the 7TM domain is responsible for the activation of G-proteins and other effector proteins. Interestingly, a salt bridge was observed in the inactive conformation of the 7TM, referred to as "ionic lock". It involves an interaction between glutamate (TM6) and lysine (TM3) residues, which stabilize the inactive (closed) conformation at the intracellular side (61,65). In addition to the "ionic lock", a hydrogen bond between ICL1 and ICL3 was observed that further stabilize the closed conformation (61). These interactions prevent G-proteins coupling.

In 2019, the full-length cryo-EM structures of the mGlu5 receptor in an active and inactive state were released (Fig. 7) (66). The structures revealed that the only contact between the mGlu5 protomers was in the VFT in the inactive receptor, while receptor activation resulted in a major conformational change and compaction of the dimer subunits with formation of contacts between the VFT, CRD and 7TM domains. The conformational rearrangement is then transmitted to the 7TM domains through CRDs, which enables the closure and reorientation of the 7TM domains. This structural change leads to a TM6-TM6 interface that is critical for receptor activation (66). However, although the overall mGlu5 was in an activate state, the 7TM domain was inactive with a closed intracellular G protein binding site probably because a G-protein is required to obtain a fully active 7TM domain. We therefore still do not have the structure of an active class C 7TM domain able to interact with the G protein.

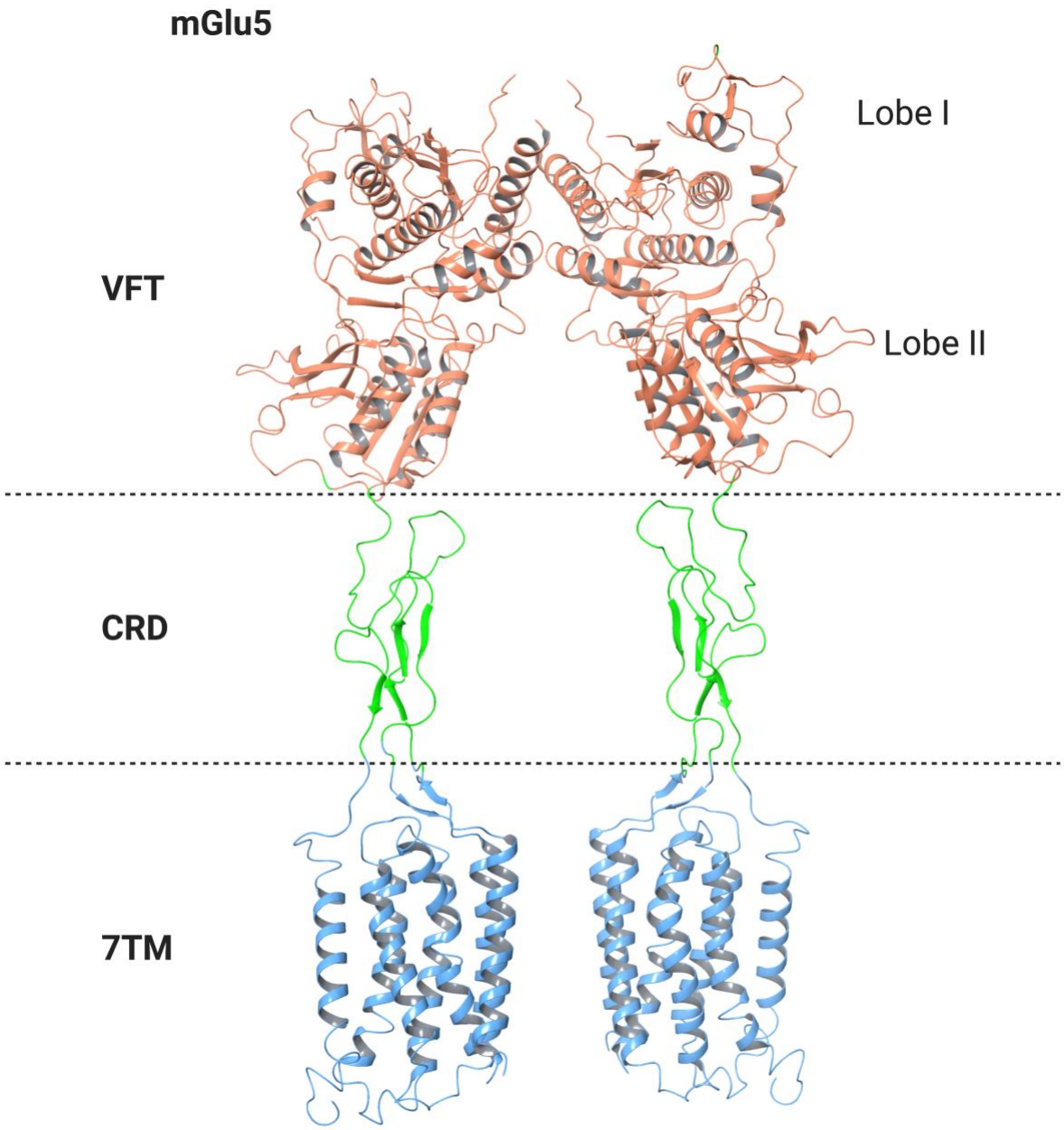

Figure 7 Cryo-EM structure of the homodimer mGlu5 receptor; metabotropic glutamate 5 receptor (PDB: 6N52). *The structural model exhibits a dimeric VFT domains; Venus flytrap domains (orange), linked to the 7TM domains; seven transmembrane domains (blue), via CRDs; cysteine rich domains (green). This structure was created using Schrödinger maestro software.*

Unlike the mGlu receptors, the $GABA_B$ receptor is an obligatory heterodimer comprised of two subunits: $GABA_{B1}$ and $GABA_{B2}$, which together form the functional unit (Fig. 8). The Venus flytrap in $GABA_{B1}$ constitutes the orthosteric binding site, whereas the helical transmembrane domain of $GABA_{B2}$ contains the allosteric binding pocket (69,70). The $GABA_{B1}$ subunit can exist in two isoforms: $GABA_{B1a}$ and $GABA_{B1b}$. The $GABA_{B1a}$ differs from $GABA_{B1b}$ by additionally possessing two sushi domains (SDs) (21). Recently, one research paper announced that these SDs are sites for a protein-protein interface (73). Numerous recognized proteins associate with these domains, but their function related to $GABA_B$ is not clear yet (73). However, it was suggested earlier that they are involved in anchoring $GABA_{B1a}$ to presynaptic terminals (74).

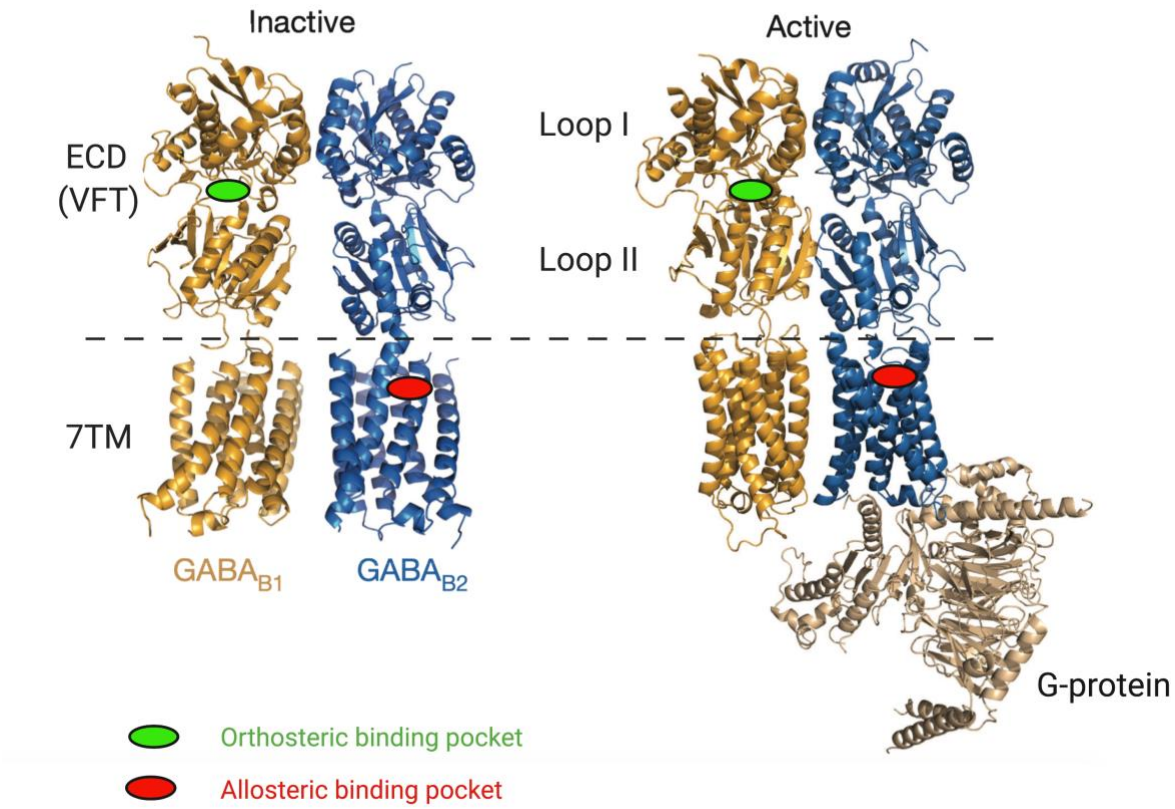

***Figure 8 Structural representation of the heterodimer GABA$_B$ receptor in the inactive and active states**. The GABA$_{B1}$ and GABA$_{B2}$ subunits are represented in yellow and blue, respectively. The VFT domains; Venus flytrap domains, are shortly linked to the 7TM domains; seven transmembrane domains, without the CRDs; cysteine rich domains observed with mGlu; metabotropic glutamate receptors. The VFT domains of the GABA$_B$ receptor are not covalently linked, as seen with mGlu. The active conformation is joined with the G-protein via GABA$_{B2}$. Figure adopted from (75).*

The VFT of GABA$_{B1}$ subunit encompasses the orthosteric binding site, whereas the VFT of GABA$_{B2}$ does not bind ligands (76). In 2012, the crystal structure of the unliganded Venus flytrap domain of the human GABA$_{B2}$ receptor was published (70). The following year, the crystal structure of the VFT dimer of GABA$_B$ in the absence of ligands and in the presence of agonists and antagonists was published (69). Our colleague investigated the receptor dynamics of GABA$_{B1b}$ VFT using metadynamics, and suggested that open/inactive and closed/active states are the main conformations adopted by the receptor, and that ligand binding is required in order to adopt the close conformation (77).

The VFT domains of GABA$_B$ are directly connected to the 7TM domains without the CRD found in other class C GPCR receptors (21). Instead, a short linker, 10-15 residues, is replacing the CRD in GABA$_B$ receptor (22). No crystal structure of the 7TM domain has been resolved so far; accordingly, limited fundamental data are available regarding the 7TM structure. However, diverse homology models were obtained thanks to the crystal structures of mGlu1 (61) and mGlu5 (62,63,65). Very recently, a publication yet to peer-reviewed introduced a full-length cryo-EM GABA$_B$ receptor structure, revealing an essential function of the ECL2 in transferring structural changes from the ECD to the 7TM domain (67,68). Also, it shows that the ECL2 of both GABA$_B$ subunits interacts with the membrane occupying the extracellular part of the 7TM, thereby providing a link between ligand binding and the receptor core that engages G protein (67). An identical TM3-TM6 "ionic lock"

observed with mGlu1 and mGlu5, is present in $GABA_B$ 7TM models stabilizing the inactive conformation of $GABA_{B2}$ 7TM domain. In contrast, the "ionic lock" is absent in $GABA_{B1}$ 7TM domain in accordance with its incapability to activate G-protein (78).

Even though the $GABA_{B1}$ subunit contains the orthosteric binding site within its VFT domain, it is incapable of activating G-proteins alone. The 7TM of $GABA_{B2}$ is responsible for binding and activation of G-proteins (Fig. 7) (79). This feature illustrates the necessity of receptor dimerization of $GABA_{B1}$ and $GABA_{B2}$. Additionally, $GABA_{B2}$ possesses an allosteric binding site within its 7TM domain, but the exact residues involved in binding allosteric modulators have not been identified conclusively (80). However, several residues were recognized to be important in binding to allosteric modulators by the use of homology modeling (81). These homology models (81) were used in virtual screening protocols, which managed to identify several hit compounds as potential allosteric modulators (unpublished results).

The C-terminal domains of $GABA_{B1}$ and $GABA_{B2}$ (about 30 residues each) are intertwined, creating a coiled-coil domain that stabilizes the heterodimeric interaction. This domain is a site for protein-protein interaction that is essential for the heterodimerization of $GABA_B$ subunits. Additionally, it is important for the migration of $GABA_B$ receptors to the cell surface (22). $GABA_B$ subunits are synthesized in the endoplasmatic reticulum (ER) and can move within the ER from the soma to axons and dendrites. $GABA_{B1}$ has an ER retention motif (RSRR) anchored to its C-terminal, preventing it from leaving the ER. The assembly of $GABA_{B1}$ and $GABA_{B2}$ coiled-coil domain inactivates the ER retention signal allowing the heterodimers to exit the ER (22). This mechanism assures that only completely functional heterodimeric $GABA_B$ receptors reach the plasma membrane. A transmembrane protein (PRAF2, prenylated Rab acceptor family), located in the ER, interacts with the $GABA_{B1}$ subunit and compete with $GABA_{B2}$ to associate with $GABA_{B1}$. Therefore, the amount of $GABA_{B2}$ compared to PRAF2 determine the number of heterodimeric $GABA_B$ expressed on the cell surface (82).

The $GABA_B$ receptors can also exist as large complexes, by protein-protein interactions (83). It can be joined with diverse proteins to obtain optimal signal transduction. It can form oligomers through interaction between $GABA_{B1}$ subunits (84). Also, a K^+ channel tetramerization domain (KCTD) proteins have been recognized. They serve as a supporting subunit by stabilizing $GABA_B$-G-protein interaction by getting attached to both the $G_{\beta\gamma}$ subunit and the C-terminal of $GABA_{B2}$ (85). There are four isoforms of KCTD (KCTD 8, 12, 12b, 16), and each can provide distinct properties. For example, KCTD 12 isoform decreases $GABA_B$ internalization, hence increasing the number of $GABA_B$ on the cell surface (86). Other proteins than KCTD have been identified to form core complex with $GABA_B$ (73), and therefore examining such proteins can explain the functional diverseness observed with $GABA_B$.

1.3.3 Development of $GABA_B$ allosteric modulators

As previously mentioned, GABA (Fig. 10, a) is produced by decarboxylation of glutamate. This process occurs in the CNS because GABA is incapable of penetrating the BBB due to its high hydrophilicity (logP= -3,17) (23). GABA also works on different type of receptors; therefore, GABA itself cannot be applied as a drug. In 1962, baclofen (Fig. 10, b) was synthesized in attempt to find lipophilic analogous of GABA. In 1972 Baclofen was

marketed as Lioresal@, and so far, it is the only FDA-approved orthosteric agonist that are available in the market for the $GABA_B$ receptor (23). It is used to treat muscle spasticity and rigidity associated with spinal cord injuries and multiple sclerosis, overactive bladder, gastroesophageal reflux diseases, addiction disorders, and anxiety (22). Spasticity occurs in approx. 50% of patients harmed by these disorders. Intrathecal baclofen is also used in patients with spasticity that do not get enough response from the maximum oral dose of baclofen (87). However, baclofen has pharmacokinetic limitations such as rapid clearance, short half-life (3-4 hours), narrow therapeutic window, rapid tolerance, and poor penetration to the brain. It is usually administered in high doses, owing to all these limitations. Therefore, the clinical use of baclofen is limited due to numerous side effects, including sedation, dizziness, nausea, muscle weakness, and mental confusion (22). However, there are many drugs under the development phase that target the $GABA_B$ receptor, including agonists for the treatment of gastroesophageal reflux disease, positive allosteric modulators (PAMs) that shows anxiolytic activity, and antagonists that shows memory and attention improvement (23). Few novel allosteric modulators of $GABA_B$ are known compared to $GABA_A$ receptors.

The majority of the drugs in the market target the same domain of the receptor that recognizes the natural ligand at the orthosteric binding site (33). These binding sites are usually highly conserved, making it challenging to obtain better drug selectivity for a specific receptor target (88). The discovery of allosteric modulators helped to overcome such challenges. Allosteric modulators do not bind to the orthosteric binding sites, but rather bind to a topological different site called the allosteric binding sites. Various endogenous allosteric modulators such as proteins, lipids, sterols, and ions can affect such binding sites (22).

Allosteric modulators can display multiple pharmacological characteristics (Fig. 9). They can modulate the affinity of the orthosteric ligands by causing a conformational change in the orthosteric binding pocket or by stabilizing the structure. This will result in a change of the association or dissociation rate of the orthosteric ligand. They can also modulate the efficacy of the orthosteric ligand by changing the signal capacity of the orthosteric ligand and thereby either facilitates or inhibits receptor coupling to downstream receptors. Interestingly, some allosteric modulators can activate the receptor without the necessity of an agonist, referred to as positive agonist modulators (agoPAMs) (88). Allosteric modulators that potentiate the response of orthosteric agonists are referred to as “positive allosteric modulators” or PAMs. In contrast, allosteric modulators that decrease the activity of orthosteric agonists are known as “negative allosteric modulators” or NAMs. Furthermore, another type of allosteric modulators has been recognized, referred to as “silent allosteric modulators” or SAMs (89). These ligands bind to the allosteric binding site, without mediating any effect. However, depends on their structural properties they may compete to displace PAMs or NAMs (40).

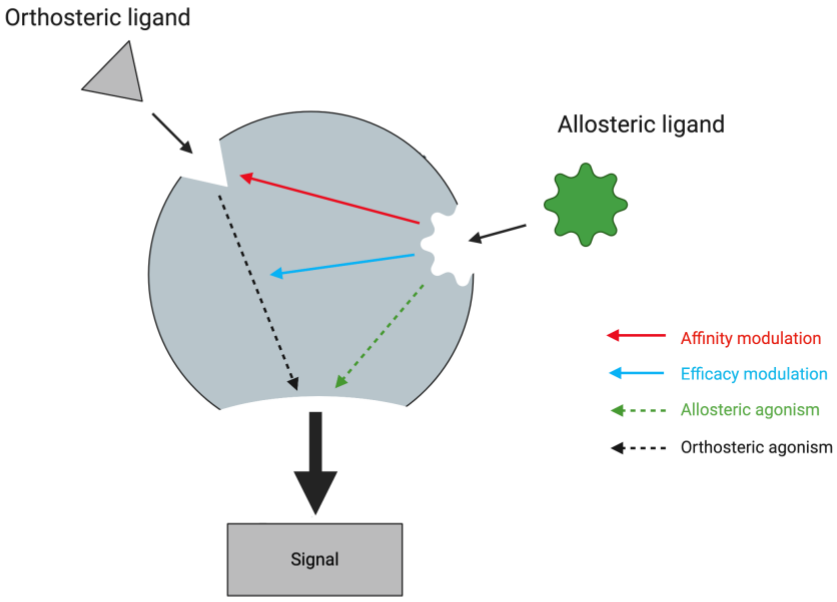

Figure 9 Mode of action of allosteric modulators. The figure is adopted from (88).

Allosteric ligands have several advantages over orthosteric ligands as therapeutic molecules (88). The allosteric binding sites are less conserved than the orthosteric binding sites. This feature provides allosteric ligands an excellent potential for selectivity. The effect of some drugs slowly decreases when the drug is taken repeatedly over a long-time duration. Desensitization and tolerance are the terms used to describe this phenomenon. Desensitization occurs within a few minutes, whereas tolerance takes hours, days, or weeks to develop (3). Allosteric modulators are not expected to result in receptor desensitization or tolerance compared to traditional orthosteric ligands. Therefore, they can be used in a prolonged term without developing tolerance (90). The allosteric modulators (except for allosteric agonists) apply their effects only when the orthosteric agonist is present. This cooperativity provides a fine-tuning of the physiological signal rather than turning the signal on or off by themselves. This characteristic increase safety in case of a drug overdose (40). Furthermore, a lower dose of allosteric ligands is required to obtain the desired pharmacological effect because of their non-competitive action mechanism (22).

Recently, synthetic allosteric modulators have been identified for many GPCRs, as promising drug candidates. In 2001, the first PAM of $GABA_B$, di-tert-butylbenzenes (Fig. 10, c), also referred to as CGP7930, was discovered (91). This PAM could enhance an agonist mediated $GABA_B$ receptor response, and a few years later, it was shown that CGP7930 indeed binds to the allosteric binding site but could cause a receptor activation even in the absence of an orthosteric ligand. (92). In 2003, a more potent PAM was discovered referred to as N,N-Dicyclopentyl-2-methylsulfanyl-5-nitropyrimidine-4,6-diamine (GS39783) (93). The lead structures, CGP7930 and GS39783, was then optimized to develop allosteric modulators such as NVP-BHF177 (94) and rac-BHFF (95). All four PAM compounds have shown activity to

relive anxiety (23). Currently, there are more than 72 known allosteric modulators that act as PAMs on the $GABA_B$ receptor (81).

In 2014, the first NAM (Fig. 10, d) of $GABA_B$, (CLH304a), was discovered in an analysis to find more potent analogs of CGP7930 (80). Unfortunately, CLH304a has limitations in pharmaceutical and pharmacokinetic progress. It possesses a phenol group and an electrophilic unsaturated ketone that may cause a toxicological effect (22). Therefore, safer and more potent NAM analogs are required. Two years after the identification of CLH304a, the bindings site for CLH304a was suggested to be in the 7TM domain of $GABA_{B2}$ (96). The same research group demonstrated that modification of CLH304a resulted in two analogs, CLH391 and CLH393, that showed the same inhibitory effect as CLH304a (96). $GABA_B$ antagonists have shown to have many beneficial effects in animal studies, mainly in depression, cognitive deficiencies, Down's syndrome, and absence epilepsy (23). Therefore, NAMs of the $GABA_B$ are expected to produce similar effects with fewer side effects. Our colleagues have earlier identified potential negative allosteric modulators by virtual screening using homology models of $GABA_{B2}$ 7TM domain (unpublished results).

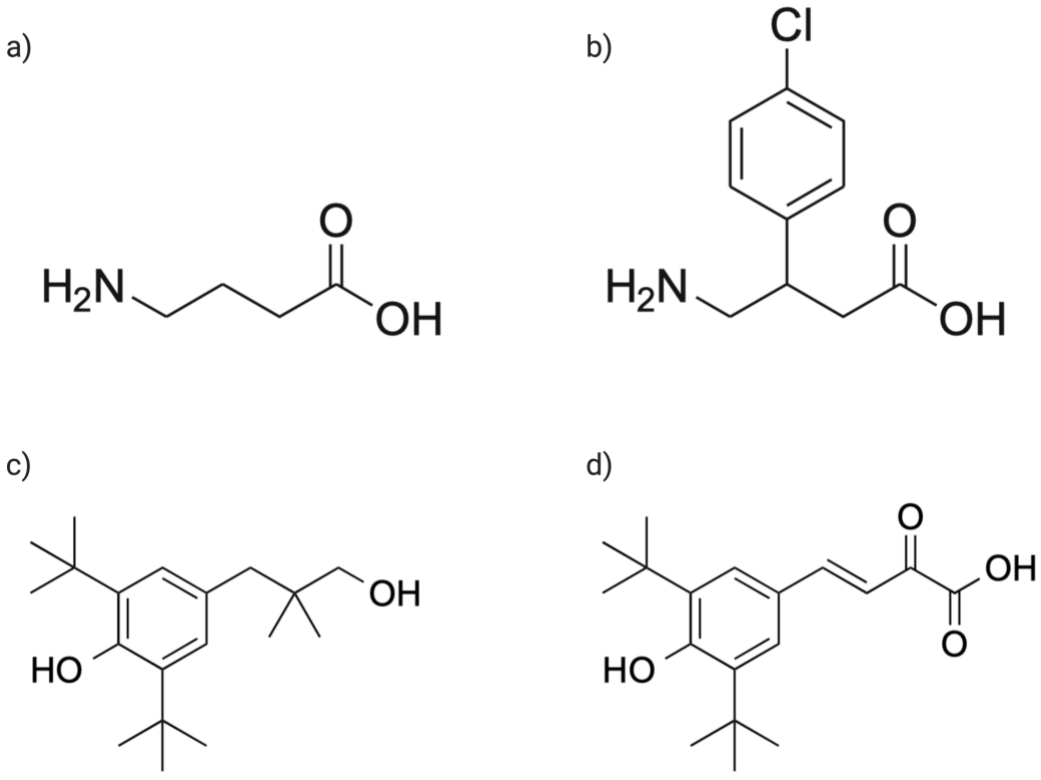

Figure 10 Structures of a) GABA (natural agonist), b) Baclofen (agonist), c) CGP7930 (PAM), d) CLH304a (NAM)

1.4 Computer-based methods in structural biology and drug discovery

The first performance in the scientific method is to create a logical assumption. If it is compatible with known data, a theory or model is then generated. The model is a conceptional idea and can be demonstrated in mathematical equations to facilitate calculations and prediction. The utilization of computers to solve equations of a model is usually referred to as computational chemistry (97). The terms computational chemistry and molecular modeling are used interchangeably. In recent years, the use of molecular modeling has increased due to the development of easily operated computer software, and today, computer-aided drug discovery or design (CADD) is an important part of many drug development projects, both in academia and by the industry (98). There are two major categories of CADD, the ligand-based drug discovery (LBDD), and the structure-based drug discovery (SBDD). The ligand-based approaches only depend on the information of ligands of interest. In contract, the structure-based approaches require a three-dimensional knowledge of target structure and ligand structure to put in practice (99).

1.4.1 Molecular modeling

Molecular modeling is a collection of different computational methods to study molecular structures and relate them to biological activity. For example, it is applied to model a molecular system of a specific molecule before synthesizing it in the laboratory (97). Molecular modeling helps to study molecular geometry, calculate energies of molecules conformation, create an energy minimum by modifying the structure, derive molecular properties, among others (100). Some molecular properties are more easily obtained computationally than by experimental analyses, and some molecular features can only be determined computationally. Also, molecular modeling provides insight into processes and mechanisms that might be impracticable or too costly to investigate by traditional experimental methods (97). However, molecular models do not replace experimental techniques, but they are frequently proper enough to rule out many compounds that are not suitable for their expected use (101).

The first step in a molecular modeling study is to generate a model of the molecule in the computer by defining relative positions of the atoms in space using a set of Cartesian coordinates. The 3D-structure of the molecules of interest can be an experimentally determined structure obtained by for instance X-ray crystallography or cryo-EM. However, determining the 3D-structure of proteins may be difficult, especially for the membrane proteins. Fortunately, the 3D-structures can also be predicted by homology modeling based on the homology with proteins of a known three-dimensional structure (100).

1.4.1.1 Molecular mechanics (MM)

Molecular mechanics (MM) and quantum mechanics (QM) are the two main approaches applied in molecular modeling to calculate molecular geometries and energies. The quantum mechanical methods are subdivided into two categories: ab initio and semi-empirical (100). These methods estimate the energy and wavefunction of a molecule by solving the Schrödinger equation. The wavefunction enables the calculation of electron distribution, which makes it possible to derive properties such as electrophilic attacks (break and form bonds) (101).

Molecular mechanics use the Born-Oppenheimer approximation, which assumes that nuclei in an atom are more massive and hence very slow, almost stationary, compared to the electrons (101). Therefore, molecular mechanics apply the laws of classical physics only to the nuclear position and ignore the motion of electrons (100). In molecular mechanics, a molecule is represented as a collection of particles that interact with each other via harmonic forces where atoms are represented as balls of various sizes (atom types) held together by springs with varying lengths (the bonds) (102). The molecular mechanics method is broadly applied to generate reasonable structure geometries before different calculations (101).

1.4.1.1.1 Force fields

Molecules are not rigid but at permanent motion, because all atoms in a molecule, at room temperature, have sufficient motional energy to move. Each molecule can exist in different conformers or rotamers with different energy levels, and when a molecule structure changes, the energy of the molecule also changes. Therefore, the change from one geometry of a molecule to another will correspond to change in the potential energy (102). Commonly, all living molecules try to reach a structural configuration with the lowest possible potential energy. Therefore, only conformations with low energy are found in nature. The most stable molecular system is usually defined as the system with the lowest potential energy. Therefore, all computational chemistry techniques try to find the shape of a molecule with the lowest energy (97).

In molecular mechanics, the mathematical representation of the system (the potential energy function) and the force parameters (the force constants) are known as the force field. Force fields can be written as the following equation:

$$E_{tot} = E_{bonded} + E_{non\text{-}bonded}; \text{ or}$$
$$= (E_{bond} + E_{angle} + E_{dihedral}) + (E_{vdr} + E_{elec}) \qquad \text{Eq. (6)}$$

The E_{tot} is the total potential energy, and the E_{bonded} and $E_{nonbonded}$ is the covalent and non-covalent bonding energy terms, respectively. The E_{bonded} can be divided into the bond stretching energy (E_{bond}), angle bending energy (E_{angle}), and energy for rotation around a bond (E dihedral). The $E_{non\text{-}bonded}$ can likewise be divided into van der Waals interaction energy (E_{vdw}) and electrostatic interaction energy (E_{elec}). All molecular modeling software programs utilize force fields to obtain molecular mechanics predictions. The reliability of the force field calculation is reliant on the included potential energy function and the quality of force constants. Some force fields are more suitable for small molecules, while others are primarily for proteins and biomolecules (102).

1.4.1.2 Homology modeling

Generally, proteins that have developed from a mutual ancestor are considered homologous. The homology modeling approach takes advantage of the observation that even if the sequence similarity of homologous proteins can vary, due to mutations, their overall 3D-structure similarity is more preserved (103). Homology modeling is applied to construct a theoretical 3D-model of proteins with unknown structures (i.e., the target) by using the experimentally determined 3D-structure of homologous proteins (i.e., the template).

Homology modeling is acknowledged to be the most reliable available computational method for studying drug targets with unknown structure and are extensively used in drug discovery (104).

Homology modeling generally covers the following steps which can be repeated until a proper model is obtained: (i) template selection; (ii) target–template sequence alignment; (iii) 3D model structure building; (iv) model refinement; and (v) model quality evaluation (104). These steps are shown in Fig. 11.

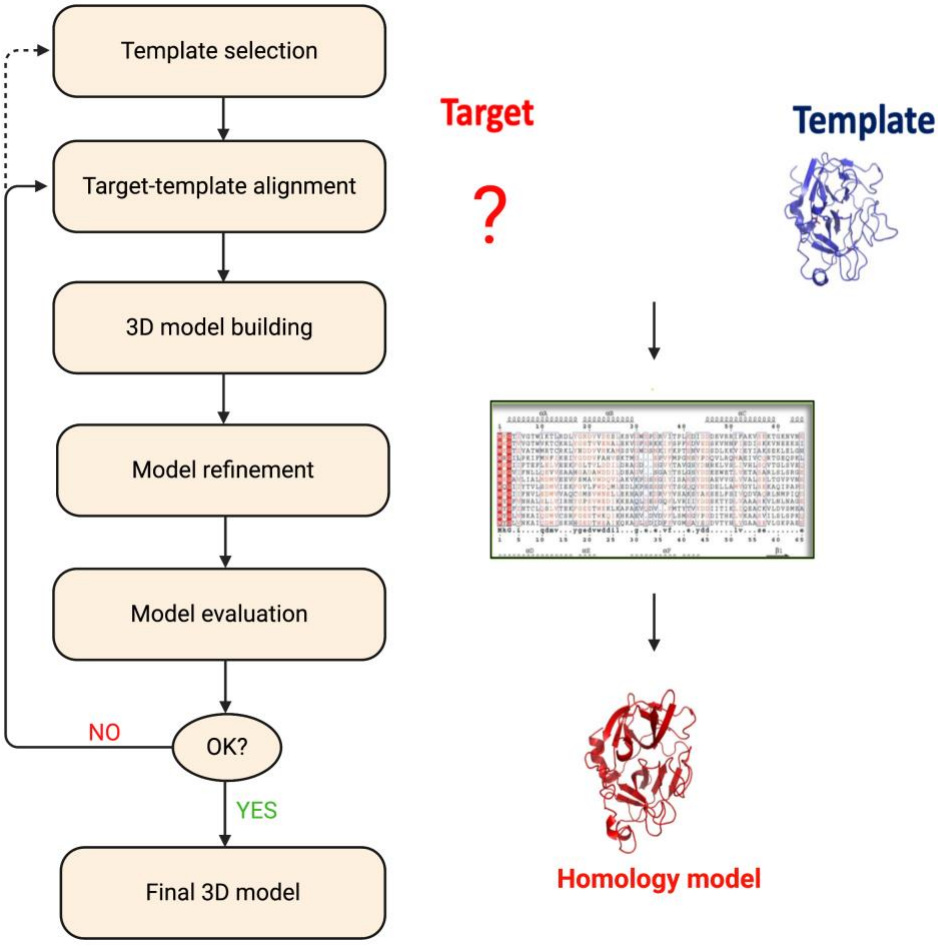

Figure 11 The main steps in homology modeling.

Template selection

The first step in homology modeling is the selection of an appropriate template structure. In many cases, there are few template structures available, and the researcher working in the field would know which structures to retrieve from the PDB database. In other projects, a BLAST search of the PDB databank using the target sequence as query would be performed to identify the most appropriate template structure(s) (105).

The success of the homology modeling depends strongly upon how close the target sequence is to the template sequence. The selection of the template should also be based on the quality of the template structure. It is important to analyze the resolution of the template if it is an X-ray structure. Generally, a structural resolution of 2.0 Å or lower is considered reliable enough to give an accurate 3D-model (102); however many membrane proteins have a structural resolution between 2-3 Å. Depending on the purpose of using the 3D-model, other conditions should be evaluated. If the aim of modeling is ligand docking, the template structure should be co-crystallized with a ligand. For instance, if it is desired to model receptors in an active state, the selected template should, if available, be bound to an agonist, whereas the template representing the inactive conformation should be bound to an antagonist (44).

Target-sequence alignment

Following template identification, an amino acid alignment between the target and the template is generated. This process is a crucial step that profoundly influences the quality of the constructed model. During this procedure, correspondence coordinates between amino acids of the template and target are identified.

Usually, the sequence alignment is first accomplished automatically by the program, followed by manual analysis and adjustments to correct for mistakes or inaccuracies (44). Due to low sequence identity and variations in lengths and locations of conserved regions, gaps are often presented in the sequence alignment complicating the procedure. Therefore, it is often necessary to locate and remove gaps by manually adjusting the sequence alignment (102). It is also recommended to include more than two homologous sequences in the alignment, creating a multiple sequence alignment (MSA), in order to recognize structurally conserved regions efficiently. In this case, the target sequence is aligned with different template sequences to increase the chance of correct alignment and thus improve the modeling procedure (106).

Model building

The 3D-structure of the target protein is constructed based on the target-template sequence alignment by the use of a suitable modeling program. Model construction usually consists of (1) backbone generation of structurally conserved regions, (2) generation of non-conserved regions (loop regions), and (3) adding the side chains.

The core of proteins contains the secondary structure elements that are usually conserved throughout the entire protein family. These segments are called conserved regions because only small changes are tolerated in order to maintain the overall fold (102). Therefore, the core regions, e.g. the 7TM domain of GPCRs, are the most reliable regions of a homology model as they are the most conserved parts (44). On the contrary, modeling the loop regions is the most challenging task. Query sequence regions that are not aligned to the template, due to differences in the number of amino acids, are modeled as loops (102). A suitable conformation for loop sequences can be obtained by searching the PDB for a similar loop sequence of another protein. As an alternative, loop conformations of right length and endpoints can also be generated by Monte Carlo and molecular dynamics methods (100). However, the incorporation of loops in the model depends on the purpose of the model (107). For example, models lacking loops or parts of loops can still be successfully used in

structure-based virtual screening (SBVS) as long as the loops are not involved in ligand binding (104).

Drugs are expected to interact with low-energy conformations of their target. Although the structure we put into the program is "chemically correct," it is seldom "geometrically correct," and we must adjust the geometry. This adjustment is usually performed by using energy minimization (100). The energy minimization process usually begins by measuring the energy of the original molecule and then varies the parameters such as bond length and angles to create a new structure geometry. Changing the geometry until the lowest energy is found, is called geometry optimization (100).

Model refinement

After model construction, the 3D structure of the target protein can be refined by energy minimizations, Monte Carlo simulations (see 1.4.1.3.1), or molecular dynamics simulations (see 1.4.1.3.2). The purpose is to shift nearby unusual connection between amino acids and to optimize the energy of high-energy conformations added in the building step. The refinement is regularly performed as a stepwise process where the most problematic parts of the model are often optimized first. If the constructed model is based on a low similarity or alignment between the target and template, the refinement process may not guarantee the improvement of the model (107).

Model evaluation

The ultimate step is the estimation of the accuracy and quality of the constructed model. Model evaluation can be performed online by necessary analyzing tools that provide information about the quality of the built model. The Structural analysis and verification server (SAVES) (http://nihserver.mbi.ucla.edu/SAVES) is one of the commonly used servers that evaluate the stereochemical properties of the model structure. The Ramachandran plot describes the backbone conformation of the protein by showing the rotation of dihedral angles, Phi (Ψ), and Psi (Φ) of each amino acid. These backbone dihedral angels, in addition to side-chain packing, secondary structure packing, and side-chain geometry are displayed in the SAVES server (107).

Molecular docking can be used to evaluate the constructed model, especially if the purpose of the model is an investigation of the binding site or to use the model in a docking-based virtual screening. In the latter case, the ability of the model to discriminate between active and inactive compounds should to be evaluated. It is usually performed by docking a collection of well-known active compounds and a large number of inactive compounds into the binding site of the target receptor (108). However, for most proteins, the number of known inactive ligands is small; therefore, decoys are often used. Decoys are molecules that exhibit similar physical properties (e.g., molecular weight and calculated log P−values) of active compounds but, at the same time, are topologically dissimilar (109,110).

1.4.1.3 Conformational analysis

The starting point in molecular modeling is often a 3D-structure, determined experimentally (e.g., by X-ray) or theoretically (e.g., homology modeling). The 3D-model is usually used to facilitate calculations related to the 3D-structure, followed by calculation results analysis. A 3D-model can be used to study time-dependent structural changes (e.g., molecular dynamics simulations), and predict affinity (e.g., molecular docking and scoring), among others (111). One single molecule can have many low-energy conformations, but there is only one biologically active conformation among the low-energy conformations. It is noteworthy that the bioactive conformation is not necessarily the lowest-energy conformation. The search for bioactive conformation is one of the critical tasks in molecular modeling because this will present the opportunity to design new drugs based on the bioactive conformation. The 3D-structures determined experimentally only provide information about a single or few conformations. Therefore, a variety of conformational analysis methods have been developed. Conformational search and energy can be calculated by using quantum mechanical or molecular mechanical methods. However, almost all the conformational search programs apply molecular mechanics because the quantum mechanical methods are very time-consuming and can only be used on a limited number of atoms (102).

The transformation from one conformation to another is primarily due to the dihedral angles because only small changes in bond length and angles occur. Accordingly, the conformational search is usually performed by altering the dihedral angles of a molecule to generate different conformations. Depends on the step size implemented in the program and the number of rotatable bonds (n) in the molecule, a certain number of conformations will result. This can be written as:

$$\text{Number of conformations} = (360/\text{step size})^{n} \qquad \text{Eq. (7)}$$

For example, if the molecule has six rotatable conformations and the step size applied in the program is 30 degree (full rotation is 360 degree), the number of produced conformations is 12_6 or 2985 984 structures.

Conformational search is obtained mainly by two methods Molecular dynamics (MD) and Monte Carlo (MC) simulations (102).

1.4.1.3.1 Monte Carlo methods

Monte Carlo is a random search method (stochastic method). The initial structural conformation is changed randomly in order to obtain new conformation, and so on. At each step, the resulting conformation is energy minimized and compared to the previously generated conformations, if the new structure is unique it is then kept. Usually, Monte Carlo is operating as several parallels, where each parallel is beginning with a different initial conformation. Once the results from each parallel are identical or almost identical, then the procedure is considered complete (102).

1.4.1.3.2 Molecular dynamics methods

The molecular dynamics method is a simulation of the time-dependent behavior of a molecular system, such as vibrational motion. It starts with calculating the energy of the molecular system by the use of specific force field, and randomly generation of velocities.

This energy is then used to compute the forces on the atoms at a given geometry. At regular time intervals (determined in advance), the classical equation of motion described by Newton's second law is solved:

$$F_i = m_i a_i(t) \qquad \text{Eq. (8)}$$

Where F_i is the force on atom i at time t, m_i is the mass of atom i, and a_i is the acceleration of atom i at time t. Based on the initial atom coordinates of the system, new positions and velocities can be calculated at time t, and accordingly, the atoms will move to the new positions. As a result of these calculations, a new conformation is generated (102).

1.4.1.4 Molecular docking

The docking method is the search for precise 3D ligand conformation and orientation (posing) within a predefined binding site of the 3D structure of target protein (112). Information obtained from the best ligand pose is then used to predict how well the ligand binds to the protein (binding affinity) by using scoring functions. Following docking protocol, scoring is usually used to rank the different ligands. (113)

Identification and description of the binding pocket are also necessary for docking and is a critical step in structure-based virtual screening. 3D -ligands binds within a predefined size and shape of a specific active site or binding pocket. Therefore, the success of the docking procedure and structure-based virtual screening of potential drug ligands is highly reliant on the quality of the predefined binding pocket architecture (114).

Many different docking programs are available nowadays that differ in the docking algorithm, scoring functions employed, and ligand and protein treatment. The conformation of a ligand bound to its receptor may be different from the unbound conformation. Generally, when the ligand is unbound, it exhibits many different conformations, and only a few of these conformations are relevant to the bound state. Therefore, it is necessary to consider the ligand flexibility during the docking procedure (115). Proteins are dynamic systems in their natural way and exhibit great flexibility in their structure, including their binding pocket. Therefore, taking the target and binding site flexibility into account is quite important in computer-aided drug design (CADD) (Schmidt2014). Most docking programs use a rigid target structure and a flexible ligand during docking; however, the most recent advances also include flexibility into the target structure (115).

1.4.2 Virtual screening

The high-throughput screening (HTS), experimental screening of large libraries of compounds against a specific target, is the dominant technique used for the identification of new lead compounds in drug discovery. The HTS is expensive and time-consuming but has its place in the pharmaceutical industries because of the enormous HTS capacities provided. Virtual screening (VS) methods, on the other hand, are frequently used as a complementary for HTS, especially in academia (116). VS is broadly applied in drug discovery and in a range of computational methods that facilitate the selection of lead compounds from an extensive chemical database (117). Virtual screening is a technique used to computationally

screen libraries of compounds in order to identify those structures which are most likely to bind to a drug target. Virtual screening protocol accesses a large number of possible new ligands that are then purchased and tested experimentally (118).

The virtual screening is divided into two typical strategies: the widespread structure-based virtual screening (SBVS) and the ligand-based virtual screening (LBVS). The former approaches can be employed when the 3D-structure of the target protein is available. The ligand-based methods, however, use only information about a compound or set of compounds that are acknowledged to have a biological activity or are known to bind to the desired target. The LBVS are the methods of choice when detailed 3D-structure data of the target protein is lacking. Using a combination of both methods is also very common (116).

1.4.2.1 Filtering

Physicochemical filters are usually applied before the aforementioned VS methods to reduce the number of compounds in the databases before they are screened. It is especially useful to apply filters when the size of the prepared screening database is up to one million compounds or above (115).

Lipinski's rule-of-five is an empirical set of rules (more correctly, guidelines) based on molecular weight, lipophilicity, and hydrophobicity, that increases the likelihood to retrieve compounds with satisfactory oral bioavailability (Tab. 2). Due to the simplicity of Lipinski's rule-of-five, many virtual libraries apply it as a standard filtering protocol (119). Veber's rule is a different filter that narrows the rotatable bonds or the polar surface area of hit compounds with acceptable bioavailability (Tab. 2) (120). Additional filters can also be implemented to remove compounds containing specific chemical substructures associated with poor chemical stability or toxicity (115), or the other way around, by selecting compounds with desirable properties. For instance, one study applied such filters in order to achieve compounds with protonated amines (121).

Table 2 Drug-like property filters. *HBD; hydrogen bond donor, HBA; hydrogen bond acceptor, MW; molecular weight, logP; octanol/water partition coefficient, RB; rotatable bonds, PSA; polar surface area.*

Filters	Criteria	Value
Lipinski's rule-of-five	HBD HBA MW LogP	< 5 > 10 ≤ 500 < 5
Veber's rule	RB PSA	≤ 10 ≤ 140 Å$_2$

1.4.2.2 Ligand-based virtual screening

Ligand-based virtual screening is based on the principle that structurally similar molecules are expected to exhibit similar properties. Therefore, the screening is often dependent on structures with known activity, so-called reference structures. 2D- and 3D-similarity (including pharmacophore models) search methods are examples of LBVS approaches (116).

2D fingerprinting is a valuable tool that is favorably applied in drug discovery to retrieve active compounds from large databases. Compounds are divided into different fragments, where each fragment is described as a binary bit. The presence of a specific chemical moiety within a ligand is represented as "on" bit, whereas the absence as "off" bit (Fig. 12). The "on" bits is represented as one and the "off" bits as zero. The assembling of these bits (binary numbers) yields a binary fingerprint (122).

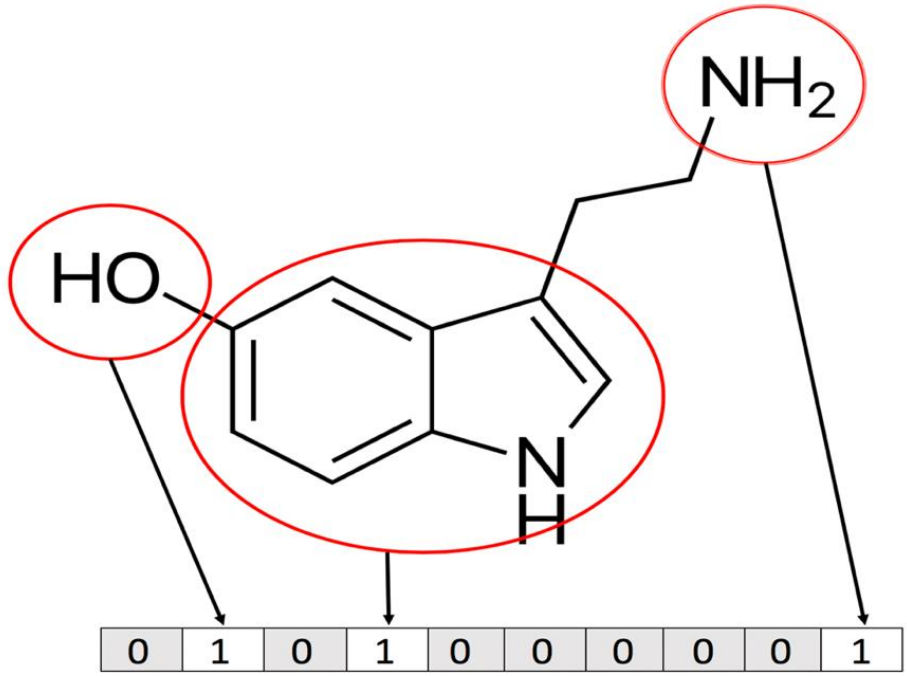

Figure 12 An example of 2D-fingerprinting. *Each chemical feature of the structure is represented as 1 (on bit) or zero (off bit) forming a binary number (fingerprint) (123).*

The atom-type scheme determines which atoms are treated as chemically distinct, and therefore how many unique chemical features a structure possesses (122). Fingerprints usually encode the presence or absence of chemical fragments. However, if it is desired to account for how many times a chemical fragment appears in a structure, a bit-scaling can be used (124).

Similarity metrics are used to compute the similarity between the reference structure(s) and the structures that are available in the database to be screened. Tanimoto coefficient (Tc) is the most used among similarity metrics that calculate the similarity between two compounds based on the common fragments they share. The Tc can be formulated as:

$$\frac{a}{(a + b + c)} \qquad \text{Eq. (9)}$$

Where:
a - count of bits on in compound 1 but not in 2

b - count of bits on in compound 2 but not in 1
c - count of bits on in both compound 1 and 2

The Tc gives a range of values from 0 to 1, where zero represents no common similarity and one are identical (102,117).

Ligand-based virtual screening can also be performed using 3D pharmacophore models. A pharmacophore model can be built by superimposing a collection of known active compounds (reference ligands), then extracting a general chemical hallmark that is crucial for their biological activity (125).

1.4.2.3 Structure-based virtual screening

Structure-based virtual screening usually covers subsequent computational stages, starting with target and database preparation, docking and post-docking analysis, and prioritization of compounds for in vitro testing (115).

In addition to the application of docking protocols in ligand-receptor interaction optimization in an attempt to improve potency or selectivity, docking protocols are also widely used in the in silico virtual screening, where a chemical library of compounds is docked into the target binding site and scored (126). Generally, there are two stages of the docking applied in the virtual screening: 1) prediction of the accurate pose of compounds within the binding site using docking algorithms, and 2) the generated ligand-target complexes are scored to predict the likelihood of the ligand actually to bind to the target using scoring functions (126). When it comes to the search algorithm, speed, and effectiveness in finding suitable conformational space are the two decisive factors. The docking calculations should be rapid, but also accurate enough, which is difficult to obtain because an increase in the speed of the calculations will reduce accuracy. Therefore, a reasonable balance between speed and accuracy should be implemented in the docking programs (100). For example, Glide docking by Schrödinger software package are provided with different accuracies, where extra precision (XP) Glide docking employs a more sophisticated scoring function than standard precision (SP) Glide docking, which makes XP docking take longer running time than SP docking (127).

First and foremost, structure-based virtual screening involves automatic docking of compounds present in a virtual library against a target to find active ligands (115). Accordingly, docking protocols are usually characterized as a combination of a search algorithm and scoring function.

Induced Fit Docking is one of the protocols that introduce flexibility to both ligand and receptor. It causes small backbone relaxations and significant changes in the side-chain conformation of the receptor. Induced Fit Docking uses the advantage of combining two programs, Glide and Prime (128). Glide is first used to generate a different set of ligand poses while temporarily excluding flexible side chains of the receptor. For each pose of the ligand generated, a Prime is then used to embed the ligand by reorienting the nearby side chains, followed by energy minimization of the ligand and nearby residues. Eventually, each ligand pose is re-docked into its corresponding energy minimized protein structure, and complexes are ranked according to GlideScore (129).

Scoring is used to describe the interaction between a protein and a ligand. Scoring functions are used to rank the quality of the poses generated from the docking procedure. A specific compound pose is usually compared to other poses of the same compound, and with the other compounds in the database. The term scoring is also used to rank compounds according to their binding affinity during the screening of databases (115). The Gibbs-Helmholtz equation defines the free energy of binding (ΔG) as:

$$\Delta G = \Delta H - T\Delta S = -RT\ln K_i \qquad \text{Eq. (10)}$$

Where ΔH is the enthalpy, T is the temperature in kelvin, ΔS is the entropy, R is the gas constant, and K_i is the binding constant (102). In SBVS, the inability to correctly estimate free energies of ligand binding severely limits the accuracy of scoring functions and, consequently, compound ranking (116). Few scorings functions are used to predict relative free energy, described in Tab. 3.

Table 3 Description of scoring algorithms (112,113).

Scoring algorithm	*Description*
Force-filed based	Quantify the sum of two energies: the interaction energy between the receptor and the ligand, and the internal energy of the ligand
Empirical	Are based on the idea that binding energies can be approximated by a sum of several individual uncorrelated terms
Knowledge-based	Are based on the statistical analysis of interacting atom pairs from protein-ligand complexes with experimentally determined structures

1.5 In Vitro screening

GPCR drug discovery usually relies on high-throughput screening (HTS) for hit compounds identification. The use of HTS technologies in pharmaceutical industries accelerates the testing of millions of compounds. Nevertheless, in vitro ligand screening is also applicable in the academic research and stands as a fundamental and complementary to the in-silico part of the drug discovery (130). The combination of these methods reduces both time and cost by decreasing the number of compounds to be tested experimentally. Furthermore, it increases the possibility of identifying new compounds (131). Currently, the main aims in GPCR drug discovery have extended to the search for allosteric modulators in addition to regular orthosteric ligands (132).

In vitro drug discovery requires a well-designed and verified assays that can be implemented for different purposes. Assays can be applied for hit identification, classification of ligand activity (e.g. agonist, antagonist, PAM, NAM etc.), studying signaling pathways, and estimating efficacy and potency. An extensively used assay in early drug discovery is the ligand-binding assays. There are multiple variants of ligand binding assays that are used to measure the binding affinity of compounds and the site of interaction (131). In a concept of allosteric modulators, these assays are used to understand the influence of allosteric ligands on orthosteric ligands (132). Traditionally, ligand binding assays that use radioactive ligands are widely applied in drug discovery. The compound of interest must be custom synthesized and labeled with a radioisotope, which is costly and time-consuming. Also, these assays are hazardous due to the use of radioactive ligands (133). High-affinity radioligands for allosteric ligands are less available than for orthosteric ligands (132). All these drawbacks make this type of assay less attractive in HTS nowadays. Consequently, different read-out methods have been developed, including fluorescence and luminescence (134).

Still, these binding assays do not provide information about ligand activity nor the potency of a compound under physiological conditions (131). Therefore, new signaling-dependent cell-based functional assays have been developed. Commonly used in vitro assays that are used when studying GPCRs are functional assays that measure either G-protein activation, such as GTPγS binding assay (135), or second messengers mediated by G-proteins, such as cAMP assays (131). The GTPγS binding assay measures the accumulation of non-hydrolyzable GTP analog, such as [^{35}S]-GTPγS, from cells expressing GPCR of interest after receptor stimulation. The cAMP assay detects cellular levels of cAMP produced by intact cells (131). In this study, cAMP assay was used for compound testing.

1.5.1 cAMP assay

Several cAMP assays are commercially available with advantages and disadvantages for each method. Screening GPCRs that couple to G_s proteins is generally straightforward, whereas GPCRs coupled to $G_{i/o}$ are challenging to perform with high precision because a direct activator of adenylyl cyclase, forskolin, is often added to maximize the inhibition signal (136). Furthermore, the accessibility of highly sensitive plate readers enabled the detection of sub-nanomolar levels of cAMP produced by cells (132). HitHunter™ assay (Fig. 12) from DiscoverX is one of the luminescence-based assays. The assay consists of cAMP labeled with a small peptide fragment of a β-galactosidase enzyme (enzyme donor, ED) also referred to as ED-cAMP, an antibody (Ab) with binding sites for both ED-cAMP and cellular cAMP, and a remaining fraction of β-galactosidase (enzyme acceptor, EA). Cellular cAMP, produced by cells, competes with ED-cAMP to bind the antibody. When ED-cAMP is bound to the antibody, it cannot complement with EA; the remaining fraction of β-galactosidase. Therefore, upon addition of β-galactosidase substrate, no enzyme activity is present and no luminescence signal is produced. When the level of cellular cAMP increase, it competes with ED-cAMP at the antibody, which enables the ED-cAMP to dissociate from the antibody and complement with the EA fragment. Substrate addition now can produce a luminescence signal. The amount of signal produced is directly proportional to the amount of cAMP produced by the cells (132).

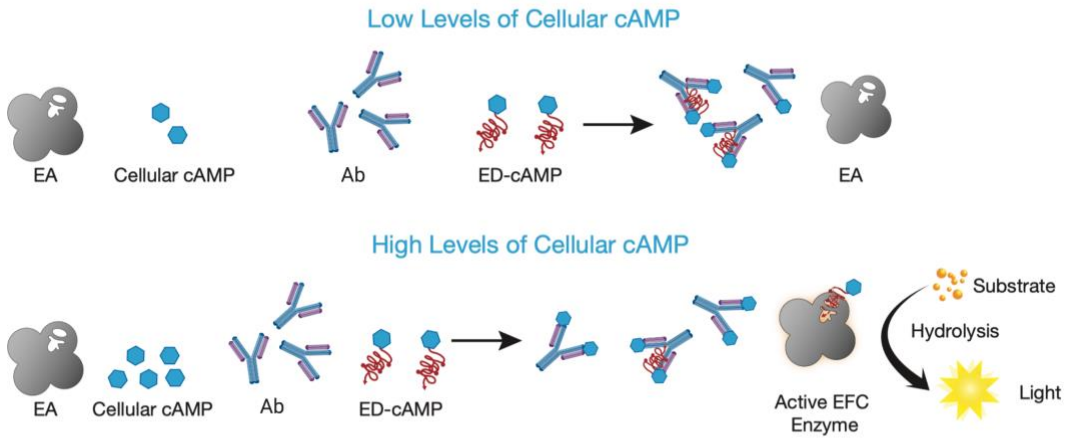

Figure 13 The mechanism of cell-based cAMP assay. *EA; enzyme acceptor, Ab; antibody, ED-cAMP; cyclic adenosine monophosphate labeled with enzyme donor, EFC; enzyme fragment complementation (137).*

1.5.2 Cell culture

Cell culture is defined as the removal of animal cells from tissues, and its growth in a suitable artificial environment (in vitro) outside its native environment (in vivo). Cell culture technology is a valuable tool that provides suitable model systems for many types of biological research, including drug screening and development (138).

There are two different cell types: primary cells and cell lines. Cells directly taken from tissue or organ of interest are referred to as primary cells. Once primary cells are sub-cultured or passaged, they become cell lines. Cell lines can be further subdivided onto finite cell lines and continuous cell lines. Finite cell lines are cultures of cells that can be sub-cultured for a limited number of population doublings, whereas continuous cell lines can be sub-cultured indefinitely (139).

Organs and tissues isolated from animals are difficult to standardize because they require a complicated environment and nutritious, and because of the heterogeneity between individuals (140). Primary cells are often a mixture of different cell types because diverse cell types exist in a single blood or tissue sample (139). Furthermore, they have a limited lifetime and alter their nature when cultured over time, which is difficult to standardize (140). Cell lines, on the other hand, are beneficial for long-term research because they can be stored in liquid nitrogen for later use. Different continuous cell lines are used in the pharmaceutical industry and academic research, including the CHO-k1 cell lines that originated from the Chinese Hamster ovary (139).

Understanding the cell cycle is important for cell synchronization during cell culturing. Cells need to be synchronized so they will be at the same phase at the same time, which makes it more straightforward to determine the growth rate and to minimize variations between cells (138).

Normal mammalian cellular proliferation is strictly regulated at each phase of the cell cycle. The cell cycle consists of five different phases: the gap phases (G_0, G_1, and G_2), M-phase, and S-phase. During G_0, the cells remain at an inactive state, while during G_1 and G_2, the RNA and protein syntheses occur. Throughout S-phase, the cell's DNA is replicated, and finally, the cell undergoes mitoses and cytokinesis during M-phase. There are several checkpoints in between cell cycle phases to ensure normal cell function. The primary checkpoint, known as the restriction (R) point, acts at the end of G_1 phase to ensure healthy cell progression. The second checkpoint exist at S-phase to check the quality of replicated DNA and to activate the DNA repair mechanism if necessary. The third checkpoint is at the G_2/M transition to ensure that DNA has been completely replicated and is unharmed before the cell enters M-phase. Finally, there are several checkpoints within M-phase to ensure that conditions are still suitable during cell division (cytokinesis). The time spent at each phase of the cell cycle varies and depends on the cell type, but cells spend most of the time at G_1 phase, as shown in figure 16 (141).

2 AIM

Baclofen, a $GABA_B$ orthosteric agonist, is currently the only marketed drug available that targets the $GABA_B$ receptor. It is used to treat many disorders, including muscle spasticity and rigidity associated with spinal cord injuries and multiple sclerosis. However, side effects provided by baclofen limit its use for the treatment of many disorders. Antagonists of the $GABA_B$ receptor are expected to have beneficial effects, especially in depression, cognitive deficits, Down's syndrome, and absence epilepsy, as revealed by studies in rodents. For instance, allosteric modulators may provide the benefit to dissociate the undesired side effects observed with baclofen. GABAB receptor antagonists are suspected of having beneficial effects, especially in depression, cognitive deficits, Down's syndrome, and absence epilepsy, as reported by studies in rodents. Accordingly, negative allosteric modulators are expected to exhibit the same effects as antagonists, but with fewer side effects observed with antagonists. Hence, the primary aim of this study was to identify promising new negative allosteric modulators that can potentially be new drugs by using a combination of structure-based methods (docking and scoring) and ligand-based methods (2D fingerprinting similarity screening) and in vitro evaluation.

This study is part of an ongoing project that has continuous testing of new $GABA_B$ allosteric modulators where previous homology modelling and virtual screening has led to the identification of possible novel $GABA_B$ NAMs. Earlier, four negative allosteric modulators identified by VS of the MolPort database and one negative allosteric modulator from DrugBank were identified (manuscripts in preparation). These negative allosteric modulators, in addition to one published negative allosteric modulator, will be used as reference structures in the current study.

The main aim of this study was to identify analogous of the previously identified NAMs using a combination of virtual screening and in vitro evaluation.

Additional purposes of the study were:

- Achieve a more comprehensive understanding and skill in the use of computational methods and in vitro methods.
- Homology modeling of an active $GABA_B$ receptor.
- Evaluate the combination of ligand- and structure-based virtual screening.
- Optimization of instruments and methods used during the in vitro testing.

3 METHODS

3.1 Part I: in silico

3.1.1 Software

3.1.1.1 Molsoft Internal Coordinates Mechanics (Version 3.8-7c)

Internal Coordinate Mechanics (ICM) software is a molecular modeling package with various tasks such as protein and small-molecule prediction, docking, and structure-based design. The use of this program performed the target-template sequence alignment and the construction of the homology model.

3.1.1.2 Schrödinger Maestro (Version 12.2.012)

Schrödinger is a software package with products used for computational technology. Maestro software is the graphical user interface (GUI) for about all the Schrödinger's computational programs. Protocols applied by this program were sketching of known NAMs, preparation of ligands (LigPrep), preparation of protein (Protein Preparation Wizard), Glide docking (SP and XP), Glide scoring (Emodel scoring and GlideScore), and (IFD) and QikProp.

3.1.1.3 Schrödinger Canvas (Version 4.2.012)

Canvas software is part of the Schrödinger package providing cheminformatics tools such as fingerprint-based similarity searching and structural clustering of compounds. This program provided the calculation of physicochemical properties, 2D-fingerprinting, ligand similarity screening, and compounds clustering. (https://www.schrodinger.com/canvas)

3.1.2 Databases

The universal Protein Resource Knowledgebase (UniProtKB)

UniProtKB is a database that supplies users with a scientific collection of useful data and knowledge about protein and protein sequences. This database consists of two sections: a section including manually annotated documents with data extracted from literature (UniProtKB/Swiss-Prot), and a section with computationally analyzed records that await comprehensive manual annotation (UniProtKB/TrEMBL). The primary amino acid sequence of $GABA_{B2}$, used for target-template sequence alignment and homology modeling, was downloaded from the Swiss-Prot section of the UniProtKB. (https://www.uniprot.org/).

MolPort Database

MolPort database was built in 2006 to supply users with compounds in order to quicken drug discovery. This database was used because it contains information for over 7 million compounds purchasable from stock and over 20 million made-to-order compounds. MolPort specializes in sourcing thousands of compounds from dozens of trustworthy suppliers. On the 25th of October 2019, the MolPort database was used to retrieve 7,608,598 compounds, that

were available in stock, in order to find potentially active binders. (https://www.molport.com/shop/index)

3.1.3 Virtual screening of MolPort database

3.1.3.1 Workflow with MolPort database

In the current study, a multi-step strategy combining ligand-based and structure-based virtual screening was applied to screen the MolPort database. The purpose of this method is to find new negative allosteric modulators (NAMs). 7,608,598 compounds from the MolPort database were reduced to 6,444,706 using Lipinski's rule of five and Veber's rule (Tab. 2). Subsequently, 41,984 compounds were extracted using the MOLPRINT2D fingerprint method and the Tanimoto similarity metrics. These compounds were docked into $GABA_{B2}$ 7TM homology model using SP Glide docking, which resulted in 18,845 compounds, after removing the duplicates. Exclusively 10% of these compounds (with top score) were re-docked using XP Glide docking. Afterward, a score cut-off value of -9,0 kcal/mol was used to end up with 376 compounds that were clustered into 18 clusters. Finally, 16 hit compounds were selected to be purchased and tested experimentally. The workflow of the study with MolPort database is shown in Fig. 14.

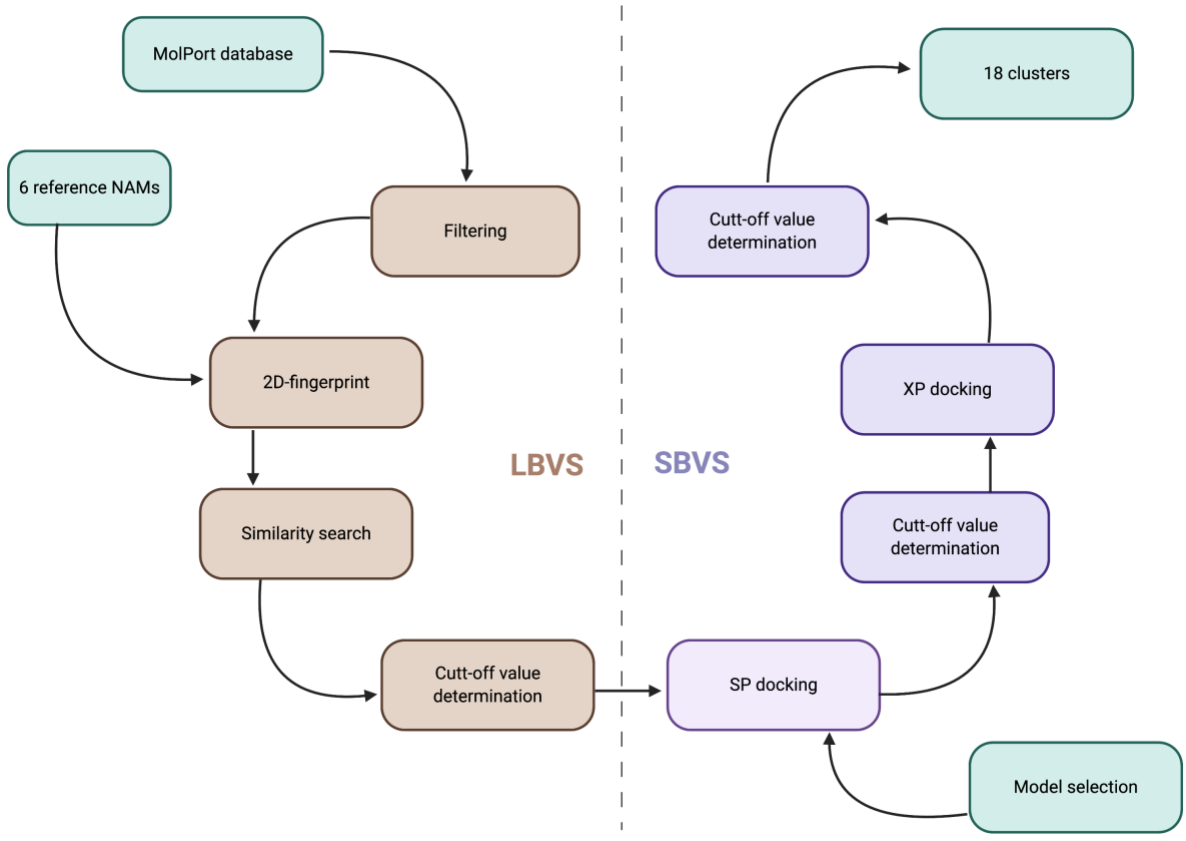

Figure 14 Workflow with MolPort database.

3.1.3.2 Ligand-based virtual screening

3.1.3.2.1 Database filtering

7,608,598 compounds were downloaded from the MolPort database (25th of October 2019) into Schrödinger Canvas (142). The following molecular properties were calculated for all compounds: number of hydrogen bond donors and acceptors (HBD, HBA), the molecular weight (MW), number of rotatable bonds (RB), partition coefficient (LogP), and polar surface area (PSA), were calculated for all the compounds. These properties were then used to filter the database using Lipinski's rule of 5 (119) and Veber's rule (120). Their default property cut-off values were used (Tab. 2).

3.1.3.2.2 Reference ligands

The reference ligands used in this project were five potential NAMs that have been identified through VS and in vitro evaluation by the Molecular Pharmacology and Toxicology research group, IMB, UiT (manuscripts in preparation) and a CLH304a , a NAM retrieved from literature (80) (Fig. 15).

The 2D-sketcher in Schrödinger Maestro (143) was used to sketch the reference NAM structures in a 2D representation. Due to the similarity between benzydamine and its metabolite benzydamine N-oxide, only the metabolite was selected for screening the MolPort database. Also, the metabolite had a better docking score than its parent compound (manuscript in preparation). In total, six different NAM structures (Fig. 15) were used to screen the MolPort database. The six unique reference NAMs were added to the list of compounds downloaded from the MolPort database into Schrödinger Canvas (142) after the application of Lipinski's rule of 5 and Veber's rule.

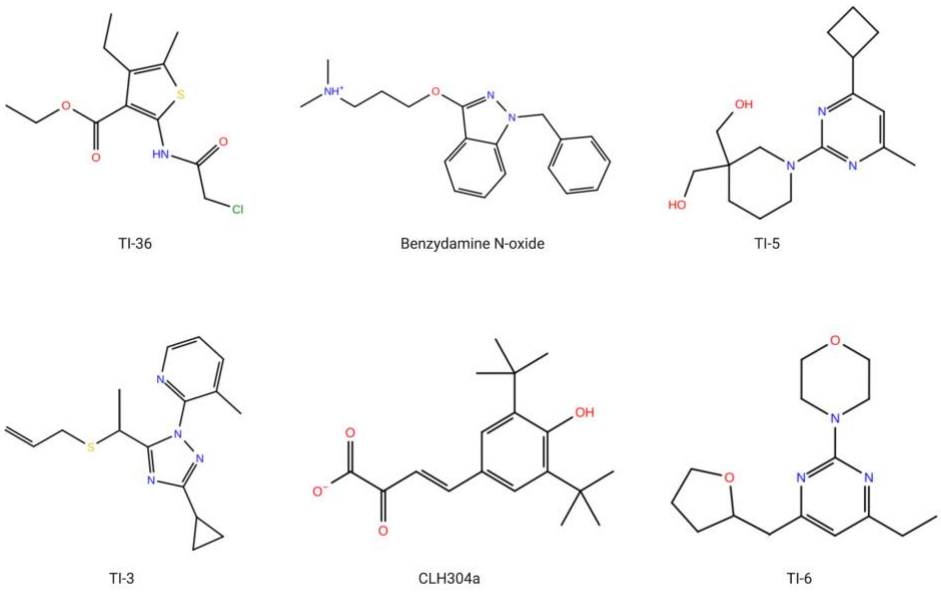

Figure 15 Reference NAMs used in the screening of MolPort database. *Ligands starting with TI in their name are identified from MolPort database, benzydamine N-oxide from DrugBank and CLH304a from literature.*

3.1.3.2.3 Calculation of 2D fingerprint

MOLPRINT2D fingerprints for all compounds, including the six reference NAMs, were calculated using default settings. MOL2 was used as an atom type-scheme, and each fingerprint is encoded by hashing each chemical pattern into a 32-bit size. No bit-scaling was used.

3.1.3.2.4 Similarity screening

The Tanimoto metric (Eq. 9) was used to calculate the similarity between the six reference NAM structures and the structures retrieved from the MolPort database. All six reference NAM structures were manually selected as reference structures in the employment of the similarity screening.

3.1.3.2.5 Determination of similarity cut-off value

The output from the filtering step was screened to identify new compounds that are similar to the reference structure. For each group, the similar compounds were arranged in descending order of the similarity value. In other words, compounds most similar to their reference NAM were ranked at the top, and those with the lowest similarity value were ranked at the bottom. The cut-off value for each group was based on a structural examination and a sensible quantity of compounds for each reference NAM (Tab. 8; results). Totally, 41,984 structures were retrieved using the 2D-fingerprint-screening.

3.1.3.3 Structure-based virtual screening

3.1.3.3.1 Selection of inactive $GABA_{B2}$ homology models for VS

The primary purpose of this selection step was to choose the most suitable model among the seven available models for the structure-based virtual screening (see below). Due to the limited time available to perform the virtual screening, only one model was be selected.

3.1.3.3.1.1 Generation of inactive $GABA_{B2}$ models

In the present study, seven homology models of the 7TM domain protomer of $GABA_{B2}$ subunit that had previously been generated by Thibaud Freyd were used for the structure-based steps of the VS protocol (81). The $GABA_{B2}$ homology models had been constructed using Modeller software and two different crystal structures as templates: the class C mGlu1 (PDB: 4OR2) and mGlu5 (PDB: 4OO9) receptors (61,65), and in order to select the best $GABA_{B2}$ models for virtual screening, 72 unique PAMs, divided into five different clusters, and a large number of decoys had been docked into the generated models (81). In the current project, the seven models were displayed in Schrödinger Maestro (143) and the protein preparation step was not required because the models were already prepared from the recent study (81). The Protein Preparation step helps to ensure structural correctness of the target protein, such as missing hydrogen atoms, incomplete side chains and loops, ambiguous protonation states, and flipped residues (144).

3.1.3.3.1.2 Generation of active compounds and decoys

The 2D structures of the reference ligands were converted to 3D structures using Schrödinger LigPrep (145) and the OPLS3e force field. The following settings were applied in the LigPrep process:

- standard ionization states at pH (7,0 ± 2,0),
- Epik option to predict the protonation state
- generate at most 32 conformations per ligand
- for the reference negative allosteric modulators with chiral centers, both enantiomers were kept

The option to generate tautomers was likewise not applied because it will increase the number of compounds to be docked and so the computational time. The ionization of a ligand can influence ligand-target interaction and binding affinity exponentially. It is known that the use of "Epik" improves virtual screening performance, and it was the selected default option recommended by Schrödinger. Furthermore, "Epik" adds energetic penalties to the predicted protonation state that helps to differentiate active from inactive compounds during docking protocol (146)**.**

Decoys were retrieved from the previous study (81) that were selected from the ZINC database (147). They were selected based on that they have similar physical properties, but chemically dissimilar to the active compounds. LigPrep step for decoys was not necessary since it was already performed from the last study (81).

3.1.3.3.1.3 Glide docking

Receptor Grid Generation was initially used to assemble a grid map that represent the allosteric binding site of the $GABA_{B2}$ model, using Schrödinger Glide (148). One grid box was generated for each model by centering around the residue Tyr564, a binding site residue (81), with an outer grid box size of 25 Å and an inner box size of 10 Å, according to the previous study (81).

The decoys that were retrieved from the last study (81) together with the prepared reference NAMs were docked into each grid map generated from the seven models using the Schrödinger Glide docking with “Standard Precision” (148). The docking procedure was applied with default settings using the OPLS3e force field. The default settings are:

- flexible ligand sampling
- sample ring conformations
- sample nitrogen inversions
- bias sampling of torsions for all predefined functional groups
- add Epik state penalties to docking score

The reference NAMs were docked with XP docking using the same setup implemented in the SP docking.

Following docking, the results were analyzed using the docking score and visual inspection of the receptor-ligand complexes to determine which model will be used further in the screening process. The purpose of the visual inspection was to investigate if the compounds docked somehow in a similar fashion, and if compounds were within the binding pocket and

between the helices. The model selection was based on the XP docking results of the reference NAMs, SP docking results of the decoys, and visual inspection.

The ability of the models to dock NAMs among a significantly higher number of decoys was used for the selection of the final model. The six references NAMs were drawn in Schrödinger Maestro as 2D structures and then transformed into eight 3D structures (Tab.4) because two of the NAMs have two isomers. 2536 decoys, together with the reference NAMs, were docked into each of the seven models. By comparing the docking results from each model shown in Tab. 4, Model c5_m2_4oo9 was appointed as the most appropriate model. Unlike some of the other models, the chosen model was able to dock all NAMs with a reasonable score. Moreover, it was the model that docked fewer decoys compared to the other models. Approval of the selection was done by visual inspection of the docking poses that revealed NAMs were better docked in model c5_m2_4oo9.

***Table 4 Docking evaluation of the models**. In each model, reference NAMs and decoys were docked. The table shows the number of NAMs and decoys that were docked in each model. In addition to the number of NAMs that were docked, the docking score range from the highest score to the lowest is given. The model highlighted with orange color, is the model that was selected.*

Models	NAMs docked with XP (kcal/mol)	Decoys docked with SP
c1.m2.s005	8 (0.258 – -6.524)	970
c2.m1.s006	8 (-2.631 – -9.532)	1864
c2.m2.s007	8 (-3.850 – -10.454)	1507
c4.m1.s008	8 (-4.814 – -8.260)	2261
c4.m2.s009	8 (-4.834 – -8.289)	2545
c5.m1.s010	8 (-7.003 – -8.638)	1007
c5.m2.s011	8 (-6.688 – -9.673)	841

3.1.3.3.2 Structure-based screening

3.1.3.3.2.1 Standard Precision (SP) docking

The output compounds from the ligand-based step of the VS protocol were converted to 3D structures using LigPrep (see 3.1.3.3.1.2) and docked into the selected $GABA_{B2}$ model using the previously set up grid box and SP Glide docking protocol (see 3.1.3.3.1.3). The number of compounds that passed the SP docking step was 18 845.

3.1.3.3.2.2 Extra precision (XP) docking

Duplicates were excluded from each of the six groups assembled from SP docking results by using the Filter Duplicates task. Following duplicate removal, the highest scored top 10 % of the resulting compounds from the SP docking step were selected to be re-docked with Glide Extra Precision (XP) using the same previously set up grid box and docking settings applied for SP docking (see 3.1.3.3.1.3).

3.1.3.3.2.3 Determination of docking score cut-off value

The number of compounds after removing duplicates are 1,785, which is still not manageable. Compounds with docking scores lower than -9,0 kcal/mol, were selected to deal with further. The number of compounds was reduced from 1,785 to 376.

3.1.3.3.3 Post-docking analysis and final selection of hits

The 72 known PAMs retrieved from the previous article (81), that are clustered into 5 clusters using Canvas Software (142). These PAMs were merged with the compounds (376) retrieved from the virtual screening in Schrödinger Canvas (142). Compounds were merged to avoid selecting already known PAMs, identify possible analogs of known PAMs, and to identify which hit compounds belongs to which reference NAM. Hierarchical clustering was then used to cluster all the compounds mentioned above using MOLPRINT2D fingerprints and Tanimoto similarity metric. The application of Kelly criterion produced 18 clusters.

QikProp is a fast and precise ADME (Absorption, Distribution, Metabolism, Excretion) prediction program (149). In addition to predicting requisite molecular properties, it grants a range for comparing a particular molecule's properties with those of 95% of known drugs. ADME descriptors, precisely the number of property that fall outside the 95% of similar values for known drugs (#stars), the number of reactive functional groups (#rtvFG), and the predicted aqueous solubility (QPlogS), were calculated and used for all compounds in the 18 conclusive clusters to facilitate the selection of the final hit compounds. QikProp properties description and recommended value for the used descriptors are shown in Tab. 5.

***Table 5 shows the QikProp descriptors that were used**. Each descriptor is explained, and the range of the recommended value is stated.*

Descriptor	Description	Recommended value
#Stars	Number of descriptor values that fall outside the 95% range of similar values for known drugs. A large number of stars suggests that a molecule is less drug-like than molecules with few stars.	0 - 5
#rtvFG	Number of reactive functional groups. The presence of these groups can lead to false positives in high-throughput screening (HTS) assays and to decomposition, reactivity, or toxicity problems in vivo.	0 - 2
QPlogS	Predicted aqueous solubility, log S. S (in $mol.dm^{-3}$) is the concentration of the solute in a saturated solution that is in equilibrium with the crystalline solid.	-6,5 – 0,5

The compounds in each cluster was ranked in an ascending order based on the Glide XP docking score. In addition to the docking score, QikProp descriptors, specified above, was displayed. The selection was based on:

- Satisfying ADME properties
- Good docking score
- Visual inspection of the XP docking results
- How similar or dissimilar are the hit compounds to the reference compounds both in ligand structure and docking orientation
- The compound-target interactions, and
- Especially reasonable price and availability of the compounds.

Finally, 16 hit compounds (A-1, A-6, A-8, A-9, A-11, A-13, A-14, A-17, A-18, A-19, A-20, A-21, A-22, A-26, A-28, and A-29) (Fig. 23) were selected and purchased to be tested experimentally.

3.2 Part II: In vitro

3.2.1 Materials

Following materials were purchased from DiscoverX: cAMP Hunter™ CHO-K1 $GABA_{B1}$+$GABA_{B2}$ G_i Cell Line (Cat.# 95-0165C2. AssayComplete™ Revive CHO-K1 Media (Cat.# 92-0016RM2S). CHO-K1 wild type cell line was kindly provided by Tumour biology research group of UiT. AssayComplete™ CHO-K1 Cell Culture Kit 35 (Cat.# 92-0018G2R2) in which it has medium, serum and antibiotics mix (Pen/Strep/Glu, Geneticin and Puromycin). AssayComplete™ Cell Detachment Reagent (Cat.# 92-0009). AssayComplete™ Freezing Reagent F2 (cat.# 92-5102FR). HitHunter® cAMP Assay for Small Molecules (cat.# 90-0075SM2). White clear bottom, tissue culture treated 384-well (cat.# 92-0013). Chemicals purchased from Sigma-Aldrich are: $CaCl_2$ (Cat.# C7902), HEPES (Cat.# H3375), $MgCl_2 \cdot 6H2O$ (Cat.# M9272), KCl (Cat.# 746436), NaCl (Cat.# 746398), D-(+)-Glucose (Cat.# G7021), NaOH (Cat.# 30620), GABA (Cat.# A5835), DMSO (Cat.# 472301), water soluble forskolin NKH477 (Cat.# N3290). Test compounds were purchased from Molport.

3.2.2 HBSS buffer preparation

Four stock solutions were prepared by dissolving a specific amount of solute into a 500 ml volumetric flask, shown in (Tab. 6). The powder solute(s) of each stock was weighted out on a weighing boat and slightly dissolved with pure water before getting transferred to a 250 ml glass backer. More water was added until the meniscus of the water reached the calibration mark on the flask. The same procedure was used to prepare all the stocks.
The stock solutions were prepared to be 20 times concentrate (20xHBSS) than the final buffer concentration required for the assay.

A 400 ml two times concentrated (2xHBSS) buffer was then prepared by adding 40 ml of each stock solution into a 250 ml glass beaker. Thereafter, 230 ml of water was added to the glass beaker, and the pH was adjusted to 7,4 by adding 3,93 ml of 1M NaOH at 25°C. Finally, 6,07 ml of water was added to reach a total volume of 400 ml. This buffer concentration was used to prepare GABA-forskolin mixture with the test compounds.

Moreover, a 50 ml volume of 2xHBSS buffer was diluted with a 50 ml volume of pure water in order to make a 1xHBSS buffer. This buffer concentration was used on the day of the assay to rinse and harvest the GABAB cells.

Table 6 The list of chemicals in each stock solution and their calculations. *The table shows the solutes used in each stock solution, in addition to their molecule weight (MW), purity, concentration (mM), and amount weighted (g/500mL). *The purity of CaCl is 96%, and therefore the amount required to obtain 26 mM is higher than expected.*

Stocks	Components	MW (g/mol)	Purity	Concentration (gram/500mL)	Concentration (mM)
Stock 1	NaCl	58,44	99%	76,8486	2630
	D-glucose	180,16	99,5%	18,016	200
	KCl	74,55	99%	3,7275	100
Stock 2	$CaCl_2$	110,98	96%*	1,502855*	26
Stock 3	$MgCl_2.6H2O$	203,3	99%	2,033	20
Stock 4	HEPES	238,3	99,5%	23,83	200

3.2.3 Cell thawing and culture

The cell culture guideline from DiscoverX, with some adjustments, was followed. Two different types of cell lines were used in the current study, GABAB cells, and wild type cells. The cells are Chinese Hamster Ovarian Cells (CHO-K1). GABAB cells are usually created by transfecting wild type cells with cDNA that has the sequence for the human GABAB receptor. In the current study, the same cell culture procedure was applied to both cells, except for the incubation time of cells and culture media composition. The incubation time for GABAB cells was 48 hours to reach approximately 75% confluence, whereas, for the wild type cells, it was 36 hours. The culture media used for both cells was with serum, but the culture media used for wild type cells did not contain selection antibiotic in its composition. The cDNA that has the sequence of GABAB receptors also contain antibiotic resistance sequence. Therefore, GABAB cells could resist the selection antibiotics, but wild type cells would die if selection antibiotics were added.

On day one, cryovials from liquid nitrogen storage, containing the cells, was placed in a 37°C water bath for approximately 30 sec to 1 min. The frozen cells were thawed until only small ice crystal remained. The cells were then placed in the LAF-cabinet and mixed with 10 mL pre-warmed cell culture media under sterile conditions. The cell suspension was then centrifuged (350 g for 4,5 min) to small pellet cells at the bottom of the tube. Following centrifugation, the supernatant culture media was aspirated, and the cell pellets were immediately resuspended with new 11 ml of pre-warmed culture media. The cell suspension was then transferred into two T25 flasks (5.5ml in each flask). The T25 flasks were then placed in the incubator for either 36 or 48 hours (at 37°C, 5% CO2) to grow the cells.

After the cells became approximately 70-90% confluent the culture media was aspirated from the flask and pre-warmed 5 mL Phosphate-buffered saline (PBS) was then added into the flask and waved to rinse the cells. The PBS was then aspirated from the flask, and this step was repeated three times. Hereafter, 1 mL of AssayComplete™ Cell Detachment Reagent was added to detach the cells from the T25 flask bottom surface. The flask was then placed in the incubator again for 2 minutes. Once the detachment of the cells was confirmed, by observing under the microscope, an additional 15 mL PBS was added to collect the cells. The cells were then removed from the flask and transferred to a 50 mL conical tube. The cell suspension was centrifuged at 350 g for 4,5 min, and the supernatant was discarded.

Subsequently, the cell pellets were resuspended in pre-warmed 16 mL of AssayComplete™ Cell Culture Media and transferred to a T75 flask. The T75 flask was then placed in the incubator for 36 or 48 hours (at 37°C, 5% CO2) for cell growth. The second T25 flask was used for backup.

After the cells in T75 flask was about 70-90%, the cells were then harvested and split into a new T75 and T175. The cell seeding density is 1.5 million cells for T75 flask and 3.5 million cells for T175 flask. Cell concentration from harvested T75 flask was determined using Trypan Blue assay. Briefly, 50 µL of cell suspension and 50 µL of trypan blue was transferred to a 0.5 mL Eppendorf tube and mixed. The Countess@ automated cell counter was used to determine the cell concentration. The cell counting procedure was repeated four times, and the average value was calculated.

On the day of assay, the procedure mentioned above was replicated where cells from the T75 flasks were transferred to a new T75 and T175 flasks. However, the cells in the T175 were harvested to run the assay. Cells from T175 flask was first harvested in PBS buffer. Cell suspension was immediately centrifuged at 350 g for 4.5 minutes, following removal of supernatant. The cell pellet was resuspended in 1xHBSS buffer, centrifuged again, supernatant discarded, and cell pellet resuspended in 15ml of 1xHBSS buffer. Cell concentration were then determined using Trypan blue assay. Based on the measured cell concentration, cell suspension was then diluted with 1xHBSS buffer to final assay concentration of 0.6 million cells/ml. The 50ml conical tube containing the cell suspension was stored in a 25 °C water bath for 150 min before running the assay. Fig. 16 shows the splitting procedure used in this study.

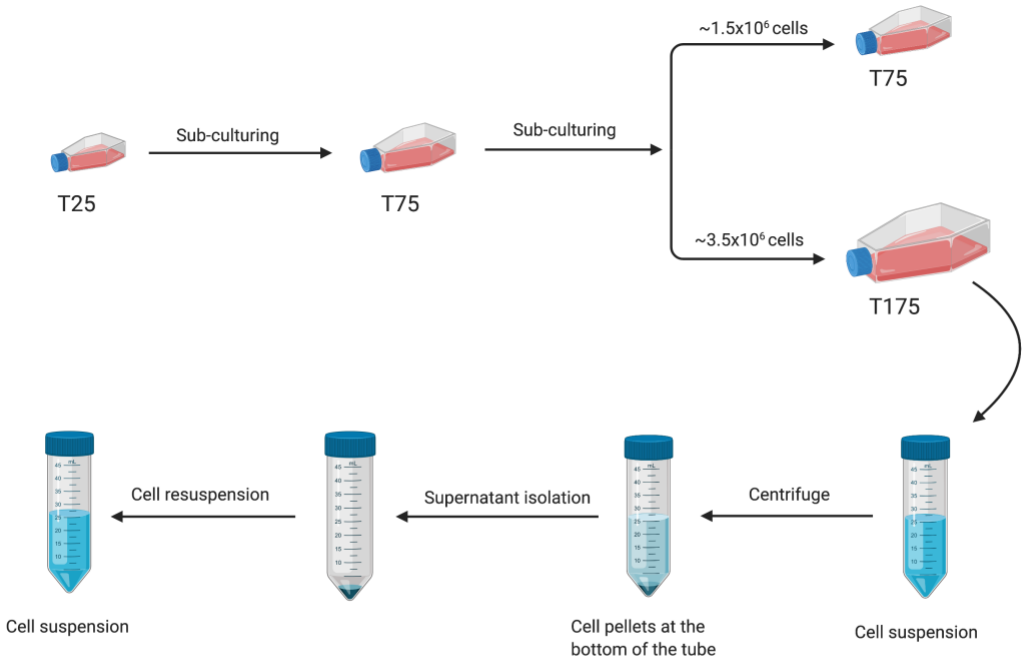

Figure 16 Schematic illustration of cell seeding workflow. *This figure shows the splitting pattern from the T25 flask to the T175 flask. Also, cell washing, and resuspension procedure are shown.*

3.2.4 Test compounds preparation and solubility test

The majority of the compounds delivered from suppliers were in powder form with ≥ 90% purity. A certain amount of each test compound was weighed and dissolved in 100% dimethyl sulfoxide (DMSO). In order to obtain an actual mass of each test compound, the impurity had to be taken into account. Therefore, the calculations had to be performed as follows:

$$\text{Actual mass} = (\text{purity\%} \times \text{weighed mass}) / 100\% \qquad \text{Eq. (11)}$$

Accordingly, the volume of DMSO was calculated, based on the actual mass, so that each test compound had a stock concentration of either 10 mM or 20 mM. The stock solution for each compound was then transferred to small Eppendorf tubes and stored in the freezer at -20 °C.

The test compounds' solubility was first tested in 2xHBSS buffer at a concentration of 60 µM of each test compound. Consequently, ten compounds of 16 passed the test. The six remaining compounds had poor solubility at 60 µM concentration and were further dissolved in 5 mM D-glucose solution. As a result, two compounds passed the test, while the remaining compounds still had poor solubility. By implementing additional solubility tests, one compound was soluble in 2xHBSS buffer at a concentration of 60 µM but only for few hours before crystallizing. Therefore, this compound was prepared and mixed with buffer right before cell dispensing in the microplate. The other compound was soluble in 10 mM NaOH solution. The two leftover compounds were sparingly soluble, yet further tests were attempted. The last compound was not soluble at all and hence was excluded from the in vitro testing.

3.2.5 cAMP assays

Different forms of cAMP assay were performed. Before compound testing, the reaction time and concentration of forskolin were first determined by running time-dependent cAMP assay and forskolin dose-response assay. Once these parameters were determined, a standard GABA dose-response assay was performed to determine the GABA EC_{20} and EC_{80} values. These two concentrations were then used for initial compound screening.

A 5 mM stock solution of forskolin in pure water was diluted to 180 µM in pure water and mixed with 2xHBSS buffer with an equal volume. Afterwards, 5 µL of the prepared mixture (90 µM forskolin in 1xHBSS) was pipetted on three rows and columns of a 384-microplate using a multichannel pipette. After pipetting the mixture, the pre-incubated cells were immediately dispensed on the microplate and placed in the plate reader (Fig. 17). The cAMP reagents, from the HitHunter™ kit, were then dispensed at different times into the microplate. Finally, the results were read after 14 hours.

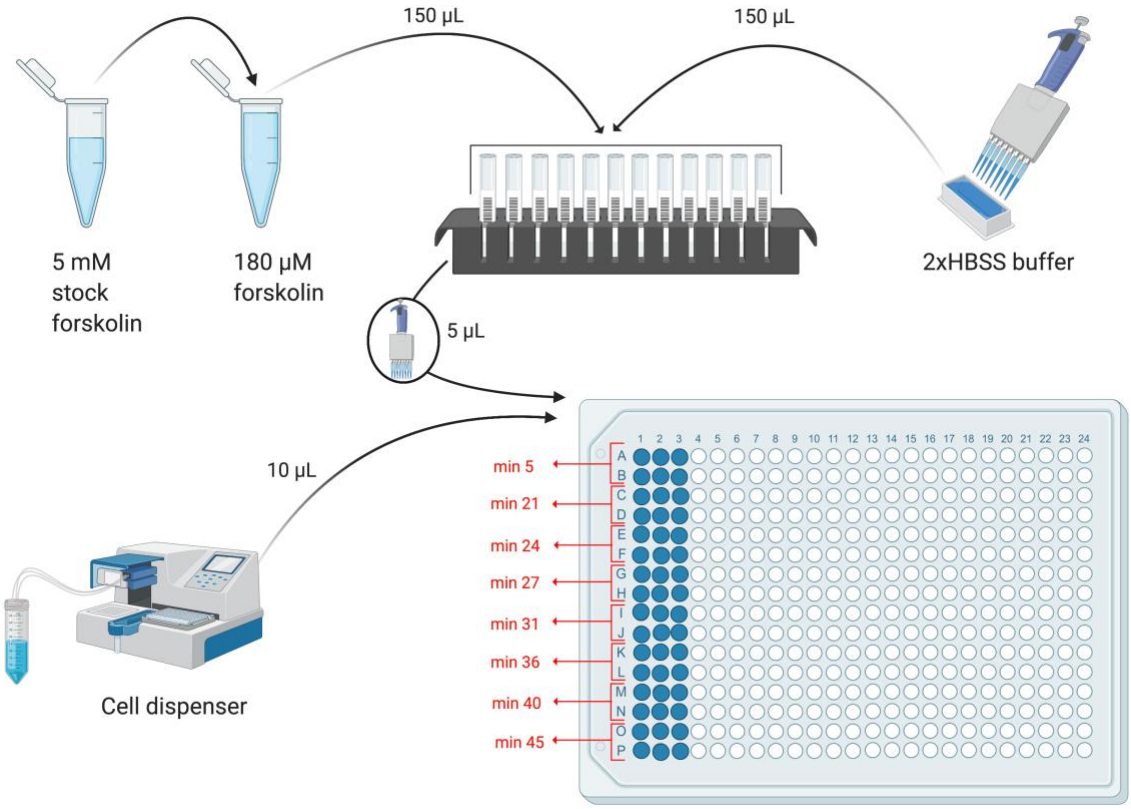

Figure 17 The time-dependent cAMP assay procedure.

3.2.5.1 Wild-type cAMP assay

Forskolin was prepared by diluting two stock solutions of 5 mM to two different solution samples of 180 µM, one stock diluted in water and the other diluted in 2xHBSS buffer. The stock solutions of the test compounds were retrieved from the freezer and placed at room temperature to thaw. Each stock solution with 20 mM was first diluted to 10 mM and then to 60 µM (6 µM for one of the compounds with poor solubility). Test compounds that were soluble at 2xHBSS solution from the solubility test, cited in 3.2.3, were diluted with 2xHBSS buffer, whereas test compounds that were soluble in D-glucose and NaOH solutions were diluted in their corresponding appropriate solution. Forskolin diluted in water was mixed with the test compounds diluted in 2xHBSS buffer with an equal volume of 100 µL each. Forskolin diluted in 2xHBSS buffer was mixed with the test compounds diluted in D-glucose and NaOH solutions with an equal volume of 100 µL of each.

Eventually, 5 µL of each prepared forskolin-test compound mixture was pipetted into the microplate using a multichannel pipette. After pipetting the mixture, the pre-incubated wildtype cells were immediately dispensed on the microplate and incubated in the plate reader for 24 minutes at 25 °C. The 24 minutes reaction time was determined from the time-dependent cAMP assay explained in 3.2.4. Following the 24 minutes reaction time, the cAMP reagents, from the HitHunter™ kit, were dispensed in the microplate, and the results were read after 14 hours.

This assay was repeated three times over three days. Fig. 18 illustrates the procedure performed.

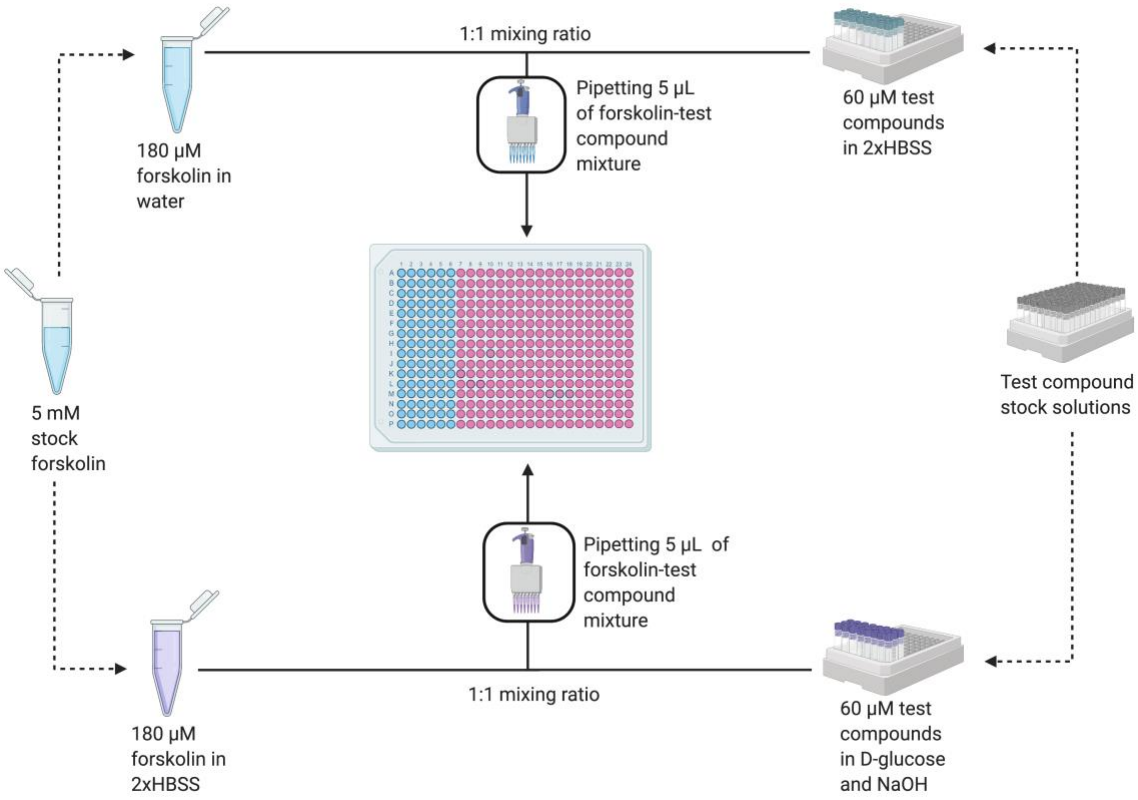

Figure 18 Wild type cAMP assay procedure.

3.2.5.2 GABA dose-response cAMP assay

Forskolin was prepared by diluting 5 mM stock solutions to a 180 µM sample solution. GABA powder was weighed to obtain a stock solution concentration of 40 mM, and a series of dilutions were performed. Eight different dilutions were selected (shown in Fig. 19) in the assay. Each sample of the GABA dilutions was mixed with the 180 µM diluted forskolin solution with an equal volume of 120 µL each.

A 5 µL of each sample mixture was pipetted into six wells of the 384-microplate with a multichannel pipette. The cell suspension was then dispensed into the microplate using a cell dispenser. Once cell suspension was dispensed, the microplate was immediately placed inside the plate reader and incubated for 25 minutes at 25 °C.

Following the 24 minutes reaction time, the cAMP reagents, from the HitHunterTM kit, were then dispensed in the microplate, and the results were read after 14 hours. Fig. 19 illustrates the procedure performed.

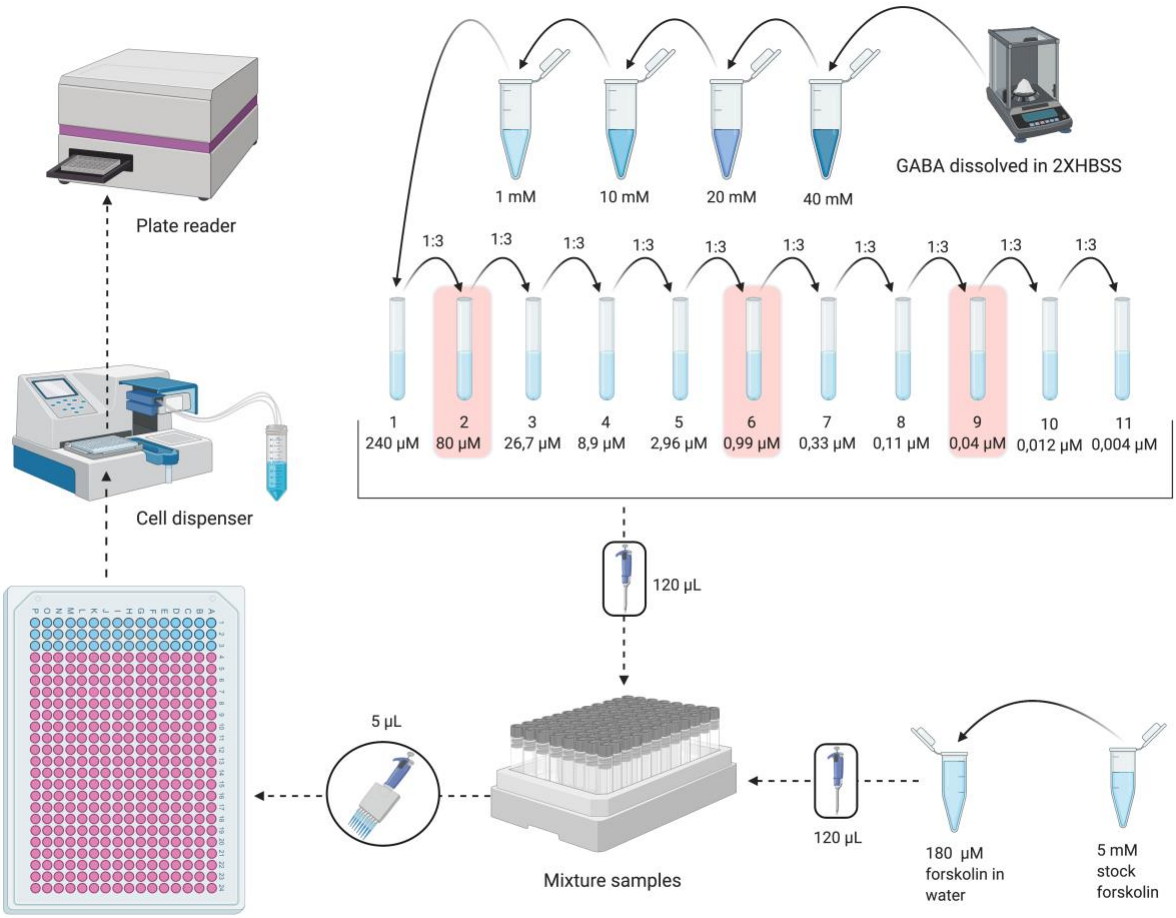

Figure 19 Dose-response cAMP assay procedure. *The dilutions marked with red color (2, 6, and 9) are excluded from the testing.*

3.2.5.3 EC_{20}/EC_{80} cAMP assay

The GABA serial dilution that most close to GABA EC_{20} and EC_{80} were used in test compound screening, which is around 27nM and 740nM, respectively. In the final assay mixture, the concentration of forskolin was 30 µM and test compound was either 10 µM or 1 µM based on their solubility. Eventually, 5 µL of each prepared forskolin-GABA-test compound mixtures were pipetted into the microplate using a multichannel pipette. After pipetting the mixture, the pre-incubated $GABA_B$ cells were immediately dispensed on the microplate and incubated in the plate reader for 24 minutes at 25 °C. The 24 minutes reaction time was determined from the time-dependent cAMP assay explained in 3.2.5.
Following the 24 minutes reaction time, the cAMP reagents were dispensed in the microplate, and the results were read after 14 hours.

This assay was repeated two times. Fig. 20 illustrates the procedure performed.

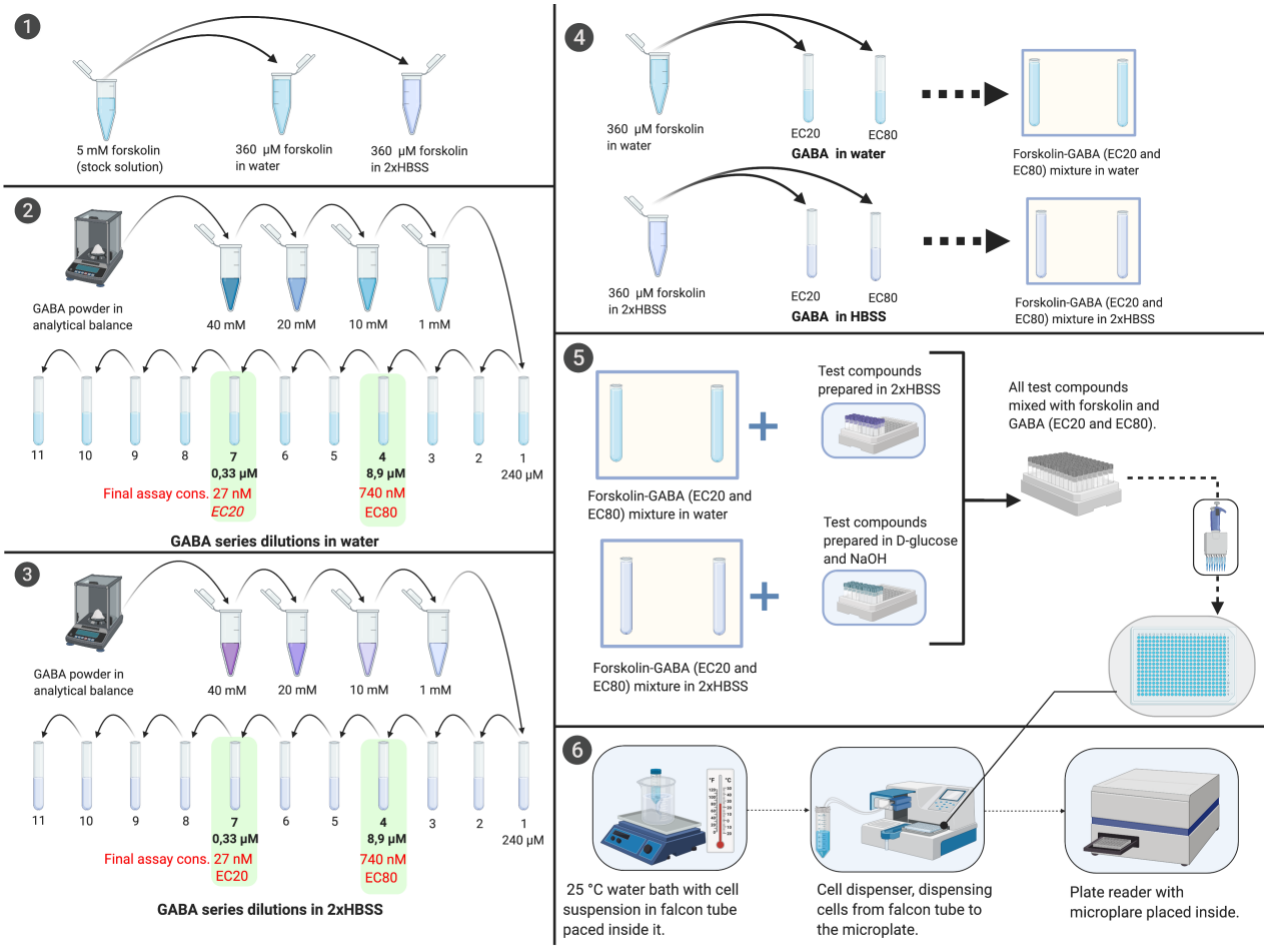

Figure 20 EC_{20}/EC_{80} cAMP assay procedure.*1. Forskolin preparation, 2. GABA series dilution in water, 3. GABA series dilution in 2xHBSS buffer, 4. GABA-forskolin mixing, 5. GABA-forskolin mixing with test compounds and pipetting into microplate, 6. Cells dispensing and incubation in plate reader.*

3.2.5.4 GABA dose-response with compound A-8

The effect of compound 8 at a fixed concentration (10 µM) towards GABA dose-response was performed. First, the same 8 serial dilutions of GABA were prepared in water. Each dilution was mixed with the same volume of 360 µM forskolin in water. The GABA and forskolin mixture were then mixed in 1:1 ratio with either 2xHBSS buffer or 60 µM compound 8 in 2xHBSS. The rest of the assay procedure and assay conditions are the same as compound screening.

This assay was not performed by us due to the coronavirus situation. Our supervisor was kind and helped to perform the remaining of the in vitro test.

3.3 Homology modeling of an active $GABA_{B2}$

Molsoft Internal Coordinate Mechanics (ICM) software (150) was used for the homology model construction of an "active" $GABA_{B2}$ model. The main purpose of homology modeling part is to gain experience and understanding of the procedure.

3.3.1 Template identification and target sequence modification

The 7TM structure of the mGlu1 receptor in its "active" form including an agoPAM was used as a template (manuscript in preparation). The entire target sequence of GABA$_{B2}$ (Uniprot accession number: O7899) were retrieved from the Uniprot database (http://www.uniprot.org). The length of the complete sequence was manually modified to code exclusively for the 7TM of GABA$_{B2}$ with 278 residues. The adjustment of the query sequence was guided by Wu (61).

3.3.2 Template-target sequence alignment

The target sequence of GABA$_{B2}$ coding for the 7TM domain was aligned with the extracted sequence of the template. Manually adjustment of the alignment was applied and guided by Wu (61). The final template-target sequence alignment used for building an active form of GABA$_{B2}$ homology model is found in Fig. 21.

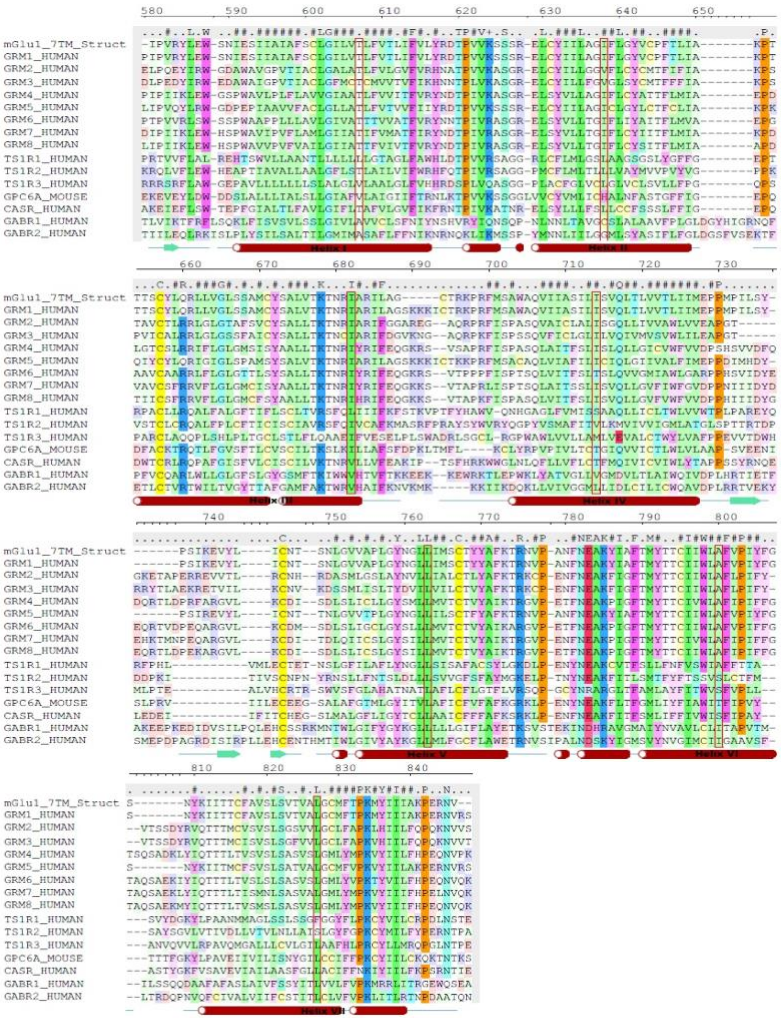

Figure 21 ***Target-template sequence alignment.*** *Sequence alignment of human class C GPCR 7TM domains. Secondary structural elements in the human mGlu$_1$ 7TM structure are shown under the sequences. Uncoloured residues show lack of conservation, while colouring highlights conserved amino acids with specific functional properties (green: hydrophobic, blue: basic, red: acidic, magenta: aromatic, cyan: small polar, orange: proline, yellow: cysteine). The graphics were prepared using ICM molecular modeling package (Molsoft LLC) (61).*

3.3.3 Model construction and refinement

Based on the target-template sequence alignment, one homology model of $GABA_{B2}$ in its "active" form was created. The constructed model was then exported to Schrödinger Maestro (143) and the protein preparation Wizard (151) was used for processing, refinement, and model evaluation. The model was processed by assigning bond orders and adding missing hydrogens using Prime.

3.3.4 Model evaluation

Following protein preparation, analysis of the Ramachandran plot was necessary to estimate the quality of the constructed model. The dihedral angles that fit perfectly to the secondary structure element will be included in the acceptable region of the Ramachandran plot. The quality of the model was evaluated using PROCHECK that provided details about the Ramachandran plot. Considering our interest lies in the allosteric binding pocket of the model, evaluation and optimization of such binding site are of more importance. Therefore, Glide docking and Induced Fit docking were applied.

3.3.4.1 Generation of active compounds and decoys

72 known PAMs and large number of decoys, retrieved from the previous paper (81), were used in the docking procedure to evaluate the model. These compounds were already prepared for docking by Schrödinger Epik (152) and Schrödinger LigPrep (145) applying OPLS2005 forcefield, from the prior study (81).

3.3.4.2 Receptor grid generation

The template includes an agoPAM in its structure. The template structure and the constructed model were superimposed, and ligand position on mGlu1 template were used to identify its corresponding position on the constructed $GABA_B$ model. Receptor Grid Generation was used to specify the allosteric binding site for the docking procedure using Schrödinger Glide. The grid box was orientated encompassing the agoPAM with an outer box-size of 20 Å and inner box-size of 10 Å, as standard settings.

3.3.4.3 Glide docking

The known PAM clusters and decoys were docked into the processed grid box. Standard precision (SP) docking protocol with default settings was utilized. Cluster 4 PAMs had the best docking score, but the docking score was not the only criterion for the selection. Ligand orientation and position in the bindings pocket were taken into account too. All the clusters docked in the center of the binding pocket, but cluster one has the most satisfactory docking poses among all other clusters (results not shown). The PAMs in cluster one docked similarly compared to the other PAM clusters. Therefore, the PAM with the best docking score, CGA 44010 (-5,268 kcal/mol) from cluster one (81), was used in the IFD procedure. The lower the docking score, the better the score and affinity a ligand have to the model (129).

3.3.4.4 Induced fit docking (IFD)

Most docking programs are using a rigid target structure and a flexible ligand while docking. However, modern improvements also introduce flexibility into the target structure. IFD starts by docking the active ligand with Glide and then adds flexibility to the binding pocket using Prime. The application of the IFD protocol with default settings produced a various number of new $GABA_{B2}$ models. Few ligand-target complexes were generated following IFD procedure, and the model with the best score was further appointed as the final model.

3.3.4.5 Glide re-docking

The known PAMs and decoys were then re-docked to the adjusted model from the IFD protocol. An identical grid box was generated using the same settings implemented earlier by encompassing the ligand in the model (see 3.2.6.4.2) and the same Glide docking set with standard precision was used as well (see 3.2.6.4.3).

4 Results

4.1 In silico

4.1.1 MolPort database screening

The overall description of the approach with the MolPort database is shown in Fig. 22.

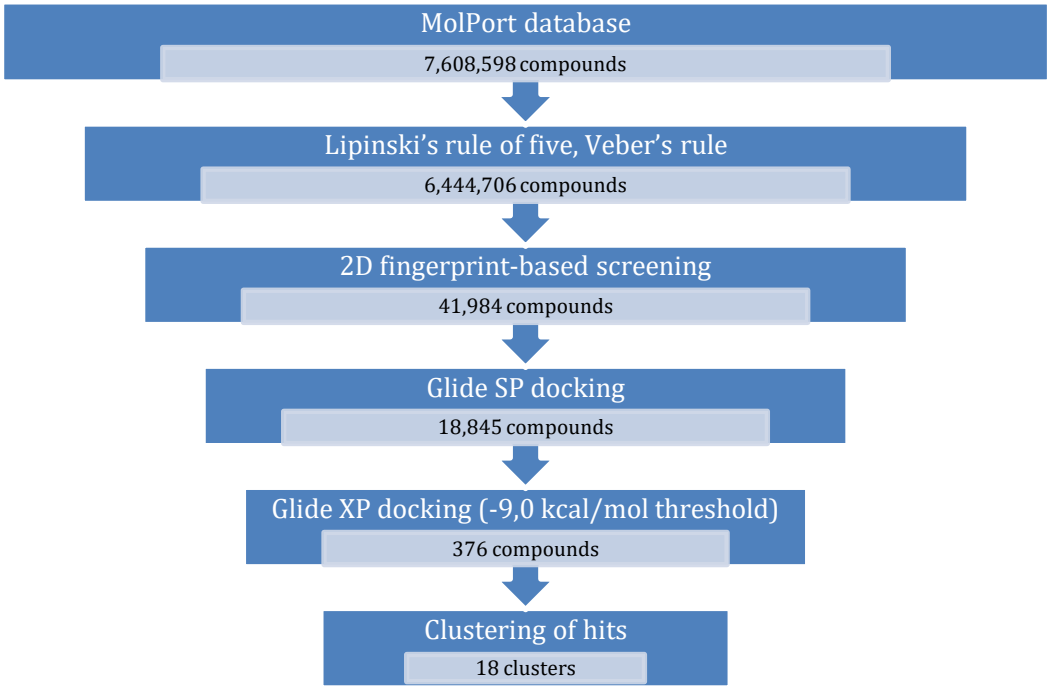

Figure 22 The overall approach with the MolPort database. *The figure demonstrates the multiple actions applied and the number of compounds in each step is presented in black. The ultimate remaining compounds in the last step is 376, which were clustered to 18 clusters in the final step.*

Based on the MOLPRINT2D fingerprint and Tanimoto similarity metric, a 2D fingerprint-based similarity screening was performed. Each reference NAM screening provided a certain number of compounds, summarized in Tab. 7. The number of compounds retrieved for all the six references NAMs combined is 41,984.

Table 7 The particular similarity screening approach and outcome regarding each reference NAM*. The table shows the name and structure of each NAM and the threshold value appropriated to accept a certain number of compounds. A typical MOLPRINT2D fingerprint and Tanimoto similarity metric were used for all the NAMs.*

Reference NAMs	Similarity threshold	Number of compounds
Benzydamine N-oxide	0,152	8,566
TI-3	0,152	2,972
TI-5	0,171	9,182
TI-6	0,171	6,849
TI-36	0,231	8,572
CLH304a	0,1	5,843

The output from LBVS, 41,984 structures, were docked into the selected model of $GABA_{B2}$ 7TM domain, c5.m2.s011. The detailed summarization of the exact number of compounds collected in each step, is shown in Tab. 8.

Table 8 Detailed summarization of the exact number of compounds collected by each action taken.

Reference NAMs	Input from LBVS	Output SP docking before duplicate removal	Top 10% docked with XP	Output -9,0 kcal/mol threshold
Benzydamine N-oxide	8,566	3,176	318	100
TI-3	2,972	1,158	116	27
TI-5	9,182	4,079	408	53
TI-6	6,849	5,951	595	94
TI-36	8,572	2,063	206	9
CLH304a	5,843	2,418	242	92

Finally, 16 hit compounds were selected to be tested experimentally in the laboratory (Fig. 23).

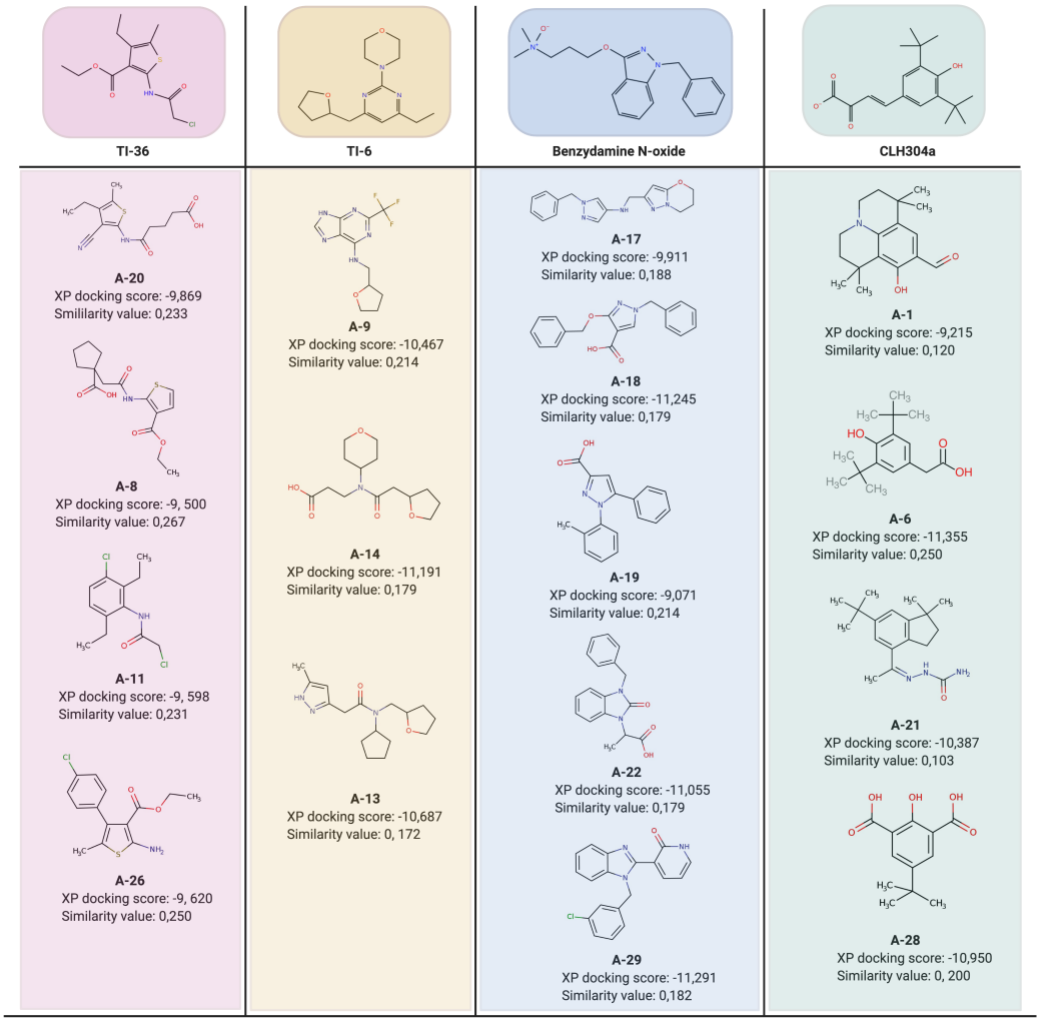

Figure 23 Final 16 hit compounds selected to be tested experimentally. *The figure also shows XP docking score and similarity value to their corresponding reference NAM structure, for each hit compound.*

4.2 In vitro results

4.2.1 Forskolin dose-response cAMP assay

The calculated forskolin EC_{50} value (3,53 µM) turned to be similar to that of manufacture's tested value, which is around 3,2 µM (Fig. 24). The cAMP assay with test compounds was performed using a close concentration of EC80 value (30,8 µM), which is 30 µM of forskolin to stimulate cAMP.

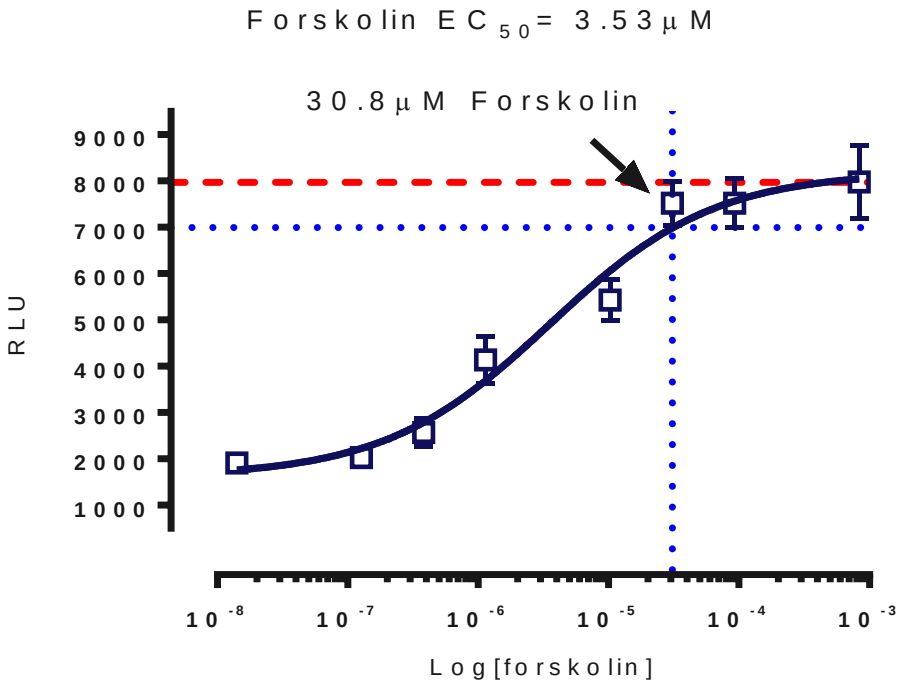

***Figure 24 Forskolin dose-response on GABA$_B$ cells**. Reaction was run at 25ºC. Prior to reaction, cells were incubated 2.5 hours at 25ºC water bath. EC80 of forskolin is 30.8 µM.*

4.2.2 Forskolin time-dependent cAMP assay

Forskolin time-dependent assay shows that cells reach a maximum stimulation at around 24 minutes and are stable for at least 3 minutes (Fig. 25). This gives us 3 minutes assay window for stopping the reaction by dispensing cAMP reagents.

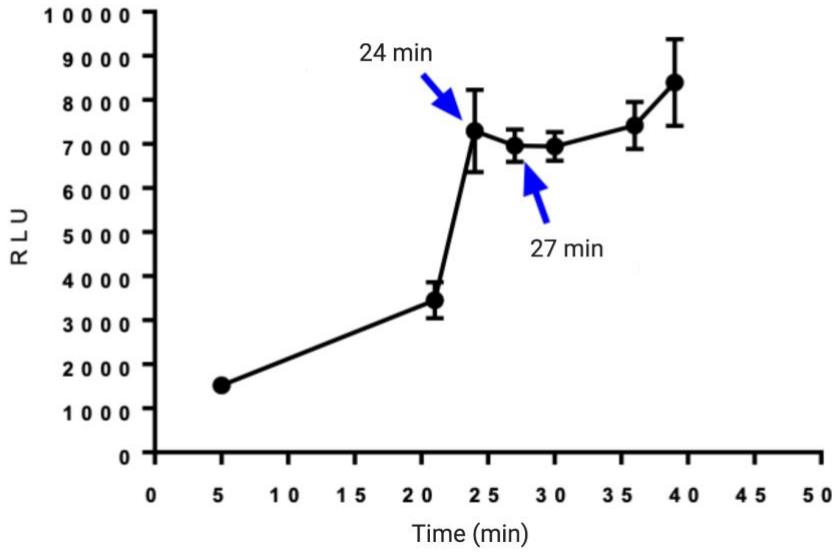

***Figure 25 Forskolin time-dependent assay on GABAB cells**. Reaction was run at 25 ºC. Prior to reaction, cells were incubated 2.5 hours at 25ºC water bath.*

4.2.3 GABA dose-response without test compounds

After 30 µM forskolin concentration was determined through forskolin dose-response assay, this concentration was used to run GABA dose-response assay to determine the $GABA_{EC20}$ and $GABA_{EC80}$ concentration for compound screening. The results show that $GABA_{EC20}$ was close towards 27 nM, and $GABA_{EC80}$ concentration was close to 740 nM (Fig. 26).

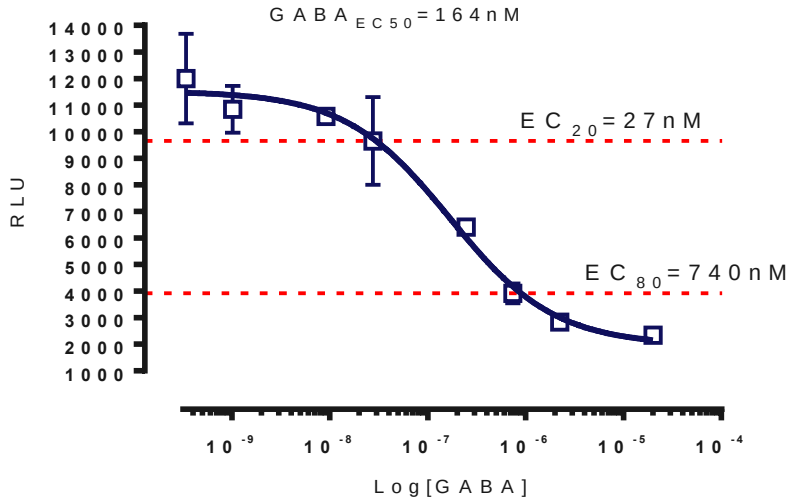

***Figure 26 GABA dose-response on GABAB cells.** 30 µ M forskolin was used. The $GABA_{EC20}$ (27 nM) and $GABA_{EC80}$ (740 nM) was determined. Reaction was run at 25 ºC. Prior to reaction, cells were incubated 2.5 hours at 25ºC water bath.*

4.2.4 Wild-type cAMP assay

This assay was necessary to determine if some of compounds have effect on cAMP signal by stimulating other targets in the cells. Since it is known that wild type CHO-K1 cells does not contain $GABA_B$ receptor, compounds that show activity on wild type (compared to forskolin control) will indicate that these test compounds affect cAMP signal by binding to other targets in the CHO-K1 cells. Therefore, the same compounds that will show similar activity on the $GABA_B$ cells can be excluded as off-target compounds. The test on wild type was repeated three times. The results from three different readouts showed that none of the test compounds have significant activity on wild-type cells (within 10% range of forskolin control). Therefore, none of the compounds were excluded from the upcoming test assays.

4.2.5 Functional $GABA_{EC20/EC80}$ cAMP assay

In the $GABA_{EC80}$ screening group (Fig. 27-30), compared to the control, compound A-8 and A-9 increased the cAMP signal, while compound A-1, A-20 and A-29 decreased cAMP signal. In the $GABA_{EC20}$ screening group (Fig. 27-30), compared to the control, compound A-8 and A-9 increased the cAMP signal, while the rest of the compounds showed inconsistent results from two repeat of the assay. In the forskolin only screening group (Fig. 27-30) where GABA is absent, compared to the control, compound A-9 increased the cAMP signal, while compound A-20 showed most significant decrease of the cAMP signal. The rest of the compounds either showed inconsistent results or the increase or decrease of the cAMP signal were not significant, considering the standard deviation.

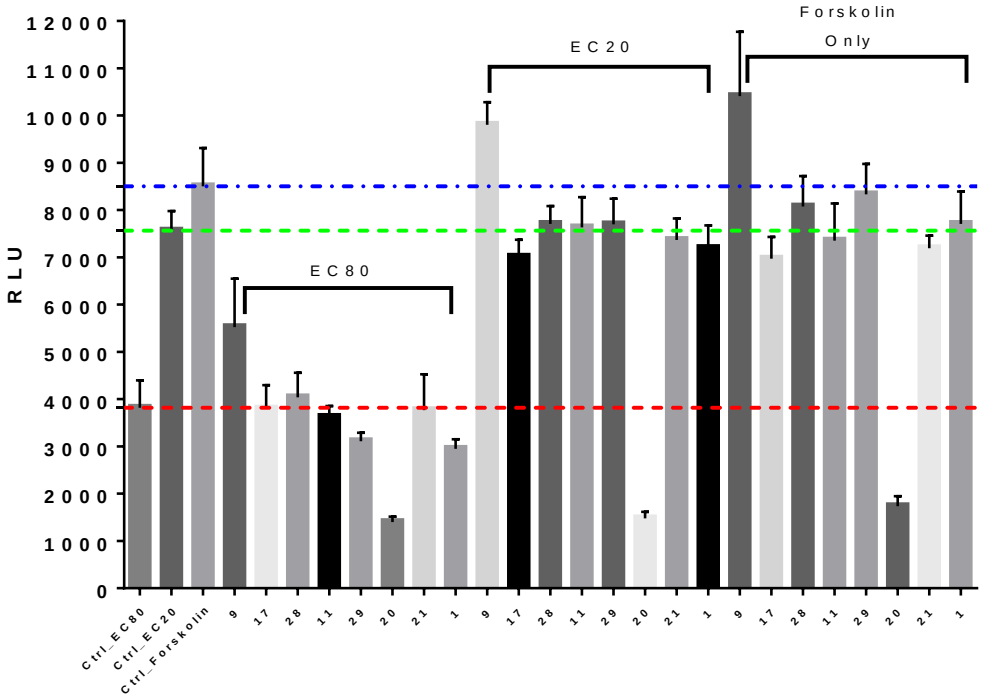

Figure 27 Functional GABA$_{EC20/EC80}$ cAMP assay (first read). *Reaction was run at 25 ºC. Prior to reaction, cells were incubated 2.5 hours at 25ºC water bath. Test compound screening at the presence of GABA$_{EC20}$ (27 nM), GABA$_{EC80}$ (740 nM) and forskolin (30 µM) only on GABA$_B$ cells. The Y-axes shows the relative light unit (RLU), while X-axes shows the test compounds. The dotted line is displayed to facilitate the comparison between controls and test compounds.*

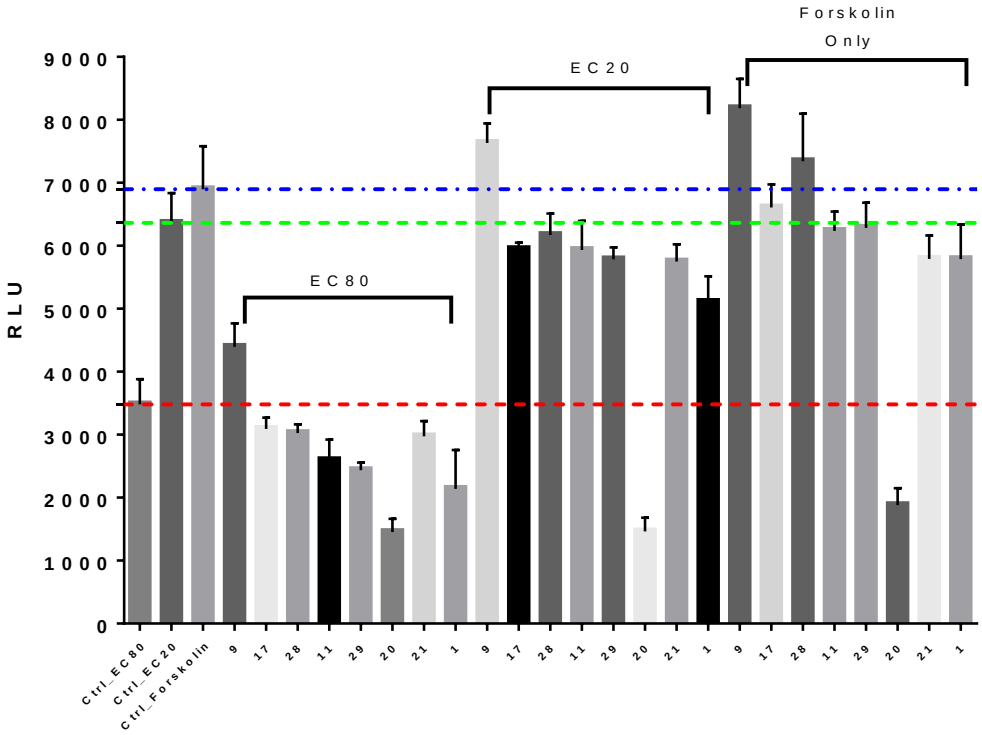

Figure 28 Functional GABA$_{EC20/EC80}$ cAMP assay (second read). *Reaction was run at 25 ºC. Prior to reaction, cells were incubated 2.5 hours at 25ºC water bath. Test compound screening at the presence of GABA$_{EC20}$ (27 nM), GABA$_{EC80}$ (740 nM) and forskolin (30 µM) only on GABA$_B$ cells. The Y-axes shows the relative light unit (RLU), while X-axes shows the test compounds. The dotted line is displayed to facilitate the comparison between controls and test compounds.*

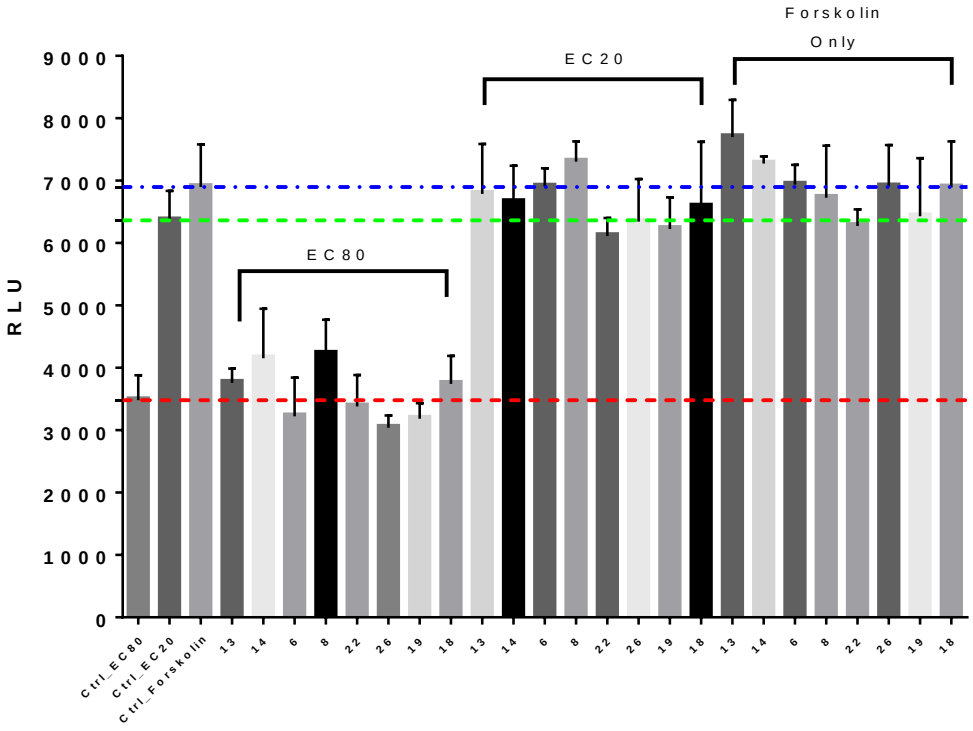

***Figure 29 Functional GABA$_{EC20/EC80}$ cAMP assay (first read)**. Reaction was run at 25 ºC. Prior to reaction, cells were incubated 2.5 hours at 25ºC water bath. Test compound screening at the presence of GABA$_{EC20}$ (27 nM), GABA$_{EC80}$ (740 nM) and forskolin (30 µM) only on GABA$_B$ cells. The Y-axes shows the relative light unit (RLU), while X-axes shows the test compounds. The dotted line is displayed to facilitate the comparison between controls and test compounds.*

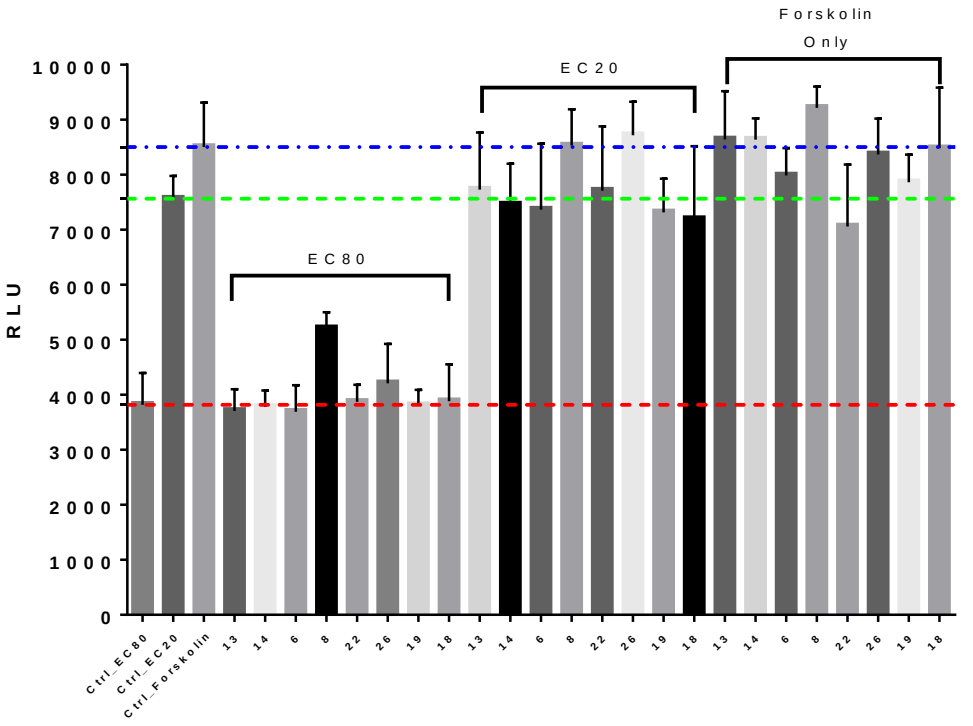

***Figure 30 Functional GABA$_{EC20/EC80}$ cAMP assay (second read).** Reaction was run at 25 ºC. Prior to reaction, cells were incubated 2.5 hours at 25ºC water bath. Test compound screening at the presence of GABA$_{EC20}$ (27 nM), GABA$_{EC80}$ (740 nM) and forskolin (30 µM) only on GABA$_B$ cells. The Y-axes shows the relative light unit (RLU), while X-axes shows the test compounds. The dotted line is displayed to facilitate the comparison between controls and test compounds.*

4.2.6 GABA dose-response cAMP assay with test compounds

Comparing to GABA dose-response curve compound A-8 (Fig. 31) increased $GABA_{EC50}$ value from 294 nM to 442 nM.

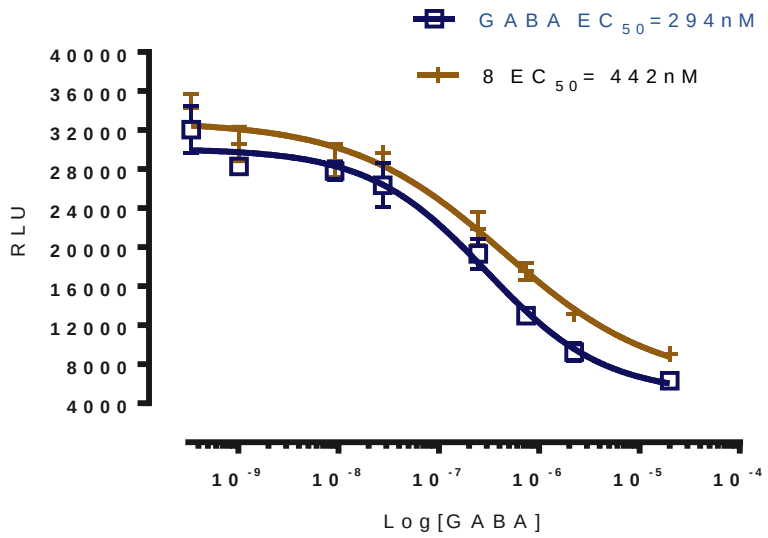

Figure 31 GABA dose-response assay on $GABA_B$ cells with or without 10 µM test compound A-8.

4.3 Homology modeling

One homology model of the 7TM of $GABA_{B2}$ was constructed using ICM. The amino acid sequence similarity between the mGlu1 template and the $GABA_B$ 7TM domain was 22,36%. Following model refinement, Ramachandran plot evaluation was necessary to check the quality of the constructed model. None of the residues of the constructed model are outside the disallowed region, as shown in Fig. 32. The majority of the amino acids are located in a favorable region.

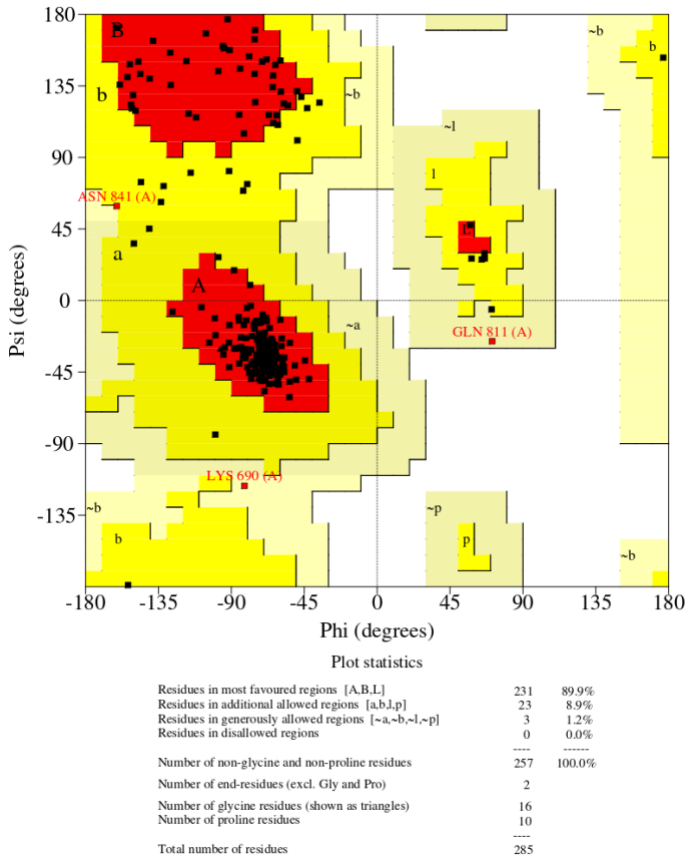

Figure 32 Ramachandran plot of the built model. *The plot shows the dihedral angels of amino acid residues present in the "active" homology model. The Phi torsional angles values are plotted on the Y-axes and Phi values on the X-axes. The red area represents the most favored regions, the dark yellow area represents additional allowed regions, light yellow represents the generously allowed regions, and the white area represents the disallowed regions.*

The induced-fit docking protocol provided several new different receptor complexes. The complex with the highest docking score was accepted as the ultimate model. The IFD procedure was necessary to optimize the binding pocket of the constructed model. Following IFD, docking of the same PAMs used before the IFD was implemented. By using the IFD protocol, the binding site of the constructed model was improved. All the PAMs docked before the IFD, were able to re-dock in the new optimized bindings pocket of the generated model. The results from the dockings score (Tab. 9) shows that the binding site has improved.

Table 9 Improvement of the constructed model*. The table shows the Glide dockings score range of each PAMs cluster. The score scale gets increased for all the clusters after applying the IFD protocol.*

Clusters PAMs	Range Glide docking before IFD (kcal/mol)	Range Glide docking after IFD (kcal/mol)
1	(-4.317 – -5.268)	(-5.660 – -6.720)
2	(-5.523 – -6.796)	(-6.339 – -7.732)
3	(-4.320 – -5.800)	(-6.062 – -7.140)
4	(-5.423 – -7.914)	(-6.769 – -9.012)
5	(-5.471 – -6.554)	(-6.837 – -8.667)

5 Discussion

5.1 In silico

The main aim of the study is to identify new promising $GABA_B$ negative allosteric modulators. This is accomplished by the use of in silico virtual screening followed by in vitro testing in the wet lab. The advantage of using in silico virtual screening prior to in vitro testing is to make it feasible to process a massive number of compounds in a short time and reduce the number of compounds to be purchased and tested experimentally.

In the present study, compounds that reach the final step of the in silico virtual screening are referred to as hit compounds or hits which accounted for 376 compounds (Fig. 24), and only 16 compounds of these were tested experimentally in the laboratory for biological activity (Fig. 26). The combination strategy of ligand- and structure-based virtual screening was adopted in our study, and we were able to select 16 hit compounds from the virtual screening methods that were tested experimentally. Unfortunately, UiT was closed for students 12_{th} of mars 2020 because of the coronavirus situation and we was unable to perform the entire planned testing in the laboratory. Our chief engineer and my co-supervisor, Imin Wushur, therefore helped perform the $GABA_{EC20/EC80}$ cAMP assays and the GABA dose-response with a few compounds.

We managed to identify a promising NAM (compound A-8) and a possible PAM (compound A-20) and NAM (compound A-9) by testing their activity with the functional cAMP assay. We are more confident to conclude with compound A-8 since the compound was tested with the dose-response assay. Compound A-9 and A-20, on the other hand, require further testing to conclude assuredly. These compounds should be tested with other type of assays to be even more sure.

Our colleagues from Medical Pharmacology and Toxicology, have earlier successfully performed virtual screening in the identification of active serotonin binders (SERT) binders (121), and $GABA_B$ compounds (ongoing project; unpublished results). A combination of ligand- and structure-based modeling has become a popular strategy in virtual screening. It is believed that the unification of these two methods can improve the strengths and overcome the disadvantages of each method, hence producing more successful virtual screening (153). These methods can be combined sequentially or in parallel. The sequential combination of virtual screening methods is widely used and more successful compared to the parallel combination (153). In our approach, the sequential combination of the methods was utilized. This strategy helped to reduce the number of hits to a sensible number for in vitro testing. The initial compounds in MolPort were filtered using drug-likeness filters followed by similarity ligand-based method, and finally extensive screening by docking protocol into $GABA_{B2}$ homology models.

5.1.1 ADME properties

Approximately half of the orally administered FDA-approved small-molecules comply with Lipinski's rule of five (154), indicating that many drugs go beyond the rule of five (155). Due to the simplicity of Lipinski's rule of 5 and Veber's rule, they can be implemented early in the drug discovery to increase the chance of success. Even though these filters focus mainly on solubility and permeability, it can extrapolate to other pharmacokinetic properties such as

metabolic stability and excretion (156). MolPort is a collection of millions of compounds from many suppliers. Some databases implement ADME filtering protocols, while others do not. Therefore, the employment of Lipinski's rule of 5 and Veber's rule (Tab. 2) was necessary to weed out unsuitable compounds and to lessen the number of compounds in the virtual screening protocol.

ADME properties can be included in filter applications that can either be used before or after the virtual screening (156). We decided to apply Lipinski's rule of 5 and Veber's rule before the initiation of the virtual screening, while other physiochemical properties (QikProp; table 7) were implemented after the virtual screening to facilitate the selection of compounds tested experimentally. Modifying the lead compound structures in order to obtain better affinity and selectivity, can alter the ADME properties. On the other hand, Lipinski et al., claims that it is simpler to optimize pharmacokinetic properties in early-stage drug discovery, while receptor binding affinity is readily optimized in the late stage (119). Applying filters before the actual screening may increase the risk of removing compounds that may be drug candidates. However, by applying ADME filters on the entire virtual screening library, we managed to quicken the identification of optimal structures, and this is an absolute necessity in the current study. By performing this way, time and resources were spared and compounds with desired physical-chemical properties were obtained.

ADME properties can be predicted computationally by the use of specific software. Lipinski's rule of 5 is the most commonly used method in predicting ADME properties, which have become standard protocols for virtual screening (156).In the current study, Lipinski's rule of 5 and Veber's rules, were implemented in the search for negative allosteric modulators. Lipinski's rule of 5 is applicable only for orally administered drugs that are absorbed through passive transport mechanisms (119). Nowadays, many advanced routes of administrations and even advanced delivery systems have been developed. Many compounds can be potential drugs even though they fall outside the scope of rules implemented. Besides, some drugs are exceptions for such rules because they can have structural hallmarks making them serve as a substrate for active transporters. However, passive diffusion is still the most central for drug permeability.

5.1.2 Ligand-based virtual screening

Ligand-based methods measure the similarity of the compounds in databases to the active reference ligands. These methods are based on the concept that similar compounds have similar properties and are most likely to have the same mechanism, and hence show related biological activity (157). Most of the compounds in MolPort database have not been tested for biological activity, and based on Klopmand et al., paper, Molport compounds that are structurally similar to our reference NAMs should exhibit similar biological activity as well (157). Ligand-based virtual screening is used mainly for two reasons, the reason mentioned above and to process the excessive number of compounds (approx. 6,5 million after the application of filters in the present study) in a short time that is not possible with only structure-based virtual screening. Ligand-based virtual screening performance also allows us to estimate the method performance and suggest several improvements for further research.

5.1.2.1 2D Fingerprint-based screening

Six reference NAMs were used to screen the MolPort database. The 2D fingerprint was calculated for each reference NAM and all the compounds retrieved from the database. 2D fingerprint screening is one of the most commonly employed ligand-based techniques in virtual screening. It has been proved that similarity search based on the 2D fingerprint-based screening is more successful in identifying active compounds than docking methods, despite the absent information about interactions with the target (158). However, the same study found out that docking methods are efficient in retrieving more diverse actives than 2D methods.

In the software package Canvas (142), there are many possible fingerprint methods with a combination of different variables. For instance, there are various types of fingerprints and atom typing schemes. In our ligand-based screening, the MOLPRINT2D was used as a fingerprint type in combination with MOL2 as an atom type scheme. It is seldom known which fingerprint is the most suitable for a set of ligands. Luckily some studies compared different fingerprint types and found out that all types tested, MOLPRINT2D included, have similar retrieval rates on average, but each type has a particular property (122,124). According to Duan et al., MOLPRINT2D is the most appropriate choice when there is no prior experience about which fingerprint works best (122). Furthermore, MOLPRINT2D has the lowest variation of active compounds retrieval compared to other fingerprints (122). It was concluded that there is no optimal combination of fingerprint settings, and the MOLPRINT2D is a less sensitive method when a specific setting combination is unknown (124). We would test different fingerprint methods to optimize the screening for negative allosteric modulators if time was not a restricting factor.

The 32-bit address space has been used in our approach. The advantage of applying this bit size is that collision (different fragments setting the same bit) happens just once for every thousand structures fingerprinted, which is very small (122). To avoid losing information, we could use the 64-bit, where collisions are almost entirely eliminated, but it will consume more time to calculate the fingerprints.

An alternative approach would be to combine each fingerprint of all reference NAMs used to a single fingerprint, referred to as "modal fingerprint". Combining reference ligands into a modal print may increase the retrieval rate of active ligands compared to the use of a single reference ligand (122). Modal fingerprint, however, should not be performed using reference structures from different structural classes, as in our case. Using modal fingerprint can be a good choice in the future when more similar NAMs of $GABA_B$ receptor have been identified. However, we chose to perform a separate screen for each reference NAM to facilitate the selection of the final hits. The variation of the biological activity level of the reference NAMs is also one of the reasons for the separate screening.

Based on the MOLPRINT2D fingerprint, the similarity between the reference NAMs and each compound retrieved from the MolPort database was calculated. The main obstacle with similarity methods is their bias toward reference ligands and the struggle of deciding which reference structure to use (153). In our situation, we have limited data available from our research group, and to our knowledge, there is only one well known NAM (CLH304a) of $GABA_B$ receptor published (80).

The Tanimoto similarity metric (Eq. 9) was used to compute molecular similarities. It is a well-known coefficient and is the preferred method of fingerprint-based similarity, especially when information about investigated molecules size is absent (117). The compounds retrieved from the MolPort database were over six million and varied in size. The MOLPRINT2D fingerprint performance was tested based on the Tanimoto coefficient (122), hence choosing another similarity metric than Tanimoto may require the selection of another fingerprint type. A comparison of 12 similarity metrics, Tanimoto included, shows that there is little variation in performance. These metrics were classified in "on" bits and "off" bits, where the "on" bits class consider only the on bits. The metrics belonging to the "on" class had the best performance, and Tanimoto is one of the "on" class topping the list (124). The application of Tanimoto yielded low similarity values based on visual inspection of ligand structures. It is stated that Tanimoto has an inherent bias toward specific similarity values and produces low similarity values even when reference molecules have just a few bit sets in its fingerprint (Flower1997).

Due to the different possible combinations of fingerprint methods and similarity metrics, there is no regular cut-off value defining a specific range of similarity that yield a similar activity (159). Therefore, in order to determine the similarity cut-off value, we had to inspect the structures manually. Surprisingly, many target structures were similar to their corresponding reference NAM, even when the Tanimoto similarity value was as low as 0,1. Consequently, the cut-off value was low and different for each reference NAM group (table 10). For instance, the Tc similarity value between benzydamine and its metabolite, benzydamine N-oxide, was 0,591 (Fig. 33).

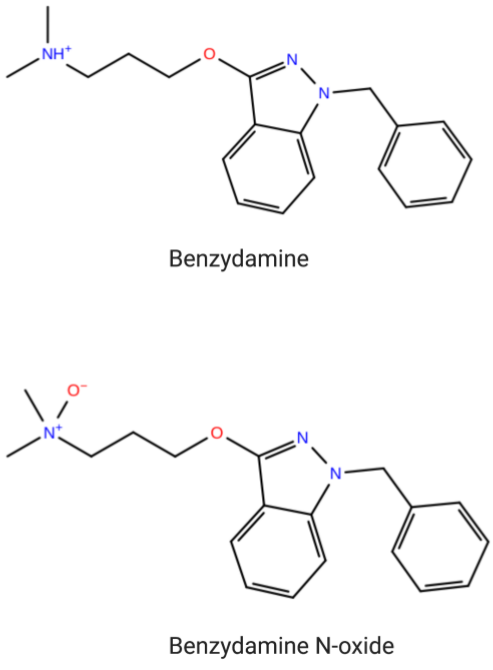

Figure 33 Benzydamine and its metabolite, benzydamine N-oxide.

Our in vitro results show that compound A-20, A-8, and A-9 are hit compounds with certain activity on $GABA_B$ receptors. The similarity value for each active hit compound seems inadequate (Fig. 23), but they display common fragments to their corresponding reference

structure (Fig. 23). It is noteworthy that high similarity value does not necessarily always mean compounds will have the same activity. The activity of a compound could dramatically change by minor structural changes because these changes can influence ligand-target interactions (159). It also seems that the receptor model allows structurally different ligands to bind its binding site.

Based on the argumentation from different research papers and our results, it is unknown whether the similarity values computed is lower than it should be, or similarity is not a reliable measure for activity. It will be helpful to test other fingerprint methods and similarity metrics with our subset of compounds to determine the most appropriate combination of variables.

Different ligand-based methods could be applied to our work, and if we had more time, we would have tried other ligand-based methods. For example, the use of 3D-shape similarity which is based on the fact that molecules with similar shapes are most likely to fit in the same binding pocket and display a related biological activity (160). Alternatively, the electrostatic potential similarity that measures the similarity between two compounds via their electrostatic potentials could also be used (159). Another method of the ligand-based approach is QSAR modeling (2D- or 3D-QSAR), where properties of a set of reference ligands can be used to construct a static model of the biological activity and then use it to retrieve new compounds (153).

5.1.2.2 Structure-based virtual screening

Unlike ligand-based virtual screening, the structure-based virtual screening is a receptor-based computational method, which involves mainly molecular docking of each database ligand, MolPort, into the binding site of the target receptors, $GABA_B$ homology models (81). The main purpose is to predict a binding pose inside the binding site and consequently measure the quality of the pose using the docking score. The docked compounds are then ranked based on the docking score, and a small subset, 16 hit compounds, are selected for experimental testing of the biological activity. Nevertheless, in order to perform this strategy, 3D-structure of the $GABA_B$ receptor is required, preferably a structure determined experimentally. So far, there is no experimentally solved 3D structure available for the 7TM domain of the $GABA_B$ receptor and homology models were our only option. Seven different conformations of $GABA_{B2}$ 7TM domain, constructed based on mGlu1 and mGlu5 templates were available (61,65). Once more, due to the limited time of the study, only one model was used to facilitate results analysis.

5.1.2.2.1 Homology models

Since our goal is to identify new NAMs, evaluation of the models had been performed by molecular docking of reference NAMs against decoys. The actual purpose of this action is to investigate which binding pocket was best in discriminating between NAMs and decoys. This is not the only possible strategy, and we could use all the seven models generated by Thibaud Freyd (81) in the docking of the MolPort database. However, our strategy first helped to appoint the most suitable model in retrieving negative allosteric modulators, and second to spare us time in our short research period. Using only a single conformation of the target receptor in the docking protocol may lead to the loss of potentially active ligands. Therefore,

we recommend using multiple conformations of the target receptor when XP Glide docking is performed, and when time is not limited.

The reference NAMs docked against decoys, are compounds with known biological activity. Decoys, on the other hand, are compounds unlikely to bind the target. The decoys were generated from the previous study (81)**,** and most of them were property-matched decoys. These decoys are not tested against our target protein but are presumed to be inactive compounds. Following the docking protocol, the visual examination revealed that many decoys were docked outside the binding pocket. Moreover, many of the decoys were large molecules that extend outside of the defined binding site. For this reason, the docking score for some decoys was better than the reference NAMs. Hence, the result analysis and model selection were based on the docking score of NAMs in the seven models and the number of decoys docked (Tab. 11), in addition to the visual inspection of compounds.

Identification and description of the binding pocket are necessary for docking performance and is a critical step in docking protocol. 3D-ligands bind within a predefined size and shape of a specific active site or binding pocket. Therefore, the success of the docking procedure and structure-based virtual screening is highly reliant on the quality of the predefined binding pocket architecture (114). It is specified in the previous paper (81) that an outer grid box size of 25 Å is critical to ensure that specific "hotspot" residues such as Gly706 and Ser710 were included in the grid map. In the context of ligand-protein interactions, a "hotspot" residue is a residue in a target protein that has a high propensity for ligand binding and hence is necessary for drug discovery in pharmaceutical research (161). Accordingly, the binding site for the docking procedure was defined precisely as the previous paper described, with a size of 25 Å. As previously discussed, there is no crystal structure of the 7TM domain of the $GABA_B$ receptor and hence comprehensive information about the allosteric binding site of $GABA_B$ receptor. Only one site-directed mutagenesis study of $GABA_B$ 7TM domain has been published, which reported the effects of implementing mutations on the 7TM subunit of $GABA_{B2}$ (162). The data from the mutagenesis study was used during the construction of the seven homology models (81).

The structure-based virtual screening of the MolPort database was performed using the "inactive" conformation of the $GABA_{B2}$ 7TM domain as the main goal was to identify NAMs. However, by modeling an "active" conformation of the $GABA_{B2}$ 7TM domain, we could compare the active conformation to the inactive conformation. Moreover, a binding site optimization of the constructed model is performed in order to retrieve positive allosteric modulators more efficiently. If further in vitro testing also validates that one of our hits is a PAM, then it would be very interesting to dock that PAM into an "active" conformation of $GABA_{B2}$ 7TM to compare docking results in the active to the inactive models.

It should be kept in mind that homology modeling studies are theoretical approaches just as docking protocols. Therefore, validation is highly required next to homology construction. Depending on the purpose of using the 3D-model, other conditions should be evaluated. If the aim of modeling is ligand docking, the template structure preferably should be co-crystallized with a ligand. For instance, if it is desired to model receptors in an active state, the selected template should be bound to an agonist, whereas the template representing the inactive conformation should be bound to an antagonist (44). The template used in our homology modeling is bound to an agoPAM, and we seek to build an "active" structure of the $GABA_B$ receptor. Since the receptor is bound to a negative allosteric modulator and built in a

way to exhibits an active-like conformation, it is most likely more efficient in identifying hit compounds during virtual screening.

The model was evaluated by using the Ramachandran plot (Figure 32), which revealed that the majority of the amino acids are located in a favorable region, indicating a pleasing quality of the model. Although 26 residues are in the additional allowed and generously allowed regions, they are found to be in the loop regions, and as earlier discussed, they are challenging to model.

Unique structure features were also evaluated and compared to the "inactive" $GABA_B$ model, c4_m2_4or2, that was constructed based on the "inactive" mGlu1 template (81). For instance, a disulfide bond was observed in our constructed model, connecting the TM3 with the ECL2. This disulfide bond is conserved through all class C GPCRs (61).

The superimposition of the "inactive" and "active" structures of the $GABA_B$ 7TM domain shows a slight conformational rearrangement of the 7TMs (Fig. 34). All TMs of the "active" structure seems to have an outward shifting, especially for TM3, TM5, and TM7. This is in agreement with the cry-EM study of $GABA_B$ receptor (68), yet to be peer-reviewed. This study demonstrated an obvious outward shifting by 5 Å of extracellular tips of TM5 and TM7. Also, the "inactive" structure seems more compact, whereas the "active" structure is slightly loose. This observation is in agreement with the fact the G-proteins connect to the intracellular face of the 7TM domain upon activation.

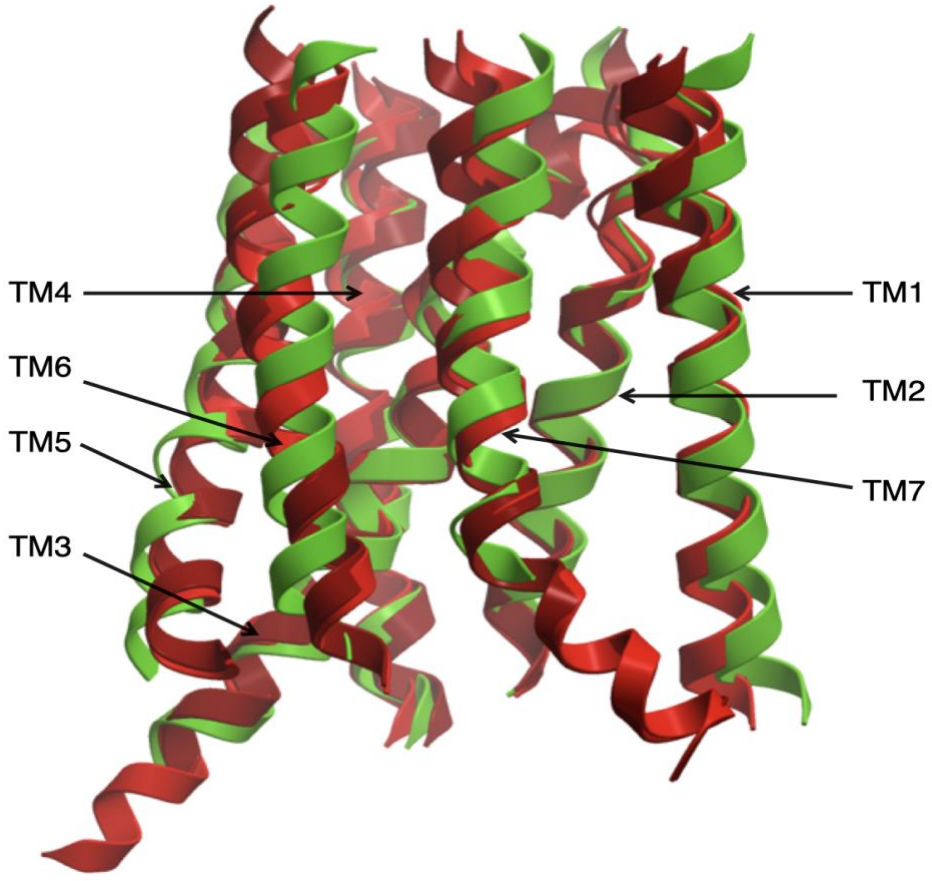

Figure 34 The "Active" and two "Inactive" $GABA_{B2}$ homology models superimposed. *The figure only shows the 7TM domains of $GABA_{B2}$ receptor, where the active conformation is in green color (based on mGlu1 active-like template), and two inactive conformations (based on inactive mGlu1 template; represented in dark red, and on inactive mGlu5; represented in light red).*

5.1.2.3 Docking and scoring

Analyzing how compounds with biological activity dock into the allosteric binding site is very crucial due to the limited information available about the binding site. Our results indicate that three compounds from our virtual screening modulate GABA$_B$ receptor. Therefore, comparing the docking pose between these compounds and analyzing the interactions of the compounds with the surrounding residues are relevant.

The docking results of hit compounds that had activity during in vitro results show a comparable docking pose with their reference NAMs. The TI-36 reference NAM, and its analogues A-8 and A-20 (Fig. 35) identified by VS in the present study occupy the same position of the binding pocket. By comparing the docking poses of similar compounds that show biological activity, we can get a better idea in evaluating new hit compounds. TI-6 (Fig. 36), reference NAM, and its analog A-9 (Fig. 36), also seems to maintain the same position of the binding site. It seems the overall structure pose of hit compounds are comparable to the reference NAMs.

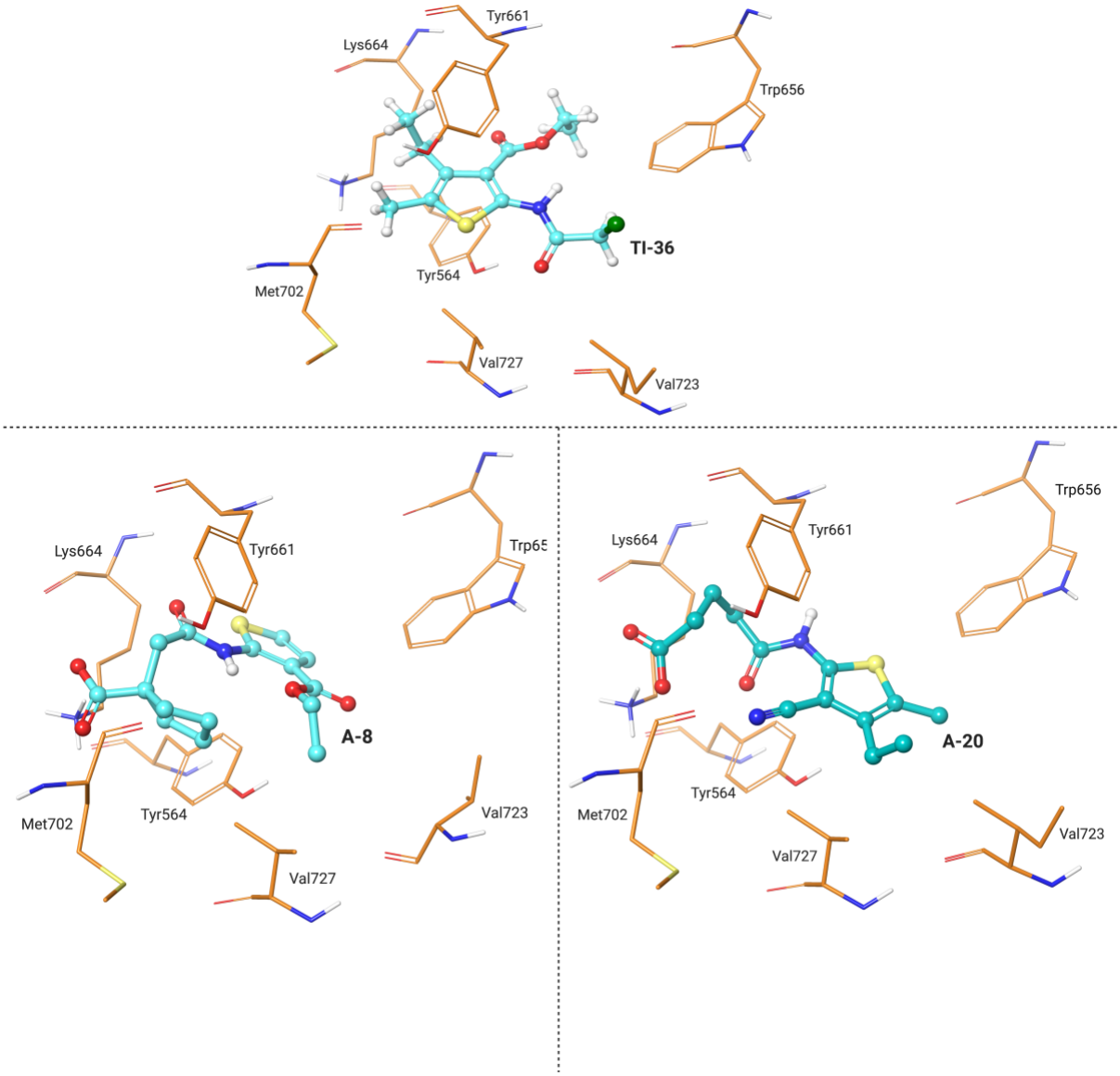

Figure 35 Docking pose of TI-36, A-8 and A-20 in the allosteric binding pocked of GABA$_B$ homology model predicted by XP Glide docking.

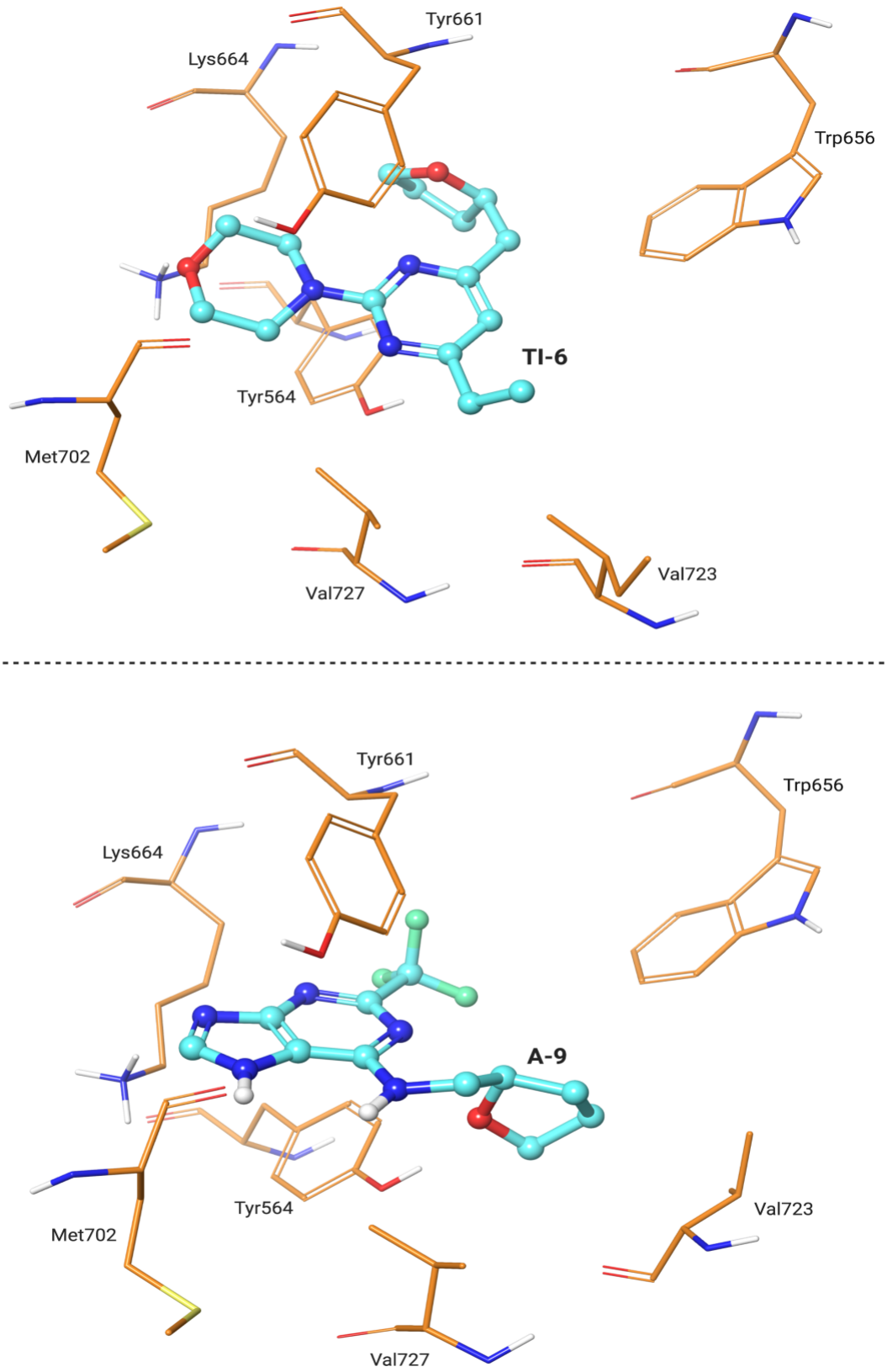

Figure 36 Docking pose of TI36 and A-9in the allosteric binding pocked of GABA$_B$ homology model predicted by XP Glide docking.

By analyzing the ligand-target interactions of the hit compounds and reference NAMs, we managed to identify common residues, for instance, Trp656, Tyr661, Lys664, and Val727. Freyd et al. identified these residues to be part of the allosteric binding site of $GABA_{B2}$ receptor (81). Moreover, Tyr661, Lys664, and Val 727 are residues that that change the potency of allosteric modulators with more than 5-fold when mutated with other class C human receptors (81). It would be interesting to implement mutations on Lys664. From the interaction diagram (Fig. 37), we can see that A-8 forms more hydrophobic interactions than A-20. TI-36 seems to have most of the hydrophobic interactions with the surrounding residues, more similar to A-8 than A-20. The main difference is that A-20 and A-8 forms an ionic interaction with Lys664, which is absent in TI-36. This is maybe the reason for the higher docking score of TI-36 (-6,688 kcal/mol) compared to A-20 (-9,869 kcal/mol) and A-8 (-9,5 kcal/mol). As earlier argued, these poses may not be the actual pose of the ligand with the target.

The same examination was performed for TI-6 and A-9. Both structures appear to have related interaction mode. Both structures form a hydrogen-bonds, but TI-6 forms a hydrogen bond with Lys664 while A-9 with Tys564 (Fig. 38). Consequently, a related score between TI-6 (-9,046 kcal/mol) and A-9 (-10,467 kcal/mol) was computed.

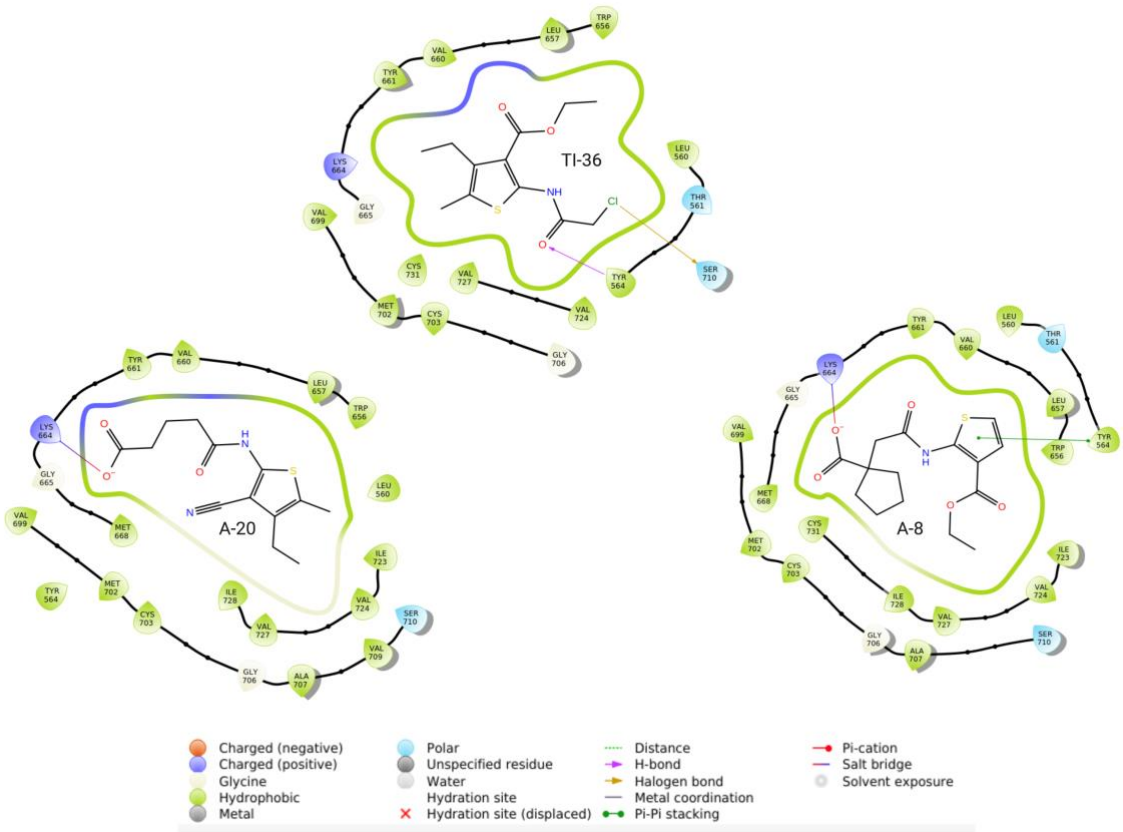

Figure 37 Interaction diagrams panels of TI-36, A-8, and A-20. *The figure shows the interactions of hit compounds with residues of the allosteric binding pocked of $GABA_B$ homology predicted by XP docking.*

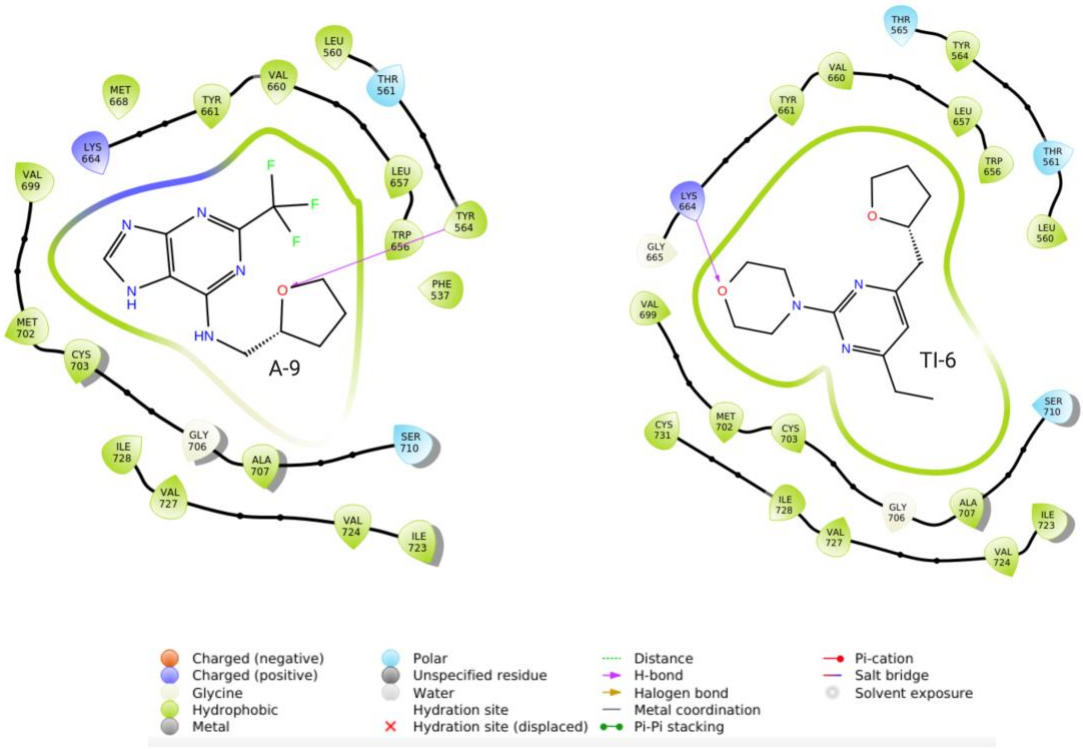

Figure 38 Interaction diagrams panels of TI-6 and A-9. *The figure shows the interactions of A-9 hit compound and reference TI-6 compound with residues of the allosteric binding pocked of GABA$_B$ homology predicted by XP docking.*

The reference structures that were used in the current study have been shown to increase cAMP with more than 20% in mixture with GABA, indicating negative allosteric modulation (unpublished results). However, cAMP functional assay results are not a measure for compounds affinity, making a comparison of activity with docking score challenging. Some of the tested compounds may have good affinity despite the low activity shown in our results since the effects allosteric modulators have on the receptors are complex (88). As earlier mentioned in the introduction of the study, there are no radioligands for the allosteric binding site of the GABA$_B$ receptor, adding more difficulties to the evaluation and characterization of the binding site and structure-based virtual screening for allosteric modulators of GABA$_B$. It is not coming into a surprise that there is only one allosteric modulator of GABA$_B$ published (80), which also add challenges to the ligand-based virtual screening.

In order to gain adequate information about the binding site, a target structure of the GABA$_B$ receptor co-crystallized with an allosteric modulator, preferably a negative allosteric modulator, is required. Enlarging the size of the binding site may increase the number of compounds docked, leading to false-positive results. Contrarily, defining a binding site dimension smaller than should be, can filter large potential active molecules. It is known that antagonists are bigger in size compared to agonists, but it is unknown if this theory applies to allosteric modulators. If so, considering having a larger binding site can be a smart move to avoid filtering potential NAMs. One study indicates that the binding site for NAMs and PAMs overlap (163), if this statement applies then definition of the binding site is even more challenging.

Most of the docking software use semi-rigid approach where the ligand is flexible, and the receptor is rigid. Our docking protocol was performed with flexible ligands and a rigid protein target. A major drawback of the applied docking procedure is that the protein is treated as a rigid structure. In nature, receptor proteins range between different conformational states with similar energies. Protein flexibility influences the binding site location and orientation and may increase the affinity between ligand and target. X-ray complexes revealed ligands buried inside the binding pocket of target proteins, which can only be accomplished by protein flexibility (164). Hence, adding flexibility to the target structure can produce better docking results. On the contrary, adding flexibility may lead to the fact that more ligands can be docked and, consequently, higher rates of false positives (153).

The conformation of a ligand bound to its receptor may be different from the unbound conformation. Generally, when the ligand is unbound, it exhibits many different conformations, and only few of these conformations are relevant to the bound state. Therefore, it is requisite to consider ligand flexibility during the docking procedure (115). There are different docking algorithms incorporated for each software, and in our study, the Monte Carlo (MC) algorithm was utilized to add ligand flexibility (127,165). The advantage of using MC methods is that they allow for a more exhaustive search of the conformation space to be performed (112). Increasing the chance of getting more "low energy" conformations of target ligands means an increased probability of getting active compounds.

To moderately overcome the drawback with protein flexibility, different conformations of the rigid target can be used during the docking procedure. Currently, some software, such as the Schrödinger Induced Fit docking (“Induced Fit | Schrödinger,” n.d.; Sherman et al., 2006), introduces partial flexibility to the binding site of the target protein. Adding flexibility to the entire protein can add further flexibility to the binding site and bring us closer to the dynamics of nature (Scior et al., 2012), but this seems unachievable yet, and super powerful computers are required to reduce the huge computational time. Generally, residues move in concert, and applying flexibility only to the binding site may not precisely resemble the actual flexibility in nature.

Another limitation of the performed docking procedures is the lack of information about solvation and entropy. Including such properties makes the docking process closer to reality. Water can form several hydrogen bonds with the surrounding molecules and can be involved in the ligand-target interactions. Water is more critical in solvent mediated interactions and may contribute up to 3 kcal/mol of the docking scoring value (166). Our target is a G-protein coupled receptor, where its 7TM is embedded in the lipophilic membrane layer. Therefore, the solvent impact may contribute to less binding energy compared to solvent-mediated interactions. It is reported that a water network is shown at the bottom of the allosteric binding site of the mGlu5 receptor, which can affect the ligand-target interaction and consequently lower the activation energy of the receptor (65). These observed phenomena could also be the case with the $GABA_B$ receptor.

One single molecule can have many low-energy conformations, but there is only one biologically active conformation among the low-energy conformations. It is noteworthy that the bioactive conformation is not necessarily the lowest-energy conformation. Providing potential orientations of the compound in the binding site by the docking search algorithm does not signify that the compound bind to the target protein. The search algorithm can fail to

predict the real pose of the ligand even if the ligand is an actual ligand of the target (159). Docking is usually considered to be successful when the root-mean-square-deviation (RMSD) value is less than 2 Å between the experimentally determined pose, and the predicted pose of the ligand (113). There is no available structure for the 7TM domain of the $GABA_B$ receptor, and accordingly, we do not have an experimentally determined pose in order to measure the RMSD value.

Many of the scoring functions used in docking programs apply simplifications to increase the computational speed, which makes them imperfect. This drawback reduces the accuracy of the scoring functions and hence the evaluation of ligand affinity (112). Glide is a combination of Emodel and GlideScore, where Emodel is more based on force field scoring functions (Tab. 3) that makes it more appropriate for comparing different conformations. Glide score, on the other hand, is an empirical scoring function (Tab. 3) used to rank poses of different ligands. XP Glide docking employs a more sophisticated scoring function than SP Glide docking, which makes XP docking take longer running time than SP docking (127).

It is recommended that SP docking should be performed first before choosing 10-30% of the best results and re-dock them with XP docking to get better results (167). Accordingly, an SP docking was applied first to all ligands resulting from the ligand-based virtual screening, and only 10% of the SP docking results were re-docked with XP docking. XP docking can penalize ligands that do not fit well into a particular receptor conformation (127). It has been reported that a combination of several scoring functions, so-called consensus scoring, can minimize the errors of individual functions. However, combining uncorrelated scoring functions can cause errors (113).

5.1.3 Selection of hit compounds to evaluate using in vitro functional assays

The 376 hit compounds resulting from the XP docking procedure, were merged with 72 well known PAMs (81) and the reference NAMs. The activity of the virtual screening hits, 367 compounds, need to be confirmed using in vitro techniques, but we did not have the capacity to test all 376 hits. Furthermore, our object was to identify analogues of the six reference NAMs, but in order to avoid purchasing compounds we already have tested, PAMs were clustered together with the hit compounds retrieved from MolPort database. It is also known that only small changes in a ligand structure can turn a PAM to a NAM or the other way around, referred to as “mode switching” (65). For instance, the discovery of CLH304a, a reference NAM, was an attempt to find more potent analogs of CGP7930, a positive allosteric modulator (80). Changing a methyl substituent on a phenyl ring, changed a NAM of mGlu5 to a PAM (65). Therefore, by mixing PAMs with our hit compounds, we could select some hits that share similarities with the well-known PAMs, and others that are structurally divergent from PAMs.

Additional ADME properties (Tab. 5) were used as a guide for the final hit selection of the in silico virtual screening. This was done as hit compounds can erroneously appear to be active during in vitro testing without interacting with the target protein. In literature, these compounds are referred to as Pan-assay interference compounds (or just PAINS), which are classified into different groups (168). For example, fluorescent compounds may give false-positive results in fluorometric assays, or compounds with reactive functional groups can also give false-positive results. We chose to implement the rtvFG descriptor, which indicates the

number of reactive functional groups in a compound that can lead to false positive results (table 5), by using QikProp from Schrödinger to promote our final hit selection. This descriptor helps to identify reactive functional groups in each hit. All the hit compounds selected for the in vitro testing have no reactive functional groups, #rtvFG value of zero (recommended value: 0-2). Two additional descriptors, QPlogS and #stars (Tab. 5), were used during the final hit selection. QPlogS predict the aqueous solubility of compounds, and #stars suggest how drug-like a compound is. We utilized these descriptors, specially QPlogS because we had problems with the solubility of compounds we have purchased. Finally, we selected 16 hit compounds to be purchased and tested in vitro. The selection was based on four reference ligands, TI-36, TI-6, benzydamine N-oxide, and CLH304a (Fig. 23).

5.2 In vitro

The 16 test compounds retrieved from virtual screening of the MolPort database were tested experimentally using functional cAMP assays. Test results showed that compound A-8 seems to exhibit NAM or antagonist activity on $GABA_B$ receptors. Compound A-9 might also be a NAM/antagonist. A further test of A-20 is needed but the preliminary tests from the GABA cells indicated that A-20 was a potent PAM (Fig. 27-28).

Based on the current results, it is difficult to final conclusion. The initial plan is to perform multiple assay readouts, but due to the situation of coronavirus, it was unfortunately not possible. However, based on the assays performed so far, we have identified a potential weak NAM, compound A-8 (Fig. 31). Except a further testing of A-9 and A-20 with cAMP assay, radioligand binding might be used to verify if these best candidates bind to the orthosteric site of the receptors.

In order to detect cAMP signals, the adenylyl cyclase has to be activated, which is usually accomplished by using forskolin. The main object of the forskolin dose-response assay, is to determine the appropriate forskolin concentration for the cAMP assays on $GABA_B$ receptors. It is recommended to select an agonist concentration between EC_{50} to EC_{80} in order to estimate the potency of antagonists (169). Choosing the maximal signal concentration will not make it possible to identify NAMs or antagonists that revers the GABA inhibition; hence, concentration of forskolin that produce the highest signal was not chosen. The EC_{80} concentration (Fig. 24), on the other hand, are more beneficial in detecting NAMs or antagonists as it leaves a small room for the signal to be increased by NAMs or antagonists. The EC_{50} concentration of forskolin (Fig. 24) is located in the middle of an S-shape curve, and small variations in forskolin concentration can contribute to significant increase or decrease of the cAMP signal, especially when pipetting small volumes. Therefore, the forskolin EC_{50} concentration was not used in this study. During the actual assay preparations, 30 µM of forskolin was used, which is close to 30.8 µM determined from the forskolin time-dependent assay. The same concentration approximation procedure was used for the selection of $GABA_{EC20/EC80}$ concentrations.

In order to optimize the assay performance, we measured the time it takes to stabilize the cAMP signal, where cells reach its maximal stimulation. We found out that the best time to add the cAMP reagents is something between 24 to 27 minutes, which gives us three minutes. Since we are using a plate reader to dispense the cAMP reagents for us, three minutes is just enough to finish the dispensing of half of the 384-well plate. We performed this way so that we have fewer variations between wells of the microplate and hence more repeatable results. Adding the cAMP reagents too early does not give enough signal because the reaction takes

time. On the other hand, adding cAMP reagents too late can cause the GABA or test compound disassociation and cAMP degradation.

The main purpose of performing the cAMP assay on WT cells is to investigate if some of the compounds can interfere with the cAMP signal in the absence of the $GABA_B$ receptor. This step is important to distinguish possible false-positive results during the performance on $GABA_B$ cells. Compounds that show activity on WT assay should be excluded from testing on $GABA_B$ cells. However, there is also a small possibility that the compound has multitarget features, which is binding to both $GABA_B$ receptor and other targets in the cells. In this case, the current functional assay would be difficult to differentiate.

The $GABAE_{C20/EC80}$ assay was performed on all selected test compounds because they did not show significant activity on WT cells. In addition to $GABA_{EC80\ and\ EC20}$ concentrations, forskolin alone was added to the compounds as well. Compounds that show activity on either EC_{20} or EC_{80} can be NAMs or PAMs, but still, there is a possibility that the compound is an agonist or antagonist, or maybe even an allosteric agonist with intrinsic activity. Therefore, the effect of the compounds on GABAB receptors without the presence of GABA was performed.

Compound A-20 has a QPlogS value of -3,303 (recommended value: -6,5-0,5), while compound A-8 and A-9 have a value of -3,085 and -3,303 respectively. During the solubility test in the laboratory, compound A-20 was not soluble in 2xHBSS buffer, while compound A-8 and A-9 were soluble. It is not a surprise some of the compounds did not dissolve good enough despite the QPlogS was within the recommended range, because these descriptors are theoretical performed by computational calculations. Predicting a pKa of a molecule is an alternative option in predicting the solubility of compounds. Additionally, pKa also affects ADME properties such as lipophilicity and metabolism (170). Predicting the pKa helps to estimate whether the molecule will be protonated in physiological pH or not. We recommend the use of Jaguar pKa software (171) from Schrödinger or the computational package MoKa (170)**.**

5.2.1 Functional assay performance

Numerous high-throughput GPCR functional assays are commercially available, including HitHunter cAMP-based assay that is used in the current study. Gabriel et al. have compared different assay platforms and reported several advantages and drawbacks of each platform; however, he suggested the use of the HitHunter™ platform for cells expressing high GPCR densities (172). Obtaining a workable cAMP assay for G_s-coupled receptors is generally straightforward, whereas screening $G_{i/o}$-coupled receptors are considered challenging because forskolin have to be added to increase cAMP production to allows for efficient detection (134,136). In addition, many factors can affect the performance of the functional assay, thereby the in vitro result. However, we worked hard to compensate for possible errors and inaccuracies. Our work was conducted during the evening for a few reasons. First, almost no people were present during this time, which helped to perform the assays constantly as planned without interruptions. Second, the cAMP reagents are light sensitive, therefore it is better to conduct the assay in the evening.

5.2.2 Cell culture

The choice of the cell line is one of the critical things that should be considered before running an assay. Two types of Chinese Hamster Ovary cell lines (CHO-k1) were used, one expressing the $GABA_B$ receptors and another one without $GABA_B$ receptors (Wild-type cell line). The culture media used for $GABA_B$ cells contained selection antibiotic, whereas the cell culture media for wild type cells does not contain selection antibiotic. $GABA_B$ cells have antibiotic resistance in its cDNA sequence, which gives it the ability to resist the antibiotic we added in. On the contrary, wild-type cells will die if antibiotics were added. The advantage of using selection antibiotics is to minimize the contamination of the cells, but also to ensure that only cells containing $GABA_B$ receptors will survive. It is also important to keep in mind that antibiotics are agents that can disrupt vital aspects of cell biology (140).

The advantage of using continuous cell lines is that they are stable over a long-term passages. Still, too many passages can alter their properties and cause irreversible changes (140). In other words, splitting $GABA_B$ cells for too many times can cause the reduced expression or even loss of $GABA_B$ receptor. Therefore, a maximum of ten passages of each frozen cryo-tube of $GABA_B$ cells was used for assay.

During the cell culture procedure, contamination can create challenges by affecting the growth of the cells (140). Therefore, this stage was performed under sterile conditions using ethanol as a disinfectant and performing the work under a laminar flow bench (LAF bench). If ethanol somehow gets mixed with the cells, it can change the functional assay results because it can inhibit forskolin-activated adenylyl cyclase (173). It is critical during cell harvesting, as ethanol contamination can create false positive agonist like results by reducing forskolin signal stimulation.

During the cell counting procedure, inaccurate cell counting can occur even with the use of Countess@ automated cell counter. In the cell suspension, cells usually sink to the bottom of the tube with time, making the cells not evenly distributed in the solution. In addition, cells can aggregate to form a cluster that affects cell counting. However, the cell suspension was always mixed gently right before cell counting. The Countess@ automated cell counter provides a visual picture of cell distribution colored with red (dead cells) and green (alive). Therefore, cell aggregates were easily identified in the sample used for cell counting. To make sure an accurate cell concentration estimation, cells were counted at least 4 times, then an average value were used.

After cell suspension centrifuge, cell pellets were appropriately resuspended to avoid cell aggregate accumulation. On the other hand, resuspending more than necessary can damage the cells. To avoid damaging the cells, we used a 10 mL graduated pipette with a wide opening during cell resuspension.

The culture media composition is one important factor to consider during cell culture. The natural medium contains rich nutrients, various hormones, isotonic osmotic pressure, and similar pH to the body environment (174). The culture medium has a complicated production process and batch to batch variations. The serum contains different essential nutrients that keep the physiological balance of promoting and inhibiting cell growth. The disadvantage of using a serum in culture media is that it can change the normal physiological condition of some cells because the serum is not the physiological fluid in vivo (174). However, we are expecting the composition of the culture media to be the same for each flask used, which will

not create variations in results. To further optimize cell condition and test results, using serum free culture media should be considered.

To ensure suitable conditions of the cells and reliable results, we had to optimize some parameters such as assay pH, temperature, osmotic pressure, and atmosphere. The HBSS buffer was prepared to have pH 7.4, because the optimal physiological pH for mammalian cells is usually 7.2 to 7.4 (140,174). Cell viability, growth, and phenotype can be significantly influenced outside this range. The buffer osmolarity was also measured, to ensure an osmolarity that is slightly lower than 300mOsm/kg (approx. 290 mOsm/kg). This is due to other compounds, such as DMSO in the test compound can contribute to increasing of osmolarity. The osmotic pressure of 260-320 mOsm/kg is known to be suitable for most mammalian cells (140,174).

The optimal temperature during cell culture depends on the type of cells involved; however, temperature above 39 ℃ is known to induce apoptosis (cell death), whereas temperature below 35 ℃ can slow down cell replication. Cells were placed inside the incubator (37 ℃, 5% CO_2) to ensure an optimal environment during cell growth. The level of oxygen and carbon dioxide is critical because a high level of both can be toxic and low levels can inhibit cell growth, which in both cases can result in cell death (140,174).

It is also essential to consider receptor expression level, especially for an obligate heterodimer $GABA_B$ receptor. The assembly of $GABA_{B1}$ and $GABA_{B2}$ allows the heterodimer to exit the endoplasmatic reticulum (ER) and transfer to the cell surface (22). However, receptors can also leave the cell surface and be recycled back to the cells through receptor-mediated endocytosis, a process referred to as receptor internalization. One study showed that a rapid receptor internalization of $GABA_B$ receptor exist and reported a 40-50% of the cell surface receptors were lost after 120 min (175). However, this observation was on Human Embryonic Kidney (HEK 293) cells, but another study also observed the same phenomena with CHO-K1 cells (176). They also reported that the internalization of $GABA_B$ receptors was induced when 100 μM GABA is used. One study reported the temperature impact on the $GABA_B$ receptor internalization using HEK cells, which revealed that the internalization rate is slower with lower temperatures (177). Therefore, cells in this study were pre-incubated at 25 ℃ for 2.5 hours before the reaction initiation.

Determining when to harvest or sub-culture the cells are very challenging, especially for the wild-type cell lines. Harvesting the cells too early will result in fewer cells to be tested, and can increase the differences between cells, which can affect the test results. Over-confluence, on the other hand, results in cell death. Therefore, we were sub-culturing and harvesting when confluence was about 70-90% to ensure an appropriate cell density and quality. The benefit of utilizing cells with 70-90% confluence is to improve the sensitivity in detecting hit compounds. On the other hand, using over confluent cells may reduce the sensitivity of the cells to the test compound stimulation. Too many cells may also saturate the cAMP assay reagents (169).

Despite all these precautions, the cultured cells can have different growth rates, which results in cells with different size, shape, cell surface, etc., (138). These cell variations may also influence receptor expression on the cell surface, and consequently, the test results. Cell synchronization is one of the methods to minimize cell variations (138). By synchronizing, the majority of cells become at the same phase of the cell cycle (Fig. 14). Usually, during the cell cycle, most of the time is spent on phase G1, which means that most of the cells will

most likely be at this phase. However, cell synchronization may provide more consistent and replicable results.

5.2.3 Assay preparation

In order to prepare the stock solutions, we had to weigh and dissolve various compounds. A small amount of compounds powder can alter the concentration of the stock solutions; hence we had to be extra cautious during this procedure. Pipetting errors can also happen during assay preparation, especially when working with small volumes in microliter (μL). The final pipetting of test compounds, GABA, and forskolin solution was, however, performed by using a multichannel pipette, which can minimize the pipetting inaccuracy. Test compounds purchased from the Molport database were not completely pure, with an unspecific amount of purity (≥90%). Necessary calculations were performed to take in to account the amount of impurities during stock solution preparation. However, unknown component in the impurity may also affect the assay results.

Calcium and magnesium are included in the composition of HBSS buffer, which is known to affect $GABA_B$ receptors. It has been shown that GABA binding to $GABA_B$ receptors increased on adding $CaCl_2$ or $MgSO_4$ (up to 2,5 mM and 5,0 mM, respectively), whereas the absence of these ions prevents detection of any binding to $GABA_B$ receptors (178). Another study claims that calcium acts as a PAM by enhancing GABA response and that calcium concentration of 0,001-1 mM can potentiate GABA stimulation of GTPγS assay prepared from CHO cells expressing $GABA_B$ receptor (179). Therefore, calcium concentration in the HBSS buffer is very critical, and variations of the concentration from batch to bach may change the results.

Test compounds, forskolin and GABA mixture, were first pipetted into the microplate, and adding the cells will immediately start the reaction. Manually adding the cells to the microplate takes long time to finish in high throughput assay format. Therefore, a well-calibrated cell dispenser was used to dispense the cell suspension quickly. The use of the robotic cell dispenser increases the accuracy and improve the test results.

6 Conclusion

A combination of in silico and in vitro approaches were applied in the search for negative allosteric modulators of the $GABA_B$ receptor. The computational screening protocols, comprising ADME-filtering and a sequential combination of ligand- and structure-based virtual screening, were utilized to screen approx. 7.5 million compounds of the MolPort database. Subsequently, 16 hit compounds were selected and purchased to be validated in vitro using functional cAMP assays. The experimental results revealed the identification of a putative new negative allosteric modulator, A-8, of the $GABA_B$ receptor. Our results also indicate a possible new allosteric or orthosteric ligands of $GABA_B$ receptor, A-9 and A-20. We highly recommend further testing of the remaining compounds, especially for compound A-9 and A-20.

Works cited

1. J. Gordon Betts, Kelly A. Young, James A. Wise, Eddie Johnson, Brandon Poe, Dean H. Kruse, Oksana Korol, Jody E. Johnson, Mark Womble, Peter DeSaix. Anatomy & Physiology. OpenStax [Internet]. 2013 Apr 25;1359. Available from: https://openstax.org/books/anatomy-and-physiology/pages/1-introduction

2. Purves D, editor. Neuroscience. 3rd ed. Sunderland, Mass: Sinauer Associates, Publishers; 2004. 1 p.

3. Rang HP, Dale MM, Ritter JM, Flower RJ, Henderson G. Rang and Dale's pharmacology. Eighth edition. Edinburgh? Elsevier, Churchill Livingstone; 2016. 760 p.

4. Barnett MW, Larkman PM. The action potential. 2007;7.

5. Roberts SM, Gibb AJ. Introduction to enzymes, receptors and the action of small molecule drugs. In: Introduction to Biological and Small Molecule Drug Research and Development [Internet]. Elsevier; 2013 [cited 2020 May 7]. p. 1–55. Available from: https://linkinghub.elsevier.com/retrieve/pii/B9780123971760000017

6. Daneman R, Prat A. The Blood–Brain Barrier. Cold Spring Harb Perspect Biol [Internet]. 2015 Jan [cited 2020 Jan 19];7(1):a020412. Available from: http://cshperspectives.cshlp.org/lookup/doi/10.1101/cshperspect.a020412

7. Pardridge WM. The Blood-Brain Barrier: Bottleneck in Brain Drug Development. 2005;2(1):12.

8. Banks WA. Characteristics of compounds that cross the blood-brain barrier. BMC Neurol [Internet]. 2009 [cited 2020 May 6];9(Suppl 1):S3. Available from: http://bmcneurol.biomedcentral.com/articles/10.1186/1471-2377-9-S1-S3

9. Pajouhesh H, Lenz GR. Medicinal chemical properties of successful central nervous system drugs. NeuroRX [Internet]. 2005 Oct [cited 2020 Jan 19];2(4):541–53. Available from: http://link.springer.com/10.1602/neurorx.2.4.541

10. Merino P. Chemical Biology of Neurodegeneration: A Molecular Approach [Internet]. 1st ed. Wiley; 2019 [cited 2020 Jan 7]. Available from: https://onlinelibrary.wiley.com/doi/book/10.1002/9783527813421

11. Olsen RW, Li G-D. GABA. In: Basic Neurochemistry [Internet]. Elsevier; 2012 [cited 2019 Sep 22]. p. 367–76. Available from: https://linkinghub.elsevier.com/retrieve/pii/B9780123749475000183

12. Rodriguez-Diaz R, Menegaz D, Caicedo A. Neurotransmitters act as paracrine signals to regulate insulin secretion from the human pancreatic islet. J Physiol [Internet]. 2014 Aug 15 [cited 2020 Jan 7];592(Pt 16):3413–7. Available from: https://www.ncbi.nlm.nih.gov/pmc/articles/PMC4229339/

13. Feng AL, Xiang Y-Y, Gui L, Kaltsidis G, Feng Q, Lu W-Y. Paracrine GABA and insulin regulate pancreatic alpha cell proliferation in a mouse model of type 1 diabetes. Diabetologia. 2017;60(6):1033–42.

14. Fuks JM, Arrighi RBG, Weidner JM, Mendu SK, Jin Z, Wallin RPA, et al. GABAergic Signaling Is Linked to a Hypermigratory Phenotype in Dendritic Cells Infected by Toxoplasma gondii. PLOS Pathog [Internet]. 2012 Dec 6 [cited 2020 Jan 7];8(12):e1003051. Available from: https://journals.plos.org/plospathogens/article?id=10.1371/journal.ppat.1003051

15. Erdö SL, Wolff JR. ?-Aminobutyric Acid Outside the Mammalian Brain. J Neurochem [Internet]. 1990 Feb [cited 2020 Jan 7];54(2):363–72. Available from: http://doi.wiley.com/10.1111/j.1471-4159.1990.tb01882.x

16. Watanabe M, Maemura K, Kanbara K, Tamayama T, Hayasaki H. GABA and GABA Receptors in the Central Nervous System and Other Organs. In: International Review of Cytology [Internet]. Elsevier; 2002 [cited 2020 Jan 7]. p. 1–47. Available from: https://linkinghub.elsevier.com/retrieve/pii/S0074769602130117

17. Scimemi A. Structure, function, and plasticity of GABA transporters. Front Cell Neurosci [Internet]. 2014 Jun 17 [cited 2020 Mar 17];8. Available from: http://journal.frontiersin.org/article/10.3389/fncel.2014.00161/abstract

18. Walls AB. GABA Synthesis and Metabolism ☆. In: Reference Module in Neuroscience and Biobehavioral Psychology [Internet]. Elsevier; 2017 [cited 2020 Mar 17]. p. B978012809324502335X. Available from: https://linkinghub.elsevier.com/retrieve/pii/B978012809324502335X

19. Olsen RW. GABAA receptor: Positive and negative allosteric modulators. Neuropharmacology [Internet]. 2018 Jul [cited 2020 Mar 7];136:10–22. Available from: https://linkinghub.elsevier.com/retrieve/pii/S0028390818300364

20. Bowery NG, Hill DR, Hudson AL, Doble A, Middlemiss DN, Shaw J, et al. (-)Baclofen decreases neurotransmitter release in the mammalian CNS by an action at a novel GABA receptor. Nature. 1980 Jan 3;283(5742):92–4.

21. Kaupmann K, Huggel K, Heid J, Flor PJ, Bischoff S, Mickel SJ, et al. Expression cloning of GABA(B) receptors uncovers similarity to metabotropic glutamate receptors. Nature. 1997 Mar 20;386(6622):239–46.

22. Colombo G. GABA B receptor. New York, NY: Springer Science+Business Media; 2016.

23. Froestl W. Chemistry and Pharmacology of GABAB Receptor Ligands. In: Advances in Pharmacology [Internet]. Elsevier; 2010 [cited 2020 Jan 7]. p. 19–62. Available from: https://linkinghub.elsevier.com/retrieve/pii/S1054358910580025

24. Simon MI, Strathmann MP, Gautam N. Diversity of G proteins in signal transduction. Science. 1991 May 10;252(5007):802–8.

25. Oldham WM, Hamm HE. Heterotrimeric G protein activation by G-protein-coupled receptors. Nat Rev Mol Cell Biol [Internet]. 2008 Jan [cited 2020 Feb 2];9(1):60–71. Available from: http://www.nature.com/articles/nrm2299

26. Rasmussen SGF, DeVree BT, Zou Y, Kruse AC, Chung KY, Kobilka TS, et al. Crystal structure of the β2 adrenergic receptor–Gs protein complex. Nature [Internet]. 2011 Sep [cited 2020 Feb 2];477(7366):549–55. Available from: http://www.nature.com/articles/nature10361

27. Chung KY. Structural Aspects of GPCR-G Protein Coupling. Toxicol Res [Internet]. 2013 Sep 30 [cited 2020 Jan 8];29(3):149–55. Available from: http://koreascience.or.kr/journal/view.jsp?kj=DSHHBQ&py=2013&vnc=v29n3&sp=149

28. DeVree BT, Mahoney JP, Vélez-Ruiz GA, Rasmussen SGF, Kuszak AJ, Edwald E, et al. Allosteric coupling from G protein to the agonist-binding pocket in GPCRs. Nature [Internet]. 2016 Jul [cited 2020 Feb 2];535(7610):182–6. Available from: http://www.nature.com/articles/nature18324

29. Gassmann M, Bettler B. Regulation of neuronal GABA B receptor functions by subunit composition. Nat Rev Neurosci [Internet]. 2012 Jun [cited 2020 Feb 2];13(6):380–94. Available from: https://www.nature.com/articles/nrn3249

30. Bowery NG, Bettler B, Froestl W, Gallagher JP, Marshall F, Raiteri M, et al. International Union of Pharmacology. XXXIII. Mammalian gamma-aminobutyric acid(B) receptors: structure and function. Pharmacol Rev. 2002 Jun;54(2):247–64.

31. Rask-Andersen M, Masuram S, Schiöth HB. The Druggable Genome: Evaluation of Drug Targets in Clinical Trials Suggests Major Shifts in Molecular Class and Indication. Annu Rev Pharmacol Toxicol [Internet]. 2014 Jan 6 [cited 2020 Jan 24];54(1):9–26. Available from: http://www.annualreviews.org/doi/10.1146/annurev-pharmtox-011613-135943

32. Fredriksson R, Lagerström MC, Lundin L-G, Schiöth HB. The G-Protein-Coupled Receptors in the Human Genome Form Five Main Families. Phylogenetic Analysis, Paralogon Groups, and Fingerprints. Mol Pharmacol [Internet]. 2003 Jun [cited 2020 Jan 22];63(6):1256–72. Available from: http://molpharm.aspetjournals.org/lookup/doi/10.1124/mol.63.6.1256

33. Sriram K, Insel PA. G Protein-Coupled Receptors as Targets for Approved Drugs: How Many Targets and How Many Drugs? Mol Pharmacol [Internet]. 2018 Apr [cited 2020 Jan 22];93(4):251–8. Available from: http://molpharm.aspetjournals.org/lookup/doi/10.1124/mol.117.111062

34. Hauser AS, Attwood MM, Rask-Andersen M, Schiöth HB, Gloriam DE. Trends in GPCR drug discovery: new agents, targets and indications. Nat Rev Drug Discov [Internet]. 2017 Dec [cited 2020 Jan 23];16(12):829–42. Available from: http://www.nature.com/articles/nrd.2017.178

35. Kolakowski LF. GCRDb: a G-protein-coupled receptor database. Receptors Channels. 1994;2(1):1–7.

36. Schiöth HB, Fredriksson R. The GRAFS classification system of G-protein coupled receptors in comparative perspective. Gen Comp Endocrinol [Internet]. 2005 May [cited 2020 Jan 8];142(1–2):94–101. Available from: https://linkinghub.elsevier.com/retrieve/pii/S001664800400396X

37. Lagerström MC, Schiöth HB. Structural diversity of G protein-coupled receptors and significance for drug discovery. Nat Rev Drug Discov [Internet]. 2008 Apr [cited 2020 Jan 22];7(4):339–57. Available from: http://www.nature.com/articles/nrd2518

38. Hu G-M, Mai T-L, Chen C-M. Visualizing the GPCR Network: Classification and Evolution. Sci Rep [Internet]. 2017 Dec [cited 2020 Mar 29];7(1):15495. Available from: http://www.nature.com/articles/s41598-017-15707-9

39. Urwyler S. Allosteric modulation of family C G-protein-coupled receptors: from molecular insights to therapeutic perspectives. Pharmacol Rev. 2011 Mar;63(1):59–126.

40. Leach K, Gregory KJ. Molecular insights into allosteric modulation of Class C G protein-coupled receptors. Pharmacol Res [Internet]. 2017 Feb [cited 2020 Jan 8];116:105–18. Available from: https://linkinghub.elsevier.com/retrieve/pii/S1043661816313068

41. Moore CAC, Milano SK, Benovic JL. Regulation of Receptor Trafficking by GRKs and Arrestins. Annu Rev Physiol [Internet]. 2007 Mar [cited 2020 Jan 24];69(1):451–82. Available from: http://www.annualreviews.org/doi/10.1146/annurev.physiol.69.022405.154712

42. Lefkowitz RJ. A Brief History of G-Protein Coupled Receptors (Nobel Lecture). Angew Chem Int Ed [Internet]. 2013 Jun 17 [cited 2020 Feb 2];52(25):6366–78. Available from: http://doi.wiley.com/10.1002/anie.201301924

43. Wang W, Qiao Y, Li Z. New Insights into Modes of GPCR Activation. Trends Pharmacol Sci [Internet]. 2018 Apr [cited 2020 Jan 8];39(4):367–86. Available from: https://linkinghub.elsevier.com/retrieve/pii/S0165614718300245

44. Strasser A, Wittmann H-J. Modelling of GPCRs: a practical handbook. Dordrecht: Springer; 2013. 218 p.

45. Hauser AS, Chavali S, Masuho I, Jahn LJ, Martemyanov KA, Gloriam DE, et al. Pharmacogenomics of GPCR Drug Targets. Cell [Internet]. 2018 Jan [cited 2020 Mar 29];172(1–2):41-54.e19. Available from: https://linkinghub.elsevier.com/retrieve/pii/S0092867417313843

46. Bortolato A, Doré AS, Hollenstein K, Tehan BG, Mason JS, Marshall FH. Structure of Class B GPCRs: new horizons for drug discovery: Structure of Class B GPCRs enable drug discovery. Br J Pharmacol [Internet]. 2014 Jul [cited 2020 Mar 29];171(13):3132–45. Available from: http://doi.wiley.com/10.1111/bph.12689

47. Dessau MA, Modis Y. Protein Crystallization for X-ray Crystallography. J Vis Exp [Internet]. 2011 Jan 16 [cited 2020 Mar 29];(47):2285. Available from: http://www.jove.com/index/Details.stp?ID=2285

48. Cooper GM, Hausman RE. The Cell: A Molecular Approach, Sixth Edition. 2013;12.

49. Privé GG. Detergents for the stabilization and crystallization of membrane proteins. Methods [Internet]. 2007 Apr [cited 2020 Mar 29];41(4):388–97. Available from: https://linkinghub.elsevier.com/retrieve/pii/S1046202307000102

50. Byrne EFX, Sircar R, Miller PS, Hedger G, Luchetti G, Nachtergaele S, et al. Structural basis of Smoothened regulation by its extracellular domains. Nature [Internet]. 2016 Jul [cited 2020 Mar 29];535(7613):517–22. Available from: http://www.nature.com/articles/nature18934

51. Zheng H, Loh HH, Law P-Y. Posttranslation Modification of G Protein-Coupled Receptor in Relationship to Biased Agonism. In: Methods in Enzymology [Internet]. Elsevier; 2013 [cited 2020 Mar 29]. p. 391–408. Available from: https://linkinghub.elsevier.com/retrieve/pii/B9780124078659000182

52. Lohse MJ, Maiellaro I, Calebiro D. Kinetics and mechanism of G protein-coupled receptor activation. Curr Opin Cell Biol [Internet]. 2014 Apr [cited 2020 Mar 29];27:87–93. Available from: https://linkinghub.elsevier.com/retrieve/pii/S0955067413001853

53. Warne T, Serrano-Vega MJ, Baker JG, Moukhametzianov R, Edwards PC, Henderson R, et al. Structure of a β1-adrenergic G-protein-coupled receptor. Nature [Internet]. 2008 Jul [cited 2020 Mar 29];454(7203):486–91. Available from: http://www.nature.com/articles/nature07101

54. Katritch V, Cherezov V, Stevens RC. Structure-function of the G protein-coupled receptor superfamily. Annu Rev Pharmacol Toxicol. 2013;53:531–56.

55. García-Nafría J, Tate CG. Cryo-EM structures of GPCRs coupled to Gs, Gi and Go. Mol Cell Endocrinol. 2019 15;488:1–13.

56. García-Nafría J, Tate CG. Cryo-Electron Microscopy: Moving Beyond X-Ray Crystal Structures for Drug Receptors and Drug Development. Annu Rev Pharmacol Toxicol [Internet]. 2020 [cited 2020 May 12];60(1):51–71. Available from: https://doi.org/10.1146/annurev-pharmtox-010919-023545

57. Bhella D. Cryo-electron microscopy: an introduction to the technique, and considerations when working to establish a national facility. Biophys Rev [Internet]. 2019 Aug [cited 2020 Mar 29];11(4):515–9. Available from: http://link.springer.com/10.1007/s12551-019-00571-w

58. Renaud J-P, Chari A, Ciferri C, Liu W, Rémigy H-W, Stark H, et al. Cryo-EM in drug discovery: achievements, limitations and prospects. Nat Rev Drug Discov [Internet]. 2018 Jul [cited 2020 May 8];17(7):471–92. Available from: http://www.nature.com/articles/nrd.2018.77

59. Alexander SP, Christopoulos A, Davenport AP, Kelly E, Marrion NV, Peters JA, et al. THE CONCISE GUIDE TO PHARMACOLOGY 2017/18: G protein-coupled receptors: THE CONCISE GUIDE TO PHARMACOLOGY 2017/18: G protein-coupled receptors. Br J Pharmacol [Internet]. 2017 Dec [cited 2020 Jan 8];174:S17–129. Available from: http://doi.wiley.com/10.1111/bph.13878

60. Kunishima N, Shimada Y, Tsuji Y, Sato T, Yamamoto M, Kumasaka T, et al. Structural basis of glutamate recognition by a dimeric metabotropic glutamate receptor. Nature. 2000 Oct 26;407(6807):971–7.

61. Wu H, Wang C, Gregory KJ, Han GW, Cho HP, Xia Y, et al. Structure of a class C GPCR metabotropic glutamate receptor 1 bound to an allosteric modulator. Science [Internet]. 2014 Apr 4 [cited 2019 Sep 23];344(6179):58–64. Available from: https://www.ncbi.nlm.nih.gov/pmc/articles/PMC3991565/

62. Christopher JA, Orgován Z, Congreve M, Doré AS, Errey JC, Marshall FH, et al. Structure-Based Optimization Strategies for G Protein-Coupled Receptor (GPCR) Allosteric Modulators: A Case Study from Analyses of New Metabotropic Glutamate Receptor 5 (mGlu $_5$) X-ray Structures. J Med Chem [Internet]. 2019 Jan 10 [cited 2020 Mar 30];62(1):207–22. Available from: https://pubs.acs.org/doi/10.1021/acs.jmedchem.7b01722

63. Christopher JA, Aves SJ, Bennett KA, Doré AS, Errey JC, Jazayeri A, et al. Fragment and Structure-Based Drug Discovery for a Class C GPCR: Discovery of the mGlu $_5$ Negative Allosteric Modulator HTL14242 (3-Chloro-5-[6-(5-fluoropyridin-2-yl)pyrimidin-4-yl]benzonitrile). J Med Chem [Internet]. 2015 Aug 27 [cited 2020 Mar 30];58(16):6653–64. Available from: https://pubs.acs.org/doi/10.1021/acs.jmedchem.5b00892

64. Thal DM, Glukhova A, Sexton PM, Christopoulos A. Structural insights into G-protein-coupled receptor allostery. Nature [Internet]. 2018 Jul [cited 2020 Mar 30];559(7712):45–53. Available from: http://www.nature.com/articles/s41586-018-0259-z

65. Doré AS, Okrasa K, Patel JC, Serrano-Vega M, Bennett K, Cooke RM, et al. Structure of class C GPCR metabotropic glutamate receptor 5 transmembrane domain. Nature [Internet]. 2014 Jul [cited 2020 Feb 2];511(7511):557–62. Available from: http://www.nature.com/articles/nature13396

66. Koehl A, Hu H, Feng D, Sun B, Zhang Y, Robertson MJ, et al. Structural insights into the activation of metabotropic glutamate receptors. Nature [Internet]. 2019 Feb [cited 2019 Oct 1];566(7742):79–84. Available from: http://www.nature.com/articles/s41586-019-0881-4

67. Papasergi-Scott MM, Robertson MJ, Seven AB, Panova O, Mathiesen JM, Skiniotis G. Structures of metabotropic GABA $_B$ receptor [Internet]. Neuroscience; 2020 Apr [cited 2020 May 6]. Available from: http://biorxiv.org/lookup/doi/10.1101/2020.04.15.004267

68. Mao C, Shen C, Li C, Shen D-D, Xu C, Zhang S, et al. Cryo-EM structures of inactive and G $_i$ -coupled GABA $_B$ heterodimer [Internet]. Molecular Biology; 2020 Apr [cited 2020 May 12]. Available from: http://biorxiv.org/lookup/doi/10.1101/2020.04.21.053488

69. Geng Y, Bush M, Mosyak L, Wang F, Fan QR. Structural mechanism of ligand activation in human GABAB receptor. Nature [Internet]. 2013 Dec [cited 2020 Jan 9];504(7479):254–9. Available from: http://www.nature.com/articles/nature12725

70. Geng Y, Xiong D, Mosyak L, Malito DL, Kniazeff J, Chen Y, et al. Structure and functional interaction of the extracellular domain of human GABAB receptor GBR2. Nat Neurosci [Internet]. 2012 Jul [cited 2020 Mar 10];15(7):970–8. Available from: http://www.nature.com/articles/nn.3133

71. Muto T, Tsuchiya D, Morikawa K, Jingami H. Structures of the extracellular regions of the group II/III metabotropic glutamate receptors. Proc Natl Acad Sci [Internet]. 2007 Mar 6 [cited 2020 Mar 29];104(10):3759–64. Available from: http://www.pnas.org/cgi/doi/10.1073/pnas.0611577104

72. Tsuchiya D, Kunishima N, Kamiya N, Jingami H, Morikawa K. Structural views of the ligand-binding cores of a metabotropic glutamate receptor complexed with an antagonist and both glutamate and Gd3+. Proc Natl Acad Sci [Internet]. 2002 Mar 5 [cited 2020 Mar 29];99(5):2660–5. Available from: http://www.pnas.org/cgi/doi/10.1073/pnas.052708599

73. Schwenk J, Pérez-Garci E, Schneider A, Kollewe A, Gauthier-Kemper A, Fritzius T, et al. Modular composition and dynamics of native GABAB receptors identified by high-resolution proteomics. Nat Neurosci. 2016 Feb;19(2):233–42.

74. Biermann B, Ivankova-Susankova K, Bradaia A, Abdel Aziz S, Besseyrias V, Kapfhammer JP, et al. The Sushi domains of GABAB receptors function as axonal targeting signals. J Neurosci Off J Soc Neurosci. 2010 Jan 27;30(4):1385–94.

75. Pin J-P, Bettler B. Organization and functions of mGlu and GABAB receptor complexes. Nature [Internet]. 2016 Dec [cited 2020 Feb 2];540(7631):60–8. Available from: http://www.nature.com/articles/nature20566

76. Kniazeff J, Prézeau L, Rondard P, Pin J-P, Goudet C. Dimers and beyond: The functional puzzles of class C GPCRs. Pharmacol Ther [Internet]. 2011 Apr 1 [cited 2019 Oct 22];130(1):9–25. Available from: http://www.sciencedirect.com/science/article/pii/S0163725811000234

77. Evenseth LSM, Ocello R, Gabrielsen M, Masetti M, Recanatini M, Sylte I, et al. Exploring Conformational Dynamics of the Extracellular *Venus flytrap* Domain of the GABA B Receptor: A Path-Metadynamics Study. J Chem Inf Model [Internet]. 2020 Apr 27 [cited 2020 May 6];60(4):2294–303. Available from: https://pubs.acs.org/doi/abs/10.1021/acs.jcim.0c00163

78. Binet V, Duthey B, Lecaillon J, Vol C, Quoyer J, Labesse G, et al. Common structural requirements for heptahelical domain function in class A and class C G protein-coupled receptors. J Biol Chem [Internet]. 2007 Apr [cited 2020 Mar 31];282(16):12154–63. Available from: https://www.ncbi.nlm.nih.gov/pmc/articles/PMC2565688/

79. Duthey B, Caudron S, Perroy J, Bettler B, Fagni L, Pin J-P, et al. A Single Subunit (GB2) Is Required for G-protein Activation by the Heterodimeric GABA B Receptor. J Biol Chem [Internet]. 2002 Feb 1 [cited 2020 Mar 31];277(5):3236–41. Available from: http://www.jbc.org/lookup/doi/10.1074/jbc.M108900200

80. Chen L-H, Sun B, Zhang Y, Xu T-J, Xia Z-X, Liu J-F, et al. Discovery of a Negative Allosteric Modulator of GABA B Receptors. ACS Med Chem Lett [Internet]. 2014 Jul 10 [cited 2020 Jan 10];5(7):742–7. Available from: https://pubs.acs.org/doi/10.1021/ml500162z

81. Freyd T, Warszycki D, Mordalski S, Bojarski AJ, Sylte I, Gabrielsen M. Ligand-guided homology modelling of the GABAB2 subunit of the GABAB receptor. Lodola A, editor. PLOS ONE [Internet]. 2017 Mar 21 [cited 2019 Sep 9];12(3):e0173889. Available from: https://dx.plos.org/10.1371/journal.pone.0173889

82. Doly S, Shirvani H, Gäta G, Meye FJ, Emerit M-B, Enslen H, et al. GABAB receptor cell-surface export is controlled by an endoplasmic reticulum gatekeeper. Mol Psychiatry. 2016 Apr;21(4):480–90.

83. Comps-Agrar L, Kniazeff J, Nørskov-Lauritsen L, Maurel D, Gassmann M, Gregor N, et al. The oligomeric state sets GABA(B) receptor signalling efficacy. EMBO J. 2011 May 6;30(12):2336–49.

84. Xue L, Sun Q, Zhao H, Rovira X, Gai S, He Q, et al. Rearrangement of the transmembrane domain interfaces associated with the activation of a GPCR hetero-oligomer. Nat Commun [Internet]. 2019 Dec [cited 2019 Oct 8];10(1):2765. Available from: http://www.nature.com/articles/s41467-019-10834-5

85. Schwenk J, Metz M, Zolles G, Turecek R, Fritzius T, Bildl W, et al. Native GABA(B) receptors are heteromultimers with a family of auxiliary subunits. Nature. 2010 May 13;465(7295):231–5.

86. Ivankova K, Turecek R, Fritzius T, Seddik R, Prezeau L, Comps-Agrar L, et al. Up-regulation of GABA(B) receptor signaling by constitutive assembly with the K+ channel tetramerization domain-containing protein 12 (KCTD12). J Biol Chem. 2013 Aug 23;288(34):24848–56.

87. Dario A, Tomei G. A Benefit-Risk Assessment of Baclofen in Severe Spinal Spasticity: Drug Saf [Internet]. 2004 [cited 2020 May 8];27(11):799–818. Available from: http://link.springer.com/10.2165/00002018-200427110-00004

88. Jeffrey Conn P, Christopoulos A, Lindsley CW. Allosteric modulators of GPCRs: a novel approach for the treatment of CNS disorders. Nat Rev Drug Discov [Internet]. 2009 Jan [cited 2020 Mar 11];8(1):41–54. Available from: http://www.nature.com/articles/nrd2760

89. May LT, Leach K, Sexton PM, Christopoulos A. Allosteric Modulation of G Protein–Coupled Receptors. Annu Rev Pharmacol Toxicol [Internet]. 2007 Feb [cited 2020 Apr 1];47(1):1–51. Available from: http://www.annualreviews.org/doi/10.1146/annurev.pharmtox.47.120505.105159

90. Brown KM, Roy KK, Hockerman GH, Doerksen RJ, Colby DA. Activation of the γ-Aminobutyric Acid Type B (GABA B) Receptor by Agonists and Positive Allosteric Modulators: Miniperspective. J Med Chem [Internet]. 2015 Aug 27 [cited 2020 Jan 10];58(16):6336–47. Available from: https://pubs.acs.org/doi/10.1021/jm5018913

91. Urwyler S, Mosbacher J, Lingenhoehl K, Heid J, Hofstetter K, Froestl W, et al. Positive Allosteric Modulation of Native and Recombinant ✐-Aminobutyric AcidB Receptors by 2,6-Di-tert-butyl-4-(3- hydroxy-2,2-dimethyl-propyl)-phenol (CGP7930) and its Aldehyde Analog CGP1350. 2001;9.

92. Binet V, Brajon C, Le Corre L, Acher F, Pin J-P, Prézeau L. The Heptahelical Domain of GABA B2 Is Activated Directly by CGP7930, a Positive Allosteric Modulator of the GABA B Receptor. J Biol Chem [Internet]. 2004 Jul 9 [cited 2020 Jan 10];279(28):29085–91. Available from: http://www.jbc.org/lookup/doi/10.1074/jbc.M400930200

93. Urwyler S, Pozza MF, Lingenhoehl K, Mosbacher J, Lampert C, Froestl W, et al. *N* , *N* ′-Dicyclopentyl-2-methylsulfanyl-5-nitro-pyrimidine-4,6-diamine (GS39783) and Structurally Related Compounds: Novel Allosteric Enhancers of γ-Aminobutyric Acid B Receptor Function. J Pharmacol Exp Ther [Internet]. 2003 Oct [cited 2020 Mar 11];307(1):322–30. Available from: http://jpet.aspetjournals.org/lookup/doi/10.1124/jpet.103.053074

94. Guery S, Floersheim P, Kaupmann K, Froestl W. Syntheses and optimization of new GS39783 analogues as positive allosteric modulators of GABAB receptors. Bioorg Med Chem Lett [Internet]. 2007 Nov [cited 2020 Mar 11];17(22):6206–11. Available from: https://linkinghub.elsevier.com/retrieve/pii/S0960894X07010542

95. Malherbe P, Masciadri R, Norcross RD, Knoflach F, Kratzeisen C, Zenner M-T, et al. Characterization of (R,S)-5,7-di-tert-butyl-3-hydroxy-3-trifluoromethyl-3H-benzofuran-2-one as a positive allosteric modulator of GABAB receptors: rac-BHFF: a positive modulator of GABAB receptors. Br J Pharmacol [Internet]. 2009 Jan 29 [cited 2020 Mar 11];154(4):797–811. Available from: http://doi.wiley.com/10.1038/bjp.2008.135

96. Sun B, Chen L, Liu L, Xia Z, Pin J-P, Nan F, et al. A negative allosteric modulator modulates GABAB-receptor signalling through GB2 subunits. Biochem J [Internet]. 2016 Mar 15 [cited 2020 Jan 10];473(6):779–87. Available from: https://portlandpress.com/biochemj/article/473/6/779-787/49353

97. Young DC. Computational chemistry: a practical guide for applying techniques to real world problems [Internet]. 2002 [cited 2020 Mar 12]. Available from: http://onlinelibrary.wiley.com/book/10.1002/0471220655

98. Sliwoski G, Kothiwale S, Meiler J, Lowe EW. Computational Methods in Drug Discovery. Barker EL, editor. Pharmacol Rev [Internet]. 2014 Jan [cited 2020 Mar 17];66(1):334–95. Available from: http://pharmrev.aspetjournals.org/lookup/doi/10.1124/pr.112.007336

99. Huang H-J, Yu HW, Chen C-Y, Hsu C-H, Chen H-Y, Lee K-J, et al. Current developments of computer-aided drug design. J Taiwan Inst Chem Eng [Internet]. 2010 Nov [cited 2020 Mar 12];41(6):623–35. Available from: https://linkinghub.elsevier.com/retrieve/pii/S1876107010000556

100. Patrick GL. An introduction to medicinal chemistry. Fifth edition. Oxford: Oxford University Press; 2013. 789 p.

101. Lewars EG. Computational Chemistry [Internet]. Dordrecht: Springer Netherlands; 2011 [cited 2020 Mar 12]. Available from: http://link.springer.com/10.1007/978-90-481-3862-3

102. Höltje H-D, Folkers G, Beier T. Molecular modeling: basic principles and applications. 3rd ed. Weinheim ; New York: VCH; 2008. 310 p. (Methods and principles in medicinal chemistry).

103. Chothia C, Lesk AM. The relation between the divergence of sequence and structure in proteins. EMBO J [Internet]. 1986 Apr [cited 2020 May 7];5(4):823–6. Available from: https://www.ncbi.nlm.nih.gov/pmc/articles/PMC1166865/

104. Schmidt T, Bergner A, Schwede T. Modelling three-dimensional protein structures for applications in drug design. Drug Discov Today [Internet]. 2014 Jul [cited 2020 Mar 17];19(7):890–7. Available from: https://linkinghub.elsevier.com/retrieve/pii/S1359644613003942

105. Protein BLAST: search protein databases using a protein query [Internet]. [cited 2020 May 7]. Available from: https://blast.ncbi.nlm.nih.gov/Blast.cgi?ALIGNMENTS=50&ALIGNMENT_VIEW=Pairwise&AUTO_FORMAT=Semiauto&CLIENT=web&DATABASE=pdb&DESCRIPTIONS=100&ENTREZ_QUERY=(none)&EXPECT=20000&FORMAT_BLOCK_ON_RESPAGE=None&FORMAT_ENTREZ_QUERY=(none)&FORMAT_OBJECT=Alignment&FORMAT_TYPE=HTML&GAPCOSTS=9+1&I_THRESH=0.005&LAYOUT=TwoWindows&MATRIX_NAME=PAM30&NCBI_GI=on&PAGE=Proteins&PROGRAM=blastp&QUERY=gapn&SERVICE=plain&SET_DEFAULTS.x=14&SET_DEFAULTS.y=5&SHOW_LINKOUT=on&SHOW_OVERVIEW=on&WORD_SIZE=2&END_OF_HTTPGET=Yes

106. Venclovas Č. Methods for Sequence–Structure Alignment. In: Orry AJW, Abagyan R, editors. Homology Modeling [Internet]. Totowa, NJ: Humana Press; 2011 [cited 2020 Mar 17]. p. 55–82. (Methods in Molecular Biology; vol. 857). Available from: http://link.springer.com/10.1007/978-1-61779-588-6_3

107. Ravna AW, Sylte I. Homology Modeling of Transporter Proteins (Carriers and Ion Channels). In: Orry AJW, Abagyan R, editors. Homology Modeling [Internet]. Totowa, NJ: Humana Press; 2011 [cited 2020 Mar 17]. p. 281–99. (Methods in Molecular Biology; vol. 857). Available from: http://link.springer.com/10.1007/978-1-61779-588-6_12

108. Costanzi S. Homology Modeling of Class A G Protein-Coupled Receptors. In: Orry AJW, Abagyan R, editors. Homology Modeling [Internet]. Totowa, NJ: Humana Press; 2011 [cited 2020 Mar 17]. p. 259–79. (Methods in Molecular Biology; vol. 857). Available from: http://link.springer.com/10.1007/978-1-61779-588-6_11

109. Cereto-Massagué A, Guasch L, Valls C, Mulero M, Pujadas G, Garcia-Vallvé S. DecoyFinder: an easy-to-use python GUI application for building target-specific decoy sets. Bioinformatics [Internet]. 2012 Jun 15 [cited 2020 Mar 17];28(12):1661–2. Available from: https://academic.oup.com/bioinformatics/article-lookup/doi/10.1093/bioinformatics/bts249

110. Mysinger MM, Carchia M, Irwin JohnJ, Shoichet BK. Directory of Useful Decoys, Enhanced (DUD-E): Better Ligands and Decoys for Better Benchmarking. J Med Chem [Internet]. 2012 Jul 26 [cited 2020 May 7];55(14):6582–94. Available from: https://pubs.acs.org/doi/10.1021/jm300687e

111. Śledź P, Caflisch A. Protein structure-based drug design: from docking to molecular dynamics. Curr Opin Struct Biol [Internet]. 2018 Feb 1 [cited 2019 Sep 22];48:93–102. Available from: http://www.sciencedirect.com/science/article/pii/S0959440X17301100

112. Sousa SF, Fernandes PA, Ramos MJ. Protein–ligand docking: Current status and future challenges. Proteins Struct Funct Bioinforma [Internet]. 2006 [cited 2019 Sep 22];65(1):15–26. Available from: https://onlinelibrary.wiley.com/doi/abs/10.1002/prot.21082

113. Gani OABSM. Signposts of Docking and Scoring in Drug Design. Chem Biol Drug Des [Internet]. 2007 [cited 2019 Sep 25];70(4):360–5. Available from: https://onlinelibrary.wiley.com/doi/abs/10.1111/j.1747-0285.2007.00571.x

114. Tripathi A, Bankaitis VA. Molecular Docking: From Lock and Key to Combination Lock. 2018;19.

115. Lyne PD. Structure-based virtual screening: an overview. Drug Discov Today [Internet]. 2002 Oct [cited 2020 Mar 16];7(20):1047–55. Available from: https://linkinghub.elsevier.com/retrieve/pii/S1359644602024832

116. Stumpfe D, Ripphausen P, Bajorath J. Virtual compound screening in drug discovery. Future Med Chem [Internet]. 2012 Apr [cited 2020 Mar 16];4(5):593–602. Available from: http://www.future-science.com/doi/10.4155/fmc.12.19

117. Willett P. Similarity-based virtual screening using 2D fingerprints. Drug Discov Today [Internet]. 2006 Dec [cited 2020 Mar 16];11(23–24):1046–53. Available from: https://linkinghub.elsevier.com/retrieve/pii/S1359644606004193

118. Shoichet BK. Virtual screening of chemical libraries. Nature [Internet]. 2004 Dec [cited 2020 Mar 16];432(7019):862–5. Available from: http://www.nature.com/articles/nature03197

119. Lipinski CA, Lombardo F, Dominy BW, Feeney PJ. Experimental and computational approaches to estimate solubility and permeability in drug discovery and development settings1PII of original article: S0169-409X(96)00423-1. The article was originally published in Advanced Drug Delivery Reviews 23 (1997) 3–25.1. Adv Drug Deliv Rev [Internet]. 2001 Mar 1 [cited 2019 Dec 8];46(1):3–26. Available from: http://www.sciencedirect.com/science/article/pii/S0169409X00001290

120. Veber DF, Johnson SR, Cheng H-Y, Smith BR, Ward KW, Kopple KD. Molecular Properties That Influence the Oral Bioavailability of Drug Candidates. J Med Chem [Internet]. 2002 Jun 1 [cited 2019 Dec 8];45(12):2615–23. Available from: https://doi.org/10.1021/jm020017n

121. Gabrielsen M, Kurczab R, Siwek A, Wolak M, Ravna AW, Kristiansen K, et al. Identification of Novel Serotonin Transporter Compounds by Virtual Screening. J

Chem Inf Model [Internet]. 2014 Mar 24 [cited 2020 May 7];54(3):933–43. Available from: https://doi.org/10.1021/ci400742s

122. Duan J, Dixon SL, Lowrie JF, Sherman W. Analysis and comparison of 2D fingerprints: Insights into database screening performance using eight fingerprint methods. J Mol Graph Model [Internet]. 2010 Sep 1 [cited 2019 Sep 14];29(2):157–70. Available from: http://www.sciencedirect.com/science/article/pii/S1093326310000781

123. Evenseth L, Warszycki D, Bojarski AJ, Gabrielsen M, Sylte I. In Silico Methods for the Discovery of Orthosteric GABAB Receptor Compounds. 2019 Mar 7 [cited 2020 May 7]; Available from: https://munin.uit.no/handle/10037/15911

124. Sastry M, Lowrie JF, Dixon SL, Sherman W. Large-Scale Systematic Analysis of 2D Fingerprint Methods and Parameters to Improve Virtual Screening Enrichments. J Chem Inf Model [Internet]. 2010 May 24 [cited 2019 Sep 14];50(5):771–84. Available from: https://doi.org/10.1021/ci100062n

125. Yang S-Y. Pharmacophore modeling and applications in drug discovery: challenges and recent advances. Drug Discov Today [Internet]. 2010 Jun [cited 2020 Mar 17];15(11–12):444–50. Available from: https://linkinghub.elsevier.com/retrieve/pii/S135964461000111X

126. Cavasotto CN, Palomba D. Expanding the horizons of G protein-coupled receptor structure-based ligand discovery and optimization using homology models. Chem Commun [Internet]. 2015 Aug 20 [cited 2019 Oct 22];51(71):13576–94. Available from: https://pubs.rsc.org/en/content/articlelanding/2015/cc/c5cc05050b

127. Friesner RA, Murphy RB, Repasky MP, Frye LL, Greenwood JR, Halgren TA, et al. Extra Precision Glide: Docking and Scoring Incorporating a Model of Hydrophobic Enclosure for Protein−Ligand Complexes. J Med Chem [Internet]. 2006 Oct [cited 2020 May 3];49(21):6177–96. Available from: https://pubs.acs.org/doi/10.1021/jm051256o

128. Sherman W, Beard HS, Farid R. Use of an Induced Fit Receptor Structure in Virtual Screening. Chem Biol Htmlent Glyphamp Asciiamp Drug Des [Internet]. 2006 Jan [cited 2020 Mar 17];67(1):83–4. Available from: http://doi.wiley.com/10.1111/j.1747-0285.2005.00327.x

129. Induced Fit | Schrödinger [Internet]. [cited 2020 Mar 17]. Available from: https://www.schrodinger.com/Induced-Fit/

130. Stein RL. High-Throughput Screening in Academia: The Harvard Experience. J Biomol Screen [Internet]. 2003 Dec 1 [cited 2020 Apr 3];8(6):615–9. Available from: https://doi.org/10.1177/1087057103260741

131. Zhang R, Xie X. Tools for GPCR drug discovery. Acta Pharmacol Sin [Internet]. 2012 Mar [cited 2020 Apr 3];33(3):372–84. Available from: http://www.nature.com/articles/aps2011173

132. Klein MT, Vinson PN, Niswender CM. Approaches for Probing Allosteric Interactions at 7 Transmembrane Spanning Receptors. In: Progress in Molecular Biology and

Translational Science [Internet]. Elsevier; 2013 [cited 2020 Apr 3]. p. 1–59. Available from: https://linkinghub.elsevier.com/retrieve/pii/B9780123945877000014

133. Sykes DA, Stoddart LA, Kilpatrick LE, Hill SJ. Binding kinetics of ligands acting at GPCRs. Mol Cell Endocrinol [Internet]. 2019 Apr [cited 2020 Apr 3];485:9–19. Available from: https://linkinghub.elsevier.com/retrieve/pii/S0303720719300243

134. Greasley PJ, Jansen FP. G-protein-coupled receptor screening technologies. Drug Discov Today Technol [Internet]. 2005 Jun [cited 2020 Apr 3];2(2):163–70. Available from: https://linkinghub.elsevier.com/retrieve/pii/S1740674905000144

135. DeLapp NW, Gough WH, Kahl SD, Porter AC, Wiernicki TR. GTPγS Binding Assays. In: Sittampalam GS, Grossman A, Brimacombe K, Arkin M, Auld D, Austin CP, et al., editors. Assay Guidance Manual [Internet]. Bethesda (MD): Eli Lilly & Company and the National Center for Advancing Translational Sciences; 2004 [cited 2020 May 7]. Available from: http://www.ncbi.nlm.nih.gov/books/NBK92011/

136. Thomsen W, Frazer J, Unett D. Functional assays for screening GPCR targets. Curr Opin Biotechnol [Internet]. 2005 Oct 28 [cited 2020 Apr 5];S0958166905001680. Available from: https://linkinghub.elsevier.com/retrieve/pii/S0958166905001680

137. DiscoverX. DiscoverX user manual HitHunter® cAMP Assay for Small Molecules [Internet]. Available from: https://www.discoverx.com/CMSPages/GetAmazonFile.aspx?path=~\discoverx\media\contentfiles\document%20resource%20library\70-317-hithunter-camp-assay-for-small-molecules_rev4_1.pdf&hash=a9fc209869aa21af311c65f3a519e3bb69958622a653b8c8c7fdfb1366bef734&ext=.pdf

138. Bhatia S. Introduction to Pharmaceutical Biotechnology, Volume 3 [Internet]. IOP Publishing; 2019 [cited 2020 Apr 4]. Available from: https://iopscience.iop.org/book/978-0-7503-1347-6

139. Doelle HW, Rokem JS, Berovic M. BIOTECHNOLOGY - Volume I: Fundamentals in Biotechnology. EOLSS Publications; 2009. 496 p.

140. Coecke S, Balls M, Bowe G, Davis J, Gstraunthaler G, Hartung T, et al. Guidance on Good Cell Culture Practice. In: Smith R, editor. Cell Technology for Cell Products [Internet]. Dordrecht: Springer Netherlands; 2007 [cited 2020 Apr 4]. p. 313–5. Available from: http://link.springer.com/10.1007/978-1-4020-5476-1_49

141. Humphrey T, Pearce A. Cell Cycle Molecules and Mechanisms of the Budding and Fission Yeasts. In: Cell Cycle Control [Internet]. New Jersey: Humana Press; 2004 [cited 2020 Apr 5]. p. 003–30. Available from: http://link.springer.com/10.1385/1-59259-857-9:003

142. Schrödinger Release 2019-4: Canvas, Schrödinger, LLC, New York, NY, 2019.

143. Schrödinger Release 2019-4: Maestro, Schrödinger, LLC, New York, NY, 2019.

144. Fradera X, Babaoglu K. Overview of Methods and Strategies for Conducting Virtual Small Molecule Screening: Overview of Virtual Small Molecule Screening. Curr

Protoc Chem Biol [Internet]. 2017 Jan [cited 2020 May 3];9(3):196–212. Available from: http://doi.wiley.com/10.1002/cpch.27

145. Schrödinger Release 2019-4: LigPrep, Schrödinger, LLC, New York, NY, 2019.

146. Sastry GM, Inakollu VSS, Sherman W. Boosting Virtual Screening Enrichments with Data Fusion: Coalescing Hits from Two-Dimensional Fingerprints, Shape, and Docking. J Chem Inf Model [Internet]. 2013 Jul 22 [cited 2020 May 3];53(7):1531–42. Available from: https://pubs.acs.org/doi/10.1021/ci300463g

147. Sterling T, Irwin JJ. ZINC 15 – Ligand Discovery for Everyone. J Chem Inf Model [Internet]. 2015 Nov 23 [cited 2019 Dec 8];55(11):2324–37. Available from: https://doi.org/10.1021/acs.jcim.5b00559

148. Schrödinger Release 2019-4: Glide, Schrödinger, LLC, New York, NY, 2019.

149. Schrödinger Release 2019-4: QikProp, Schrödinger, LLC, New York, NY, 2019.

150. http://www.molsoft.com/technology.html.

151. Schrödinger Release 2019-4: Protein Preparation Wizard; Epik, Schrödinger, LLC, New York, NY, 2016; Impact, Schrödinger, LLC, New York, NY, 2016; Prime, Schrödinger, LLC, New York, NY, 2019.

152. Schrödinger Release 2020-1: Epik, Schrödinger, LLC, New York, NY, 2020.

153. Drwal MN, Griffith R. Combination of ligand- and structure-based methods in virtual screening. Drug Discov Today Technol [Internet]. 2013 Sep [cited 2020 May 3];10(3):e395–401. Available from: https://linkinghub.elsevier.com/retrieve/pii/S1740674913000097

154. Overington JP, Al-Lazikani B, Hopkins AL. How many drug targets are there? Nat Rev Drug Discov [Internet]. 2006 Dec [cited 2020 Apr 29];5(12):993–6. Available from: http://www.nature.com/articles/nrd2199

155. Zhang M-Q, Wilkinson B. Drug discovery beyond the 'rule-of-five.' Curr Opin Biotechnol [Internet]. 2007 Dec [cited 2020 Apr 29];18(6):478–88. Available from: https://linkinghub.elsevier.com/retrieve/pii/S0958166907001279

156. Oprea T. Virtual Screening in Lead Discovery: A Viewpoint. Molecules [Internet]. 2002 Jan 31 [cited 2020 May 3];7(1):51–62. Available from: http://www.mdpi.com/1420-3049/7/1/51

157. Klopmand G. Concepts and applications of molecular similarity, by Mark A. Johnson and Gerald M. Maggiora, eds., John Wiley & Sons, New York, 1990, 393 pp. Price: $65.00. J Comput Chem [Internet]. 1992 May [cited 2020 May 3];13(4):539–40. Available from: http://doi.wiley.com/10.1002/jcc.540130415

158. McGaughey GB, Sheridan RP, Bayly CI, Culberson JC, Kreatsoulas C, Lindsley S, et al. Comparison of Topological, Shape, and Docking Methods in Virtual Screening. J Chem Inf Model [Internet]. 2007 Jul [cited 2020 May 3];47(4):1504–19. Available from: https://pubs.acs.org/doi/10.1021/ci700052x

159. Gimeno A, Ojeda-Montes M, Tomás-Hernández S, Cereto-Massagué A, Beltrán-Debón R, Mulero M, et al. The Light and Dark Sides of Virtual Screening: What Is There to Know? Int J Mol Sci [Internet]. 2019 Mar 19 [cited 2020 May 3];20(6):1375. Available from: https://www.mdpi.com/1422-0067/20/6/1375

160. Kumar A, Zhang KYJ. Advances in the Development of Shape Similarity Methods and Their Application in Drug Discovery. Front Chem [Internet]. 2018 Jul 25 [cited 2020 May 3];6:315. Available from: https://www.frontiersin.org/article/10.3389/fchem.2018.00315/full

161. Zerbe BS, Hall DR, Vajda S, Whitty A, Kozakov D. Relationship between Hot Spot Residues and Ligand Binding Hot Spots in Protein–Protein Interfaces. J Chem Inf Model [Internet]. 2012 Aug 27 [cited 2020 Mar 25];52(8):2236–44. Available from: https://pubs.acs.org/doi/10.1021/ci300175u

162. Dupuis DS, Relkovic D, Lhuillier L, Mosbacher J, Kaupmann K. Point Mutations in the Transmembrane Region of GABAB2 Facilitate Activation by the Positive Modulator N,N′-Dicyclopentyl-2-methylsulfanyl-5-nitro-pyrimidine-4,6-diamine (GS39783) in the Absence of the GABAB1 Subunit. Mol Pharmacol [Internet]. 2006 Dec 1 [cited 2019 Sep 15];70(6):2027–36. Available from: http://molpharm.aspetjournals.org/content/70/6/2027

163. Lundström L, Bissantz C, Beck J, Wettstein J, Woltering T, Wichmann J, et al. Structural determinants of allosteric antagonism at metabotropic glutamate receptor 2: mechanistic studies with new potent negative allosteric modulators. Br J Pharmacol [Internet]. 2011 Sep [cited 2020 May 5];164(2b):521–37. Available from: https://www.ncbi.nlm.nih.gov/pmc/articles/PMC3188907/

164. Teague SJ. Implications of protein flexibility for drug discovery. Nat Rev Drug Discov [Internet]. 2003 Jul [cited 2020 May 3];2(7):527–41. Available from: http://www.nature.com/articles/nrd1129

165. Friesner RA, Banks JL, Murphy RB, Halgren TA, Klicic JJ, Mainz DT, et al. Glide: A New Approach for Rapid, Accurate Docking and Scoring. 1. Method and Assessment of Docking Accuracy. J Med Chem [Internet]. 2004 Mar [cited 2020 May 3];47(7):1739–49. Available from: https://pubs.acs.org/doi/10.1021/jm0306430

166. Wang H, Ben-Naim A. A Possible Involvement of Solvent-Induced Interactions in Drug Design. J Med Chem [Internet]. 1996 Jan [cited 2020 May 3];39(7):1531–9. Available from: https://pubs.acs.org/doi/10.1021/jm950430d

167. Karthikeyan M, Vyas R. Practical Chemoinformatics. Springer; 2014. 546 p.

168. Baell J, Walters MA. Chemistry: Chemical con artists foil drug discovery. Nature [Internet]. 2014 Sep [cited 2020 May 3];513(7519):481–3. Available from: http://www.nature.com/articles/513481a

169. Wang T, Li Z, Cvijic ME, Zhang L, Sum CS. Measurement of cAMP for Gαs- and Gαi Protein-Coupled Receptors (GPCRs). In: Sittampalam GS, Grossman A, Brimacombe K, Arkin M, Auld D, Austin CP, et al., editors. Assay Guidance Manual [Internet]. Bethesda (MD): Eli Lilly & Company and the National Center for Advancing

Translational Sciences; 2004 [cited 2020 May 9]. Available from: http://www.ncbi.nlm.nih.gov/books/NBK464633/

170. Cruciani G, Milletti F, Storchi L, Sforna G, Goracci L. *In silico* p *K* a Prediction and ADME Profiling. Chem Biodivers [Internet]. 2009 Nov [cited 2020 May 3];6(11):1812–21. Available from: http://doi.wiley.com/10.1002/cbdv.200900153

171. Schrödinger Release 2019-4: Jaguar pKa, Schrödinger, LLC, New York, NY, 2019.

172. Gabriel D, Vernier M, Pfeifer MJ, Dasen B, Tenaillon L, Bouhelal R. High throughput screening technologies for direct cyclic AMP measurement. Assay Drug Dev Technol. 2003 Apr;1(2):291–303.

173. Huang RD, Smith MF, Zahler WL. Inhibition of forskolin-activated adenylate cyclase by ethanol and other solvents. J Cyclic Nucleotide Res. 1982;8(6):385–94.

174. Yang Z, Xiong H-R. Culture Conditions and Types of Growth Media for Mammalian Cells. In: Ceccherini-Nelli L, editor. Biomedical Tissue Culture [Internet]. InTech; 2012 [cited 2020 Apr 3]. Available from: http://www.intechopen.com/books/biomedical-tissue-culture/culture-conditions-and-types-of-growth-media-for-mammalian-cells

175. Grampp T, Sauter K, Markovic B, Benke D. γ-Aminobutyric Acid Type B Receptors Are Constitutively Internalized via the Clathrin-dependent Pathway and Targeted to Lysosomes for Degradation. J Biol Chem [Internet]. 2007 Aug 17 [cited 2020 Apr 4];282(33):24157–65. Available from: http://www.jbc.org/lookup/doi/10.1074/jbc.M702626200

176. González-Maeso J, Wise A, Green A, Koenig JA. Agonist-induced desensitization and endocytosis of heterodimeric GABAB receptors in CHO-K1 cells. Eur J Pharmacol [Internet]. 2003 Nov 14 [cited 2020 May 9];481(1):15–23. Available from: http://www.sciencedirect.com/science/article/pii/S0014299903023616

177. Hannan S, Wilkins ME, Dehghani-Tafti E, Thomas P, Baddeley SM, Smart TG. γ-Aminobutyric Acid Type B (GABA B) Receptor Internalization Is Regulated by the R2 Subunit. J Biol Chem [Internet]. 2011 Jul 8 [cited 2020 Apr 4];286(27):24324–35. Available from: http://www.jbc.org/lookup/doi/10.1074/jbc.M111.220814

178. Bowery NG, Hill DR, Hudson AL. Characteristics of GABAB receptor binding sites on rat whole brain synaptic membranes. Br J Pharmacol. 1983 Jan;78(1):191–206.

179. Wise A. Calcium sensing properties of the GABAB receptor. Neuropharmacology [Internet]. 1999 Nov [cited 2020 May 9];38(11):1647–56. Available from: https://linkinghub.elsevier.com/retrieve/pii/S0028390899001197